Drug release study from flexible and rigid drug carrier systems under inhomogeneous pulsed magnetic fields with applications in the molecular transport into cells

by

Basanta Acharya

B.Sc., Tribhuvan University, Nepal, 2008

M.Sc., Tribhuvan University, Nepal, 2012

AN ABSTRACT OF A DISSERTATION

Submitted in partial fulfillment of the requirements for the degree

DOCTOR OF PHILOSOPHY

Department of Chemistry

College of Arts and Sciences

KANSAS STATE UNIVERSITY

Manhattan, Kansas

2022

Abstract

This thesis focuses on the development of drug carrier systems in conjunction with an inhomogeneous pulsed magnetic field to achieve a short time release over the maximum release, in presence of magnetic nanoparticles (MNPs) as triggering agents. This thesis discusses the synthesis of both flexible (magneto-liposomal) and rigid (rattle cages of core $Fe_3O_4@SiO_2$ shell) drug carrier systems with their characterization, model drug encapsulation, and release assay under inhomogeneous pulsed magnetic field(s). Though the magneto-liposomal formulation with encapsulation of nanoparticles (NPs) at the core, at the bilayer, or the surface of liposomes is not new, the approach here is different from other works regarding the time in which the content is released. In the first project, the magnetic iron oxide nanoparticles are attached to the exterior surface of liposomes through two modifications, first, the coating of iron oxide nanoparticles with gold, and second, the surface modification of liposomes with CHOL-PEG-SH linker so that gold-coated MNPs are attached to a liposomal membrane with gold-thiol interaction. The release of carboxyfluorescein from this magneto-liposomes formulation under the application of magnetic pulses is studied. Further, the role of different types of nanoparticles on the phase transition temperature of liposomes and the effect of osmosis in model drug release from liposomes are explored. In another project, carboxyfluorescein release from magnetoliposomes with MNPs encapsulated at the aqueous lumen or, the lipid bilayer of liposomes is again investigated with applications of short magnetic pulses generated from both higher and lower inhomogeneous magnetic fields. To look further into the pulsatile release rate of the model drug, release after application of each magnetic pulse is measured. This will add a step towards our aim of the fast release kinetics of payload from magneto-liposomal systems. In addition, the release study from magnetoliposomes at different positions of magnets in both Helmholtz and anti-Helmholtz coils is

explored which strongly establishes the proof of concept for the use of the pulsed magnetic field system we developed. Besides, the release from rigid drug carrier system is discussed where rattle type mesoporous silica shell structures are used. The release of doxorubicin from these carriers with different core sizes, shell thickness, and effective volumes is investigated.

Finally, the use of the inhomogeneous pulsed magnetic field in the transportation of small molecules into the cancerous cells through the formation of micropores within those cells in presence of magnetic nanoparticles is explored. This pilot study investigated the individual and combinational effect of Dextran coated iron oxide NPs, doxorubicin, and magnetic pulses on cellular viability. Moreover, the enhancement of doxorubicin uptake and accumulation along with its effectiveness in this combinational strategy is discussed. It is expected that the use of pulsed magnetic field mediated ultrasound generation from magnetic nanoparticles will have a significant role in biological applications including targeted drug delivery.

Drug release study from flexible and rigid drug carrier systems under inhomogeneous pulsed magnetic fields with applications in the molecular transport into cells

by

Basanta Acharya

B.Sc., Tribhuvan University, Nepal, 2008
M.Sc., Tribhuvan University, Nepal, 2012

A DISSERTATION

Submitted in partial fulfillment of the requirements for the degree

DOCTOR OF PHILOSOPHY

Department of Chemistry
College of Arts and Sciences

KANSAS STATE UNIVERSITY
Manhattan, Kansas

2022

Approved by:

Major Professor
Dr. Viktor Chikan

Copyright

Abstract

This thesis focuses on the development of drug carrier systems in conjunction with an inhomogeneous pulsed magnetic field to achieve a short time release over the maximum release, in presence of magnetic nanoparticles (MNPs) as triggering agents. This thesis discusses the synthesis of both flexible (magneto-liposomal) and rigid (rattle cages of core $Fe_3O_4@SiO_2$ shell) drug carrier systems with their characterization, model drug encapsulation, and release assay under inhomogeneous pulsed magnetic field(s). Though the magneto-liposomal formulation with encapsulation of nanoparticles (NPs) at the core, at the bilayer, or the surface of liposomes is not new, the approach here is different from other works regarding the time in which the content is released. In the first project, the magnetic iron oxide nanoparticles are attached to the exterior surface of liposomes through two modifications, first, the coating of iron oxide nanoparticles with gold, and second, the surface modification of liposomes with CHOL-PEG-SH linker so that gold-coated MNPs are attached to a liposomal membrane with gold-thiol interaction. The release of carboxyfluorescein from this magneto-liposomes formulation under the application of magnetic pulses is studied. Further, the role of different types of nanoparticles on the phase transition temperature of liposomes and the effect of osmosis in model drug release from liposomes are explored. In another project, carboxyfluorescein release from magnetoliposomes with MNPs encapsulated at the aqueous lumen or, the lipid bilayer of liposomes is again investigated with applications of short magnetic pulses generated from both higher and lower inhomogeneous magnetic fields. To look further into the pulsatile release rate of the model drug, release after application of each magnetic pulse is measured. This will add a step towards our aim of the fast release kinetics of payload from magneto-liposomal systems. In addition, the release study from magnetoliposomes at different positions of magnets in both Helmholtz and anti-Helmholtz coils is

explored which strongly establishes the proof of concept for the use of the pulsed magnetic field system we developed. Besides, the release from rigid drug carrier system is discussed where rattle type mesoporous silica shell structures are used. The release of doxorubicin from these carriers with different core sizes, shell thickness, and effective volumes is investigated.

Finally, the use of the inhomogeneous pulsed magnetic field in the transportation of small molecules into the cancerous cells through the formation of micropores within those cells in presence of magnetic nanoparticles is explored. This pilot study investigated the individual and combinational effect of Dextran coated iron oxide NPs, doxorubicin, and magnetic pulses on cellular viability. Moreover, the enhancement of doxorubicin uptake and accumulation along with its effectiveness in this combinational strategy is discussed. It is expected that the use of pulsed magnetic field mediated ultrasound generation from magnetic nanoparticles will have a significant role in biological applications including targeted drug delivery.

Table of Contents

List of Figures

List of Tables

List of Abbreviations

AC – Alternating current

AMF – Alternating magnetic field

ATP – Adenosine triphosphate

CF – Carboxyfluorescein

CHOL/ TH-CHOL – Cholesterol/ Thiolated Cholesterol

DC – Direct current

Dex-IONPs – Dextran coated Iron oxide nanoparticles

DLS – Dynamic light scattering

DOX – Doxorubicin

EDX – Electron dispersive X-ray analysis

HPLC – High-performance liquid chromatography

HR-TEM/TEM – High Resolution-Tunneling electron microscopy

IONPs – Iron oxide nanoparticles

IR – Infrared

IUPAC – International union for pure and applied chemistry

kHz – Kilohertz

LMF/HMF – Lower/Higher magnetic field

LUVET – Large unilamellar vesicles by extrusion

MCM – Mobil crystalline material

MNPs – Magnetic nanoparticles

NMR – Nuclear magnetic resonance

NPs – nanoparticles

PBS – Phosphate buffered saline

PDI – Polydispersity index

PEG – Polyethylene glycol

PL – Photoluminescence

PMF – Pulsed magnetic field

RES – Reticuloendothelial system

RNA – Ribonucleic acid

Acknowledgments

I would like to express my gratitude to my major advisor, Prof. Viktor Chikan whose guidance, motivation, support, and encouragement have been invaluable throughout the years of my graduate studies. I am much thankful for the opportunity he has provided me to work under his supervision in a cozy environment. His amiable nature and the way he trained me made my learning and research easy and very interesting. The knowledge and skills I have gathered from him throughout these years are treasures for my future endeavors.

I would like to acknowledge Prof. Rafferty for providing me with an opportunity for research collaboration where I could expand my knowledge of biological systems and applications.

I would like to extend my heartful thanks to Prof. Smith who always offered me his valuable advice on all the departmental requirements for my degree.

My sincere acknowledgment to my advisory committee: Prof. Paul Smith, Prof. Ryan Rafferty, and Prof. Bret Flanders for their support and guidance during my research. A special thanks to Prof. Wang Yongqiang from Henan University at Kaifeng, China for providing the mesoporous silica shell samples to my research project. I would like to thank Prof. Matthew Basel at the K-state vet-medicine department and Dr. George Podaru (a former member of Dr. Chikan's lab) for training me on magneto-liposomal synthesis. I would like to thank Prof. Santosh Aryal and his group members for training and providing me access to the dynamic light scattering facility at NICKS, K-State.

I would like to thank Michael Hinton and Dr. Tingting Liu for training and helping me during my teaching responsibilities. I greatly appreciate our departmental technicians Tobe Eggers, Jim Hodgson, and Ron Jackson for helping me during my research. I graciously appreciate the staff at

Dedication

To my parents

and my beloved wife

Richu

Chapter 1: Introduction of Drug Carrier System

1.1 Drug carrier systems

A drug carrier can simply be defined as a substrate that is designed for the drug delivery and an assembly of such carriers makes a system that can be used for targeted and/or controlled drug delivery or release of therapeutic drugs[1]. Since the direct administration of therapeutic agents into the living body leads to the various side effects of the drug-tissue interactions, the drug carrier systems can play an important role to reduce such drug toxicity by providing a protective layer.[1, 2] In other words, the drug carrier system provides a shield to protect the drug molecules from enzymatic action so that physiochemical properties of drug molecules remain preserved during the circulation period before reaching the targeted unhealthy tissues, and at the same time, healthy tissues can be saved by avoiding unwanted chemical toxicity due to active ingredients present on drug molecules[3]. Another important advantage of the drug carriers is the lesser drug administration frequency as these carrier systems can also be used to control the rate at which drug is delivered to the targeted area[3, 4].

The candidacy of various bio-engineered systems as drug carriers requires certain properties, among them stability, stimuli responsiveness, and specificity are more important[2]. Once they enter the living body, the physiological defense system can attack these carrier systems. The carrier systems should be stable enough to preserve the encapsulated drug molecules/ loaded cargo, without being destroyed before reaching the targeted site[2, 3]. The drug carrier systems can be effective when they can be modified in a way that they can be used to target different locations as per necessity. Also, these systems must be capable of recognizing the targeted area where the drugs

need to be delivered. The drug carriers once reach the desired site should be able to respond towards an internal or external stimulus so that the drug molecules can be released.[2, 5]

The drug carrier systems usually have a few to several hundred nanometer sizes, which can be designed from organic constituents or inorganic substances and have either flexible or rigid morphology. Some of the widely used drug carriers (Figure 1) include liposomes, micelles, hydrogels, polymeric particles, dendrimers, nanospheres, nanocapsules, nanotubes, quantum dots, mesoporous silica shells, etc.[1, 2, 4, 6, 7] Among these liposomes, micelles, hydrogels, dendrimers are considered as flexible drug carriers because they can change dimensions significantly upon exposure to external stimuli while quantum dots, silica shells, nanospheres contain inorganic materials that add rigidity, hence regarded as rigid drug carrier systems providing more protection compared to the flexible drug carriers.
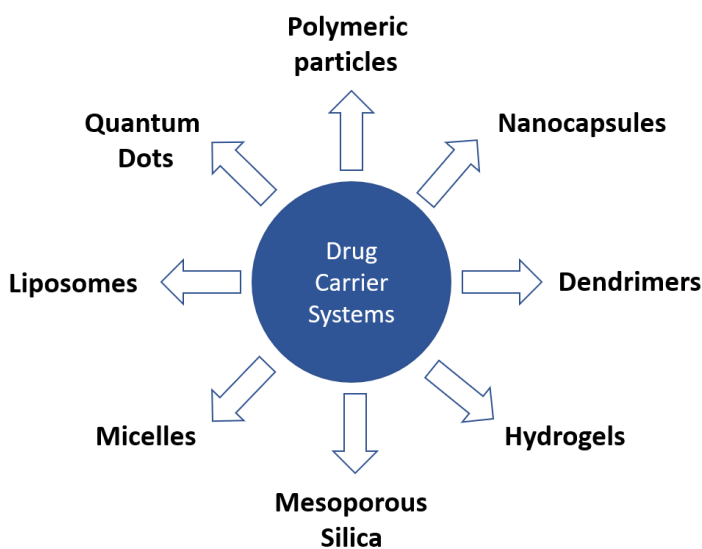
Figure 1.1. *Various nano drug-carrier systems.*

This thesis focuses on liposomal, and silica shell-based drug carrier systems and we explore how magnetic field triggering can enhance the functionality of these systems. In the next section, I will

provide some background information on liposomal and silica shell drug delivery systems and provide reasons why these systems are chosen in our studies.

1.2 Liposomes: Background and development

Since the first formulation in the 1960s, liposomes are one of the most widely used drug carrier systems in drug delivery research and clinical applications[8, 9]. With phospholipids as a chief ingredient, liposomes have spherical structures which can further be classified as unilamellar (with single phospholipid bilayer) or multilamellar (with multiple phospholipid bilayers arranged in concentric onion-like structures). It has been observed that the size between 70-300 nm is more appropriate to be used for clinical applications, thus making unilamellar liposomes as dominating lipid vesicle systems used for targeted drug delivery[10, 11]. As the lipid bilayer in liposomes resembles the natural cell membrane, they are biomimetic drug carriers that can enclose lipophilic and hydrophilic drug molecules at lipid bilayer and aqueous core respectively[12]. In addition to that, the constituent lipid and cholesterol can be so chosen that the bilayer surface of liposomes can be modified for diverse drug delivery applications[13]. The combination of phospholipids and cholesterol with hydrophilic polymers like polyethylene glycol (PEG), together known as "Stealth liposomes" has added a new avenue to the applications of liposomal drug carrier systems as they are more stable and have enhanced circulation time than conventional liposomes[9, 10, 14]. With the advancement of liposomal research, various natural and synthetic polymers have been employed during liposome formation[10, 15]. The major advantages of liposomal drug carrier systems are listed below:

1. Liposomal drug carrier systems are biocompatible[10] carriers with phospholipids as the main ingredient with relatively low cost due to its availability and ease of synthesis.[8]

2. Drug molecules or cargo with different levels of lipophilicity[16] can be loaded into the liposomes; hydrophilic drugs can be encapsulated in aqueous volume at the center and/or attached to an external surface of a lipid bilayer with surface modifications, lipophilic molecules in between the lipid bilayers, one kind at a time or simultaneously.[8] This provides a higher entrapment capacity per vesicle.

3. Liposomal drug carrier systems are bio-degradable and non-toxic hence safe to administer into a living body.[11]

4. Depending upon the toxicity level of encapsulated drug molecules, the constituent lipid molecules can be selected and combined with cholesterol at varying concentrations to add the stability of this system.[8, 11, 17] The selection of ingredients and method of preparation can reduce the problem of drug leakage before targeted delivery.[11]

5. Liposomes can prevent the biochemical degradation of drug molecules[11] and minimize the undesirable interaction of drug molecules with healthy tissues thereby improving its therapeutic applications.[11, 13]

6. Possibility of surface modifications using different types of ligands adds versatility in its use in targeted drug delivery.[18, 19] Different molecules/macromolecules can be potentially attached to the liposomal surface thereby changing the physiochemical properties of those surfaces, which in turn helps to modulate the functionality and stability of liposomal systems.[13, 18]

7. Liposomal systems can be designed and coupled with different triggering techniques to release the drug at a controlled rate. This enhances the efficiency of liposomal systems as therapeutic agents.[20]

It is important to note that the selection of constituent lipids in liposomes preparation is crucial regarding the use of liposomes in targeted drug delivery. The pharmacokinetic behavior of both

carrier (liposomes) and cargo (drugs) depends upon the physical and chemical properties of the constituent lipids[11]. First, the composition of lipids greatly influences the permeability of lipid bilayer which in turn has an impact on the rate at which payload (drugs) is released[20]. Second, the stability of liposomes is important throughout the process, i) preparation (loading), ii) administration (into the body), and iii) final release of payload at the targeted site. For this, the lipids with phase-transition temperature (T_c) slightly higher than body temperature (T_b) is the best choice. It is because, if the $T_c < T_b$, the drug is released before it reaches the targeted site and if $T_c >> T_b$ the rate of drug release is much diminished making the liposomal system a poor carrier.[11, 16, 20] For this, either the one or combination of more phospholipids is preferred for manipulating the T_c such that it will fit the needs of the specific application.

Table 1.1 Commonly used phospholipids with their phase transition temperatures.

S.N.	Phospholipids	Tc
1	1,2-dilauroyl-*sn*-glycero-3-phosphatidylcholine (DLPC, 13:0 PC)	14°C
2	1,2-dimyristoyl-*sn*-glycero-3-phosphatidylcholine(DMPC,15:0 PC)	35°C
3	1,2-dipalmitoyl-*sn*-glycero-3-phosphatidylcholine (DPPC, 16:0 PC)	41°C
4	1-palmitoyl-2-oleoyl-*sn*-glycero-3-phosphatidylcholine (POPC)	-2°C
5	1,2-distearoyl-*sn*-glycero-3-phosphatidylcholine (DSPC, 18:0 PC)	55°C
6	1-stearoyl-2-oleoyl-*sn*-glycero-3-phosphatidylcholine (SOPC)	6.7°C
7	1,2-Dioleoyl-sn-glycero-3-phosphocholine (DOPC, 16:0-18:0 PC)	49°C

Besides the composition of lipids, the liposomal stability is governed by the incorporation of cholesterol[17, 20]. Cholesterol, as an important compound in the natural cell membrane which regulates membrane permeability, imparts elasticity, adds rigidity and overall strength of membrane, finds a similar role in its bio-mimics: liposomes. Cholesterol molecules reside in the

lipid bilayer and immingles with phospholipid molecules. Studies have shown that cholesterol stabilizes the liposomes by various mechanisms like prevention of liposomes aggregation, increase in mechanical strength (forming hydrogen bonding with fatty acids chain of lipids), reduction of passive permeability (by interacting with membrane phospholipids), altering the phospholipid packing, and reducing rotational freedom of phospholipids.[21, 22]

For a system to be more effective in drug delivery, liposomes need to have a longer circulation period[10]. The conventional liposomes which contain only phospholipids and cholesterol have lesser circulation time. Once administered into the living body, these liposomes experience rapid clearance from the blood via the reticuloendothelial system (RES). Such fast removal of the liposomes by the phagocytic mononuclear cells (macrophages and monocytes) of the reticuloendothelial system (RES) can be prevented by attaching a polyethylene glycol (PEG) coating to the outside of the liposome.[23, 24] PEGylation reduces the interaction of liposomes with recognition molecules by forming a steric block around liposomes.[25, 26] As the recognition molecules cannot reach the liposomal surface, the liposomes remain inconspicuous by RES, thereby increasing the circulation time in the bloodstream[15, 25]. Another advantage of coating liposomes with PEG molecules is that it provides room for chemical modification of liposomal surface where one end of PEG is attached to the phospholipid or cholesterol molecules while another free end can be modified/ attached to the ligands[11]. Studies have revealed that ligand attachments at the PEG end improve the efficacy of liposomes in targeted drug delivery.[27, 28] A typical liposomal structure is shown in **figure 1.2**.[29]
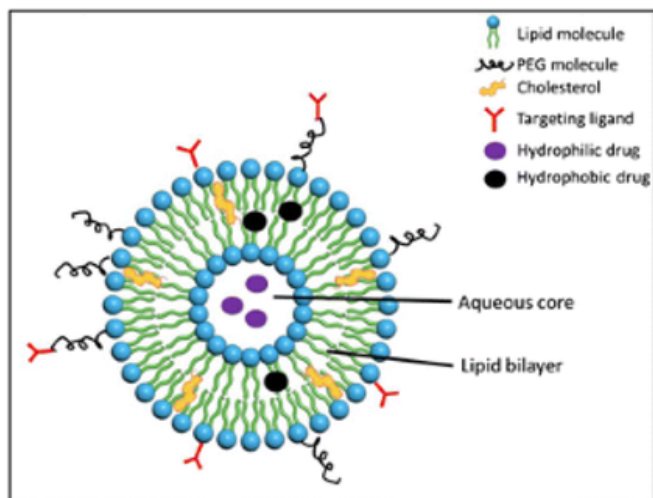
Figure 1.2. A typical liposomal structure indicating core, lipid bilayer, hydrophilic and hydrophobic drugs, surface modifications with PEG and ligands.

1.3 Triggering techniques in liposomal drug delivery

The drug carrier systems are expected to avoid drug leakage during circulation and deliver only at the targeted area. Several liposomal drug delivery systems have been developed that rely on the slow release of drugs but for the treatment of cancerous tissues and other infectious diseases, it is prudent to release the drug immediately and/or at a controlled rate after reaching the target. For this, stimuli-sensitive liposomal systems can be employed for triggered-based targeting. Stimuli-responsive systems are those which can be stimulated by changing the environmental parameters/signals. Such signals can either be internal (like change in pH, biomolecules, redox potential, enzymes, body temperatures) or external (light, heat, magnetic fields, ultrasound, mechanical forces, etc.) and upon exposure to such stimuli, these carriers release their content in a controlled manner at targeted location.[30, 31]
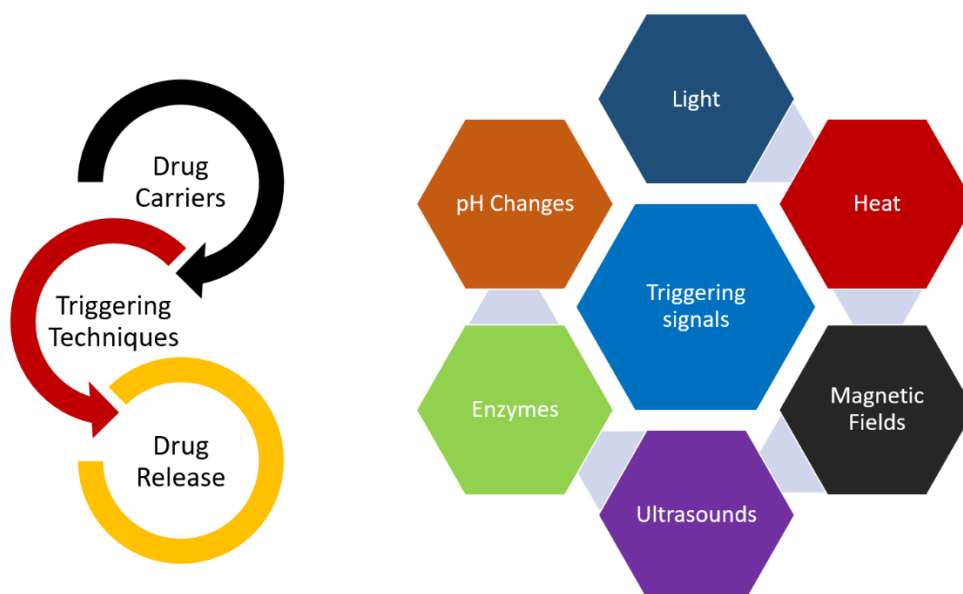
***Figure 1.3**. Internal and External stimuli for triggering the drug release from liposomes.*

1.3.1 Endogenous stimuli-based triggering

Various endogenous parameters can be used to trigger the drug release from liposomes. Such internal stimuli include a change in pH, difference in redox potential, enzymes, adenosine triphosphate (ATP), etc. Among these, pH and enzyme-based systems are discussed here.

a) ***pH-responsive liposomes***: There is a significant physiological difference between healthy and unhealthy tissues. The pH of normal tissues is around 7.4 while that infectious tissue is lower (acidic) ranging between 4.5-6.8.[32] This difference can trigger the permeability of liposomal membrane by inducing the change in morphology of lipid bilayers. In one study[33], it is found that at low pH conditions, a natural phospholipid 1,2-dioleoyl-*sn*-glycero-3-phosphoethanolamine (DOPE), exhibits a change in morphological phase behavior leading to membrane destabilization of liposomes. In other study[34], pH-sensitive liposomes are so

designed that functional group fragments are incorporated between PEG coating and lipid bilayers. These functional groups are stable at normal tissue pH but are hydrolyzed at pH lower than 6. This results in the release of PEG molecule and local drug delivery is achieved. Another approach involves the insertion of pH-sensitive peptides[35, 36]. These monomeric water-soluble peptides at normal body pH will become hydrophobic in acidic pH and lead to fusion of liposomes with cell membrane enhancing the cellular uptake and thereby releasing the payload.

b) ***Enzyme-triggered liposomes***: Certain diseases (e.g., cancer) cause the tissues to release enzymes like phospholipase, proteases, cathepsins, lysozymes, etc., in excess amount than normal healthy tissues.[11] This provides a platform to use enzyme-based liposomal triggering. The enzyme-sensitive liposomes are prepared in a way that they can release payload in response to enhanced enzyme concentrations due to pathophysiological changes.[11, 37] For example, phospholipase can degrade phospholipids when the concentration of phospholipids is higher like in liposomes. Phospholipase interacts with the liposomal membrane through its interfacial binding surface and ultimately hydrolyzes the lipid bilayer releasing the encapsulated drug.[37, 38]

1.3.2 Exogenous stimuli-based triggering

Liposomes can be designed to be triggered by various external stimuli such as heat, light, ultrasound, magnetic fields, electric fields, etc. to achieve controlled drug delivery at the desired site. Please, note that exogenous stimuli-based triggering generally provides more control than endogenous stimuli. For the specific control types, I will present the specific advantages of these stimuli.

a) ***Thermosensitive liposomes***: Phospholipids are the main ingredients of liposomal systems, and each phospholipid is associated with its unique phase transition temperature (T_m). This property makes the liposomal system inherently thermosensitive.[11] Liposomal system can be formulated using one or more phospholipids such that the phase transition occurs at around normal body temperature (37 °C). The various studies have revealed that thermosensitive liposomal systems use either lysolipids, surfactants, natural or synthetic polymers.[11, 32] On application of heat, physical and chemical properties of these thermosensitive components alter which leads to lipid bilayer destabilization and enhance the drug release. In another interesting study,[39] ammonium bicarbonate was used with a phospholipid/CHOL/PEG system. When the heat was applied, bubbles of carbon dioxide from ammonium bicarbonate induced disruption of the lipid bilayer, and the drug was rapidly released.

b) ***Light-sensitive liposomes***: During the formulation, photosensitive lipids, or photosensitive molecules, known as photosensitizers, can be incorporated into liposomes. These photosensitizing agents when irradiated with laser rupture the lipid bilayer, or lead to microporation that enables the drug release from the lipid vesicles.[40, 41] In these systems photodynamic therapy is used where light with a specific wavelength (normally near IR) activates the photosensitizers that ultimately disrupts the liposomal membrane.[32] Studies have revealed that besides photodynamic therapy, other strategies like photothermal, photo-crosslinking, photo-cleavage, and photoisomerization release have also been employed to increase liposomal drug release.[32, 41, 42]

c) ***Ultrasound-sensitive liposomes***: Due to the safe, non-invasiveness, and low cost, ultrasounds have been widely used in clinical applications. Ultrasound can trigger liposomes through different mechanisms like ultrasonic hyperthermia and acoustic cavitation.[43] Ultrasound waves

can convey energy to form gas bubbles. With an increase in acoustic pressure, these bubbles expand rapidly and finally collapse which causes deformation of liposomal bilayer membrane leading to payload release. This mechanism is known as acoustic cavitation.[43, 44] On the other hand, when some fraction of ultrasonic energy is converted to heat, during mechanical compression by ultrasonic waves, this heat facilitates the local hyperthermia resulting in drug release.[44]

d) *Magnetically triggered liposomes*: With the incorporation of magnetic nanoparticles like iron oxide nanoparticles, liposomes can be triggered to release drugs by the use of high/low frequency alternating magnetic fields or pulsed magnetic fields. DC magnetic field can also assist with the location of the liposomal drug delivery near the site of interest.[45] This is discussed in detail in section 1.4 below.

1.4 Incorporation of magnetic nanoparticles: Magneto-liposomes

1.4.1 Magnetic Nanoparticles in drug delivery: A brief discussion

Magnetic nanoparticles are the key element in a magnetic drug delivery system. Along with the properties like biocompatibility and easy surface modification, it holds the magnetic properties that open the new dimension in the field of drug delivery facilitating both localization of the liposomes and remote actuation/triggering. Magnetic nanoparticles can either be pure metals, metallic oxides, or metal alloys. Though pure metallic magnetic nanoparticles have the innate merit of high magnetic susceptibility and can be used as core substances, they tend to oxidize easily which often limits their use. While the metal oxides can be easily prepared in a controllable size and shape which adds more attention to its use for drug delivery. Iron oxides: magnetite Fe_3O_4, maghemite γ-Fe_2O_3, hematite α- Fe_2O_3, due to its excellent biodegradable nature, low toxicity to

cells, easy surface modifications, higher binding abilities with ligands and antibodies as well as ease of preparation, make it most suitable candidate for the use in drug delivery purposes. [46, 47] Below the size of critical diameter (usually <20 nm) particles behave as a single magnetic domain which makes the nanoparticles superparamagnetic. Here, the magnetic spin of the particles will be originally disordered but under the alternating magnetic field (AMF) it gets rapidly magnetized and tend to move directionally with the direction of a magnetic field. However, on the removal of the field, magnetization drops to zero which implies that, in an absence of an external magnetic field, the particles lack permanent net magnetism of the ensemble of the particles.[47, 48]

For two important reasons, the encapsulation of the magnetic nanoparticles is necessary. First, encapsulation minimizes the toxic impact and side effects of the drug(s) and nanoparticles. Encapsulation not only reduces the side effects by protecting organs from toxic drugs before reaching the desired location but also maintains a high concentration of the drugs to be released. Second, the magnetic nanoparticles alone can carry and release only a limited number of drug molecules. Thus, to increase the amount of cargo that can be delivered and to enhance the efficacy of controlled drug release by reducing the side effects of these nanoparticles, various stimuli-responsive drug delivery systems have been developed over the decades.[30] These include liposomes, micelles, hydrogels, organic polymers, dendrimers, carbon nanotubes, mesoporous silica nanoparticles, and organic-inorganic hybrid nanoparticles. The internal stimuli have limitations related to precise control of delivery time, location, and dose while external stimulus like light lacks penetration depth, the heat-responsive system can have a risk of tumor metastasis inducement during hyperthermia and ultrasound experiences blockage by bone and air.[30, 49-51] However, magnetic fields provide a suitable platform to overcome limitations discussed above. Magnetic fields are non-invasive, rather harmless, can provide size-dependent localization, and

can be precisely controlled in space and time.[30, 52, 53] In addition, magnetism does not have significant physical interactions with the body, making a more suitable stimulus.

1.4.2 Magneto-liposomes: a state-of-art

Magnetoliposomes simply refer to the drug carrier system where magnetic nanoparticles (more preferably iron oxide nanoparticles) are incorporated in liposomes along with drug molecules to meet the demand for fast and localized drug delivery. This adds a new avenue towards drug release and drug delivery phenomena allowing remote control via magnetic field application. Magnetic nanoparticles can be incorporated into the liposomes at different locations: at the core, in between the lipid bilayers, or the surface-modified liposomal membrane as shown in **Figure 1.4**.[54] Based on the lipophilicity and hydrophilicity, the drug molecules and magnetic nanoparticles are loaded at those sites. The lipid bilayer can entrap lipophilic (hydrophobic) materials while hydrophilic substances are loaded in the aqueous core or at the membrane. Advantageously, both types of substances can be loaded simultaneously in the liposomes. The aqueous core of liposomes is available for loading of hydrophilic magnetic nanoparticles of sizes 5nm or more and loading is easy. However, incorporation of hydrophobic nanoparticles in lipid bilayer is challenging due to the higher tendency of micelle formation, cluster formation, and enhanced passive release.[55, 56] The smaller lipid membrane dimension (~ 6-6.5 nm) requires nanoparticles of smaller size (<5 nm) for successful loading.[57-59] The MNPs loaded liposomes together with drug molecules make a complete carrier system that can be targeted to the desired location and triggered by externally applied magnetic fields to release the drug molecules. It is interesting to note that hydrophilic drug molecules at the core cannot easily pass through the lipid bilayer and the application of external magnetic fields can then be tuned to release the cargo in a controlled manner.

Magnetoliposomes

MNPs located inside   **MNPs located in the bilayer**   **MNPs located outside**
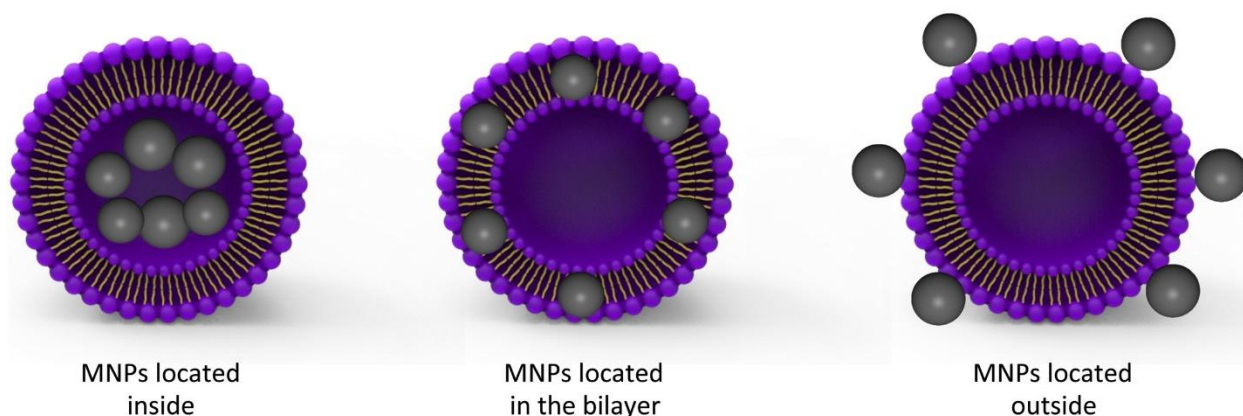
Figure 1.4. Schematic representation of magnetoliposomes with MNPs: (left) entrapped at aqueous core, (center) embedded between the lipid bilayer and (right) attached on the modified membrane.

Various studies have exhibited that magnetoliposomes add versatility in the drug delivery application of liposomes. The literature shows that different types of magnetic fields have been employed for magneto-liposomal drug release. The mechanism of drug release under the application of high or low-frequency AMF involves AC-hyperthermia where the magnetic nanoparticles facilitate the heat transfer from the magnetic field to the liposomes for drug delivery. In an alternating magnetic field, magnetic nanoparticles produce heat through Neel or Brownian relaxation depending on the size of MNPs.[60] This heat can exceed the transition temperature of constituent lipid thereby increasing the permeability of lipid bilayer and significantly enhancing drug release. Besides that, DC magnetic fields and pulsed magnetic fields have also been used for drug release as I will show in this work.

Babincova *et. al.*,[61] demonstrated the AC-hyperthermia-induced release of doxorubicin from magnetoliposomes (with iron oxide entrapped in lipid bilayer). Nobuto *et al.*,[62] used a DC dipole electromagnet with field strength fixed at 0.4 Tesla, on a tumor-bearing limb of a hamster. Doxorubicin-loaded liposomes were then administered, and a magnetic field was applied for about

an hour which led to the increase in dox concentration to 3 to 4-fold at the tumor site. In addition, tumor growth and lung metastases were also suppressed by this dox targeting. Tai *et. al.*,[63] entrapped iron oxide nanoparticles and model drug carboxyfluorescein (CF) in DPPC/Chol based thermosensitive liposomes. Application of alternating magnetic field for 5-25 min significantly released the CF (~60%) from MNPs loaded liposomes compared to the control samples. Nappini *et. al.*,[64] studied large unilamellar liposomes loaded with magnetic cobalt ferrite nanoparticles along with CF. The results showed that the application of low-frequency AMF (0.2-6 kHz) affects the bilayer structure promoting CF release. Salvatore *et. al.*,[65] with magnetoliposomes containing 5nm hydrophobic iron oxide nanoparticles in DPPC lipid bilayer achieved a high drug release percentage on exposure to LF-AMF for 5-15 min. Amstad *et. al.*,[55] incorporated stabilized iron oxide nanoparticles <5.5 nm, into the lipid bilayer and showed that application of AMF enhanced liposomal permeability through local hyperthermia. Despite several therapeutic applications, one serious disadvantage of AC-hyperthermia is that it can destroy certain anti-cancer drugs like SN-38, its prodrug irinotecan,[66] and si-RNA.[67] Guo *et.al.*,[68] demonstrated that magnetoliposomes can be formulated in a way that there is an increase in drug release under low-frequency AC magnetic field without generating hyperthermic effect. In addition, AC magnetic hyperthermia is a slow process usually in the order of a few minutes requiring a significant amount of magnetic particles loaded into liposomes.

Another mechanistic approach of drug release from magnetoliposomes is through the application of pulsed magnetic fields. Nardoni *et. al.*,[69] showed that nonthermal pulsed electromagnetic field (100 micro-Tesla with active pulse duration of 1.3 milliseconds) when exposed to high-transition temperature magnetoliposomes (loaded with hydrophilic iron oxide nanoparticles) for 3 hours, enhances the liposomal permeability without deforming liposomal

integrity. In another work, Podaru *et.al.*,[70] applied short magnetic pulses to release the payload rapidly from magnetoliposomes where ultrasound generated from MNPs increased the membrane permeability to increase drug release.

1.5 Rigid Drug Carriers

Organic drug carriers like liposomes, micelles, etc. are soft materials that have intrinsic unstable nature that often lead to the pre-leakage of drugs. The major drawbacks include limited chemical and mechanical stability, vulnerability to microbiological attacks, swelling, issues with control over the drug release rate, and costlier. Polymer nanoparticles have high polydispersity while dendrimers have a relatively high cost. On the other hand, inorganic carriers possess inherent properties like chemical stability, increased mechanical strength, resistance to biochemical attacks in an in vivo environment. Among inorganic vectors, mesoporous silica systems have been widely used as drug carrier systems due to their numerous benefits.[71-73]

1.5.1 Developments in Mesoporous Silica materials

Pores have been classified as mesopores by IUPAC when their width is between 2 nm and 50 nm.[74] Since the first design of Mobil crystalline material (MCM) in 1992 and the first report of MCM-41 type mesoporous silica in 2001, Mesoporous silica-based drug delivery systems have been explored for a variety of therapeutic agents.[75-78] With the numerous advantageous properties like uniform and tunable pore diameter (2-10 nm), large pore volume ($\geq$1cm^3/g), excellent biocompatibility, low density, and very high specific surface area (>900 m^2/g), amorphous mesoporous silica materials find potential applications in catalysis, as a carrier for drug storage and delivery, gene therapy, and biomedical imaging, etc. Among them, the mesoporous silica shell

with a hollow interior/core can provide higher cargo loading capacity compared to the conventional mesoporous silica systems.[76, 79-82]

Both bulky molecules (like enzymes and drugs) and organic compounds (dyes, pigments, etc.) can be well accommodated in mesoporous silica due to its pore size modulation ability. The guest molecules can be well adsorbed through the processes like cross-linking, covalent binding, encapsulation, and entrapment. Depending upon the pore diameter of porous silica, dimensions, and hydrophilicity/hydrophobicity of biomolecules, the guest molecules can be immobilized in mesoporous silica. Further, silanol groups (Si-OH) present on the mesoporous silica surface may favor the immobilization of organic compounds or the bulky biomolecules, accompanied by electrostatic interactions.[83-87] The number of silanol groups due to its high reactivity, can increase the multifunctionality (by reacting with other functional groups) thus providing an excellent surface modification that enables to control the transportation of different guest molecules to the pores.[88-91] In addition, hollow mesoporous silica spheres can be ingested or injected and present a homogeneous morphology which makes them very useful in drug delivery.[92]

1.5.2 Magnetic Silica Shell Systems

The mesoporous silica lacks the ability to carry cargo to the target locations in the body. To overcome this limitation, these systems can be functionalized by magnetic nanoparticles which helps to guide the drug-loaded silica materials to desired locations inside the body. The magnetic silica nanocomposites can present itself as a strong candidate in drug delivery platform because of two important merits; first, it avoids the direct contact between the magnetic nanoparticles and healthy tissues so that drug toxicity is reduced; second, the colloidal stability of nanoparticles can be well preserved even in the biological environment.[93-96] Moreover, such magnetic composite

carriers can also be utilized for hyperthermia therapy in the presence of an external magnetic field.[97, 98]

Wu *et al.*,[99] first reported the iron oxide-based magnetic mesoporous silica composites in 2004. Since then, various research groups have been involved to fabricate such composite spheres. Magnetic silica composites can be classified into 3 different types based on their structural design:

1. Magnetic silica core-shell structure.

2. Magnetic nanoparticles encapsulated in the channels of mesoporous silica.

3. Rattle-type magnetic core/mesoporous Silica shell spheres.

Since fewer drug molecules are loaded in the mesoporous channels, the first two types of magnetic mesoporous composites have lower drug loading compared to the rattle-type spheres. Rattle-type structures with vast void space and mesoporous shells possess ideal properties like low density and the high specific area, making it a leading new generation drug carrier/delivery system. Both, an interior core, and mesoporous shell provide a platform to functionalize with the desired organic groups, which favors drug loading, targeting, and delivery. In addition, the shell acts as a protective layer that avoids possible drug degradation. These hollow rattle-type structures can be divided into; first, the ordered pore particles, and second, disordered non-oriented particles. One with ordered channels is suitable for diffusion of adsorbed molecules while disordered pores are favorable for controllable and multistage release of drugs.[91, 100-102]

1.6 Actuation via application of magnetic fields

1.6.1 Motion of magnetic nanoparticles under magnetic fields

Most common magnetic nanoparticles such as iron oxide, cobalt ferrite, etc. have the remarkable property of magnetic behavior in presence of static and oscillating/alternating magnetic fields. These magnetic nanoparticles can be used in two ways under the alternating magnetic fields; first, to generate heat at their surroundings, a process known as magnetic hyperthermia. Moderate or significant heating effects can be produced by magnetic nanoparticles when subjected to low or high frequency alternating magnetic fields.[48] In addition to the hyperthermia effect, another important application of alternating magnetic fields on the magnetic nanoparticles is the generation of particle motion. Magnetic field energy can be converted into two types of particle motion, rotational and translational.[103-105] Beside alternating magnetic fields, the magnetic nanoparticle motion can also be achieved from a pulsed magnetic field induced magnetic field gradient.[106]

The discussion here is more focused on the translational motion of a particle under the magnetic field. When an external magnetic field gradient is applied, translational motion of magnetic nanoparticles is achieved in the direction of field gradient, the effect known as magnetophoresis. The magnetic field gradient can be generated using permanent magnets or electromagnets but due to the size constraints, the gradient is lower than one produced by electromagnets. In addition, both homogeneous and inhomogeneous magnetic fields can be used in the process but the magnetostriction effect makes homogeneous magnetic fields less effective. For this reason, an inhomogeneous magnetic field is used in the process (**Figure 1.5**). The particle in an inhomogeneous magnetic field can move from a region of low to high magnetic fields.[105-109]

Inhomogeneous Magnetic Field   **Homogeneous Magnetic Field**
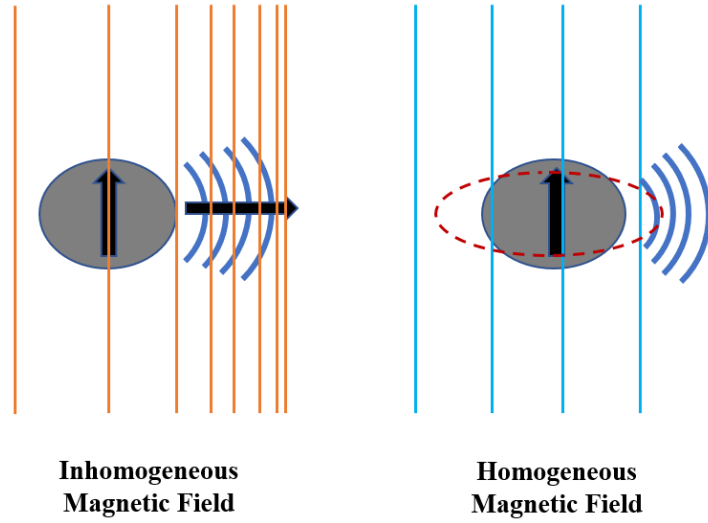
Figure 1.5. *Conceptual difference of magnetic particles in an inhomogeneous and homogeneous magnetic field. Particles experience magnetostriction in a homogeneous magnetic field so an inhomogeneous magnetic field is used in our work.*

Mathematical expression for the forces acting on the magnetic nanoparticle:[105, 107, 109]

Since the gravitational force, Brownian force, forces due to interparticle interaction, and buoyant force, are negligible, two significant forces are acting on the magnetic particle under an external magnetic field. First, the magnetic force, F_m acting on the magnetic particle is,

$$Fm \ = \ \frac{V\,(\Delta\chi)}{\mu 0} \ (\nabla.B)B$$ ………………………….. **Equation 1.1**

where, V is the volume of the magnetic particle, $\Delta\chi$ is the difference between the magnetic susceptibilities of particle and medium, μ_0 = permeability of free space, B and ∇.B are the applied external Magnetic field strength and field gradient respectively.

Second, a force known as fluidic force or viscous drag force, Fv as given by Stoke's law for spherical particles is,

$F_v = -6\pi\eta R(V_p - V_f)$ …………………………. **Equation 1.2**

where η is the viscosity of the medium where particle resides, R is the hydrodynamic radius of the particle, V_p is particle velocity and V_f is the velocity of fluid/medium.

From Newton's law, the velocity of the particle having mass m, under the forces F_m and F_v is,

m dV/dt = F_m - F_v …………………………… **Equation 1.3**

1.6.2 Ultrasound generation from magnetic particles in the presence of magnetic field gradient

The mechanical oscillation of magnetic nanoparticles under the magnetic field gradient can generate ultrasound waves. Experimental studies[105, 106] have revealed that ultrasound can be generated at different frequencies and amplitudes of magnetic field gradients from magnetic nanoparticles. Though AC coils (alternating magnetic field) can also be used for this purpose, the field gradient in a pulsed magnetic field is much larger which in turn can generate strong ultrasound.[106] Both homogeneous and inhomogeneous magnetic fields can produce ultrasound. However, magnetostriction-assisted ultrasound generation using a homogeneous field is less preferred as it leads to the change in the dimension of magnetic particles during magnetization. Thus, it is more desirable to use an inhomogeneous field. In addition, an inhomogeneous magnetic field can achieve translational motion of the magnetic nanoparticles, unlike a homogeneous field.[105, 106, 110] Since the present work also focuses on turning the magnetic field into translational motion of particles, an inhomogeneous field is used as it provides enough force for efficient actuation at the nanoscale.

1.7 Goals of this work

The key challenge in drug delivery is to develop optimal drug carrier systems. Literature suggests that maximum drug release can be achieved from various nano-drug carriers, but it takes significant time to do so. On the other hand, if we try to release the drug rapidly from the carriers in response to external stimuli, only a few percentages of total payload releases at any given application of external stimulus. However, it can be sometimes beneficial to achieve fast drug release in a small portion for two prominent reasons. First, the rate of drug release can be controlled based on the application of external stimuli. Second, the fast release of a drug can reduce the time-dependent degradation of its active moiety. To accomplish this goal, this work focuses on the following aspects of magneto-liposomal and rattle-type silica shell drug carrier systems in this dissertation:

1. We hypothesize that magnetically doped nanoparticles can be prepared with a variety of locations with reference to the liposomes. The preparation of the liposomes with magnetic nanoparticles loaded at the core, bilayer, and surface-modified membrane of liposomes is presented in the next chapter. (**Chapter 2**)

2. We hypothesize that the use of a pulsed magnetic field for the magnetic field actuation from the temporal perspective is more efficient when compared to other forms of the magnetic field-induced release mechanisms. I will present comparative data between the alternating magnetic field and pulsed magnetic field in light of the duty cycle. This is important to establish the advantage of using a pulsed magnetic field to get a short time release over maximum release (**Chapter 2**).

3. We hypothesize that the composition of the liposome and the buffer concentration can have a significant impact on the stability and release efficiency of the magnetoliposomes. I will

present the data on the effect of nanoparticles addition on the transition temperature of liposomes, the role of osmotic pressure in drug release, and thiol-gold interaction to optimize the drug release (**Chapter 3**).

4. We hypothesize that the drug release from magnetoliposomes is more efficient utilizing inhomogeneous magnetic fields than homogeneous magnetic fields. I will show the release of model drugs from magnetoliposomes at different positions of Helmholtz and anti-Helmholtz coils. This will provide the proof of concept of using pulsed magnetic field/ magnetic field gradient to maximize the drug release (**Chapter 4**).

5. We hypothesize that magnetic nanoparticles will release the drugs from magneto-liposomes under the influence of short magnetic pules. I will present data on drug release from magnetoliposomes (with both hydrophilic and hydrophobic MNPs) under the application of each pulse, in a step to achieve a short time release (**Chapter 4**).

6. We hypothesize that the intensity of the magnetic field plays an important role in determining the efficiency of drug delivery. I will present the data to show the role of the intensity of the magnetic field (generated using capacitors with different capacitance) on magneto-liposomal drug release (**Chapter 4**).

7. We hypothesize that the drug delivery can be achieved with not only soft drug delivery carriers such as magnetoliposomes but utilizing hard-sphere rattle cage type magnetically doped silica shells. I will investigate the drug release under a pulsed magnetic field using a rigid drug carrier system, i.e., rattle-type silica core-shell structures (**Chapter 5**).

8. We hypothesize that the drug delivery from magnetic rattle type cage silica shells is impacted by the silica shell's physical characteristics such as the thickness of the silica shell. I will

present the data to show the effect on drug release with varying shell-thickness and size of magnetic core (**Chapter 5**).

9. We hypothesize that in the presence of magnetic nanoparticles, microporation can be induced on the cell membrane using a pulsed magnetic field which can facilitate the transport of small drug molecules into the cells. I will present the data to show the potential application of a pulsed magnetic field to trigger passive molecular transport into cells using a combination of inhomogeneous magnetic fields and magnetic nanoparticles. (**Chapter 6**)

Chapter 2: Experimental Techniques

2.1 General method of synthesis of liposomes/ magneto-liposomes

Liposomes used in this thesis were prepared according to the method described by Podaru *et. al.*,[70] using a thin film hydration method coupled with the extrusion method in sequence. Briefly, chloroform solutions of lipids DPPC and DSPC were mixed in a vial along with cholesterol in a molar ratio of 88:1:10 such that the total lipid mixture was 10 mg. The chloroform was first evaporated from the solution at around 55°C, followed by vacuum evaporation for about an hour. The hydration of thin film of lipid was carried out by adding 1mL of phosphate-buffered saline (1xPBS, prepared by dissolving 4 g of NaCl, 0.1 g of KCl, 0.72 g of Na_2HPO_4, and 0.12 g of KH_2PO_4 in 500 mL of distilled water buffered to pH 7.4). A 100 mM solution of model drug 5(6)-carboxyfluorescein (CF) was prepared in PBS followed by titration with 3M NaOH which gave a dark red solution of dye CF. To load the liposomes with CF, 1 mL of this dark red solution was added to the lipid thin layer instead of pure PBS. After addition, the mixture was vortexed for 5 minutes to help create multilamellar liposomes. Then freeze/thaw process was carried out where the vial containing a sample was placed in a water bath (50°C) for 5 min and then placed in dry ice for 5 min, repeatedly for 10 times such that at the end of the cycle, the sample solution remained in a hot water bath. In the next step, unilamellar liposomes were produced using a process called large unilamellar vesicles by extrusion (LUVET). For this, multilamellar liposomes at 50°C were extruded (Figure 2.1 A) through a 0.2 µm pore diameter polycarbonate filter 11 times, which yielded around 250 nm diameter liposomes, as verified by dynamic light scattering (DLS) measurements. Finally, the non-entrapped free dye was separated by gel filtration chromatography using the Sephadex G-50 size exclusion column (Figure 2.1 B). The liposomes were collected in the first fraction of the column. The DLS measurements (Malvern Zeta-sizer Nano, Malvern

Instruments) showed that the size of liposomes was about 200 nm. The liposomes sample lacking surface modifications and/or without nanoparticles incorporation are called *regular liposomes* throughout this thesis.

A   **B**
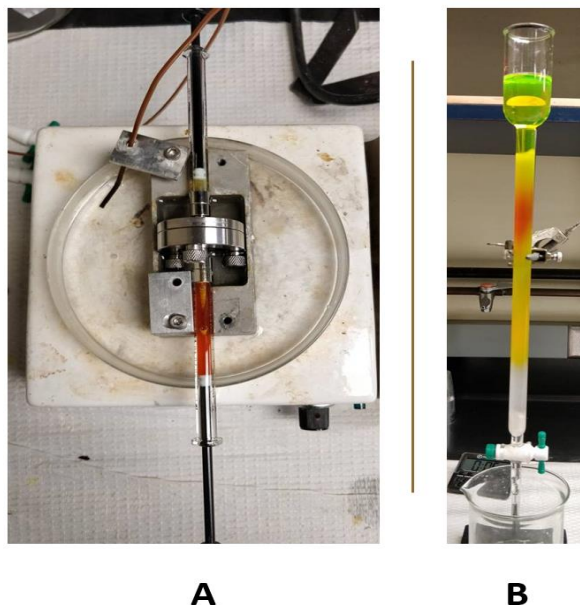
Figure 2.1. *(**A**) Extrusion of liposomes loaded with CF dye and magnetic nanoparticles to create unilamellar liposomes. (**B**) Size-exclusion gel filtration for separation of the free dye and free nanoparticles from magnetoliposomes.*

2.1.1 Surface modified magneto-liposomes

For the liposomes where gold-coated magnetic nanoparticles were intended to attach to the liposomal surface, bifunctional polyethylene glycol (PEG) molecules are used as chemical linkers (Figure 2.2, *Left*). The modified cholesterol, Cholesterol-PEG-SH (Figure 2.2, *Right*) was used instead of regular cholesterol. Here, one end of the PEG molecule is functionalized with cholesterol to facilitate the attachment to lipid bilayer while another end contains thiol (-SH) functional group which provides efficient attachment to the gold. All other steps of liposomal synthesis remain the same as described in section 2.1. This liposomal formulation was used for the surface decoration of liposomes with gold-coated magnetic nanoparticles. These liposomes are denoted as *thiolated liposomes* and their use is described in **chapter 3** in detail.
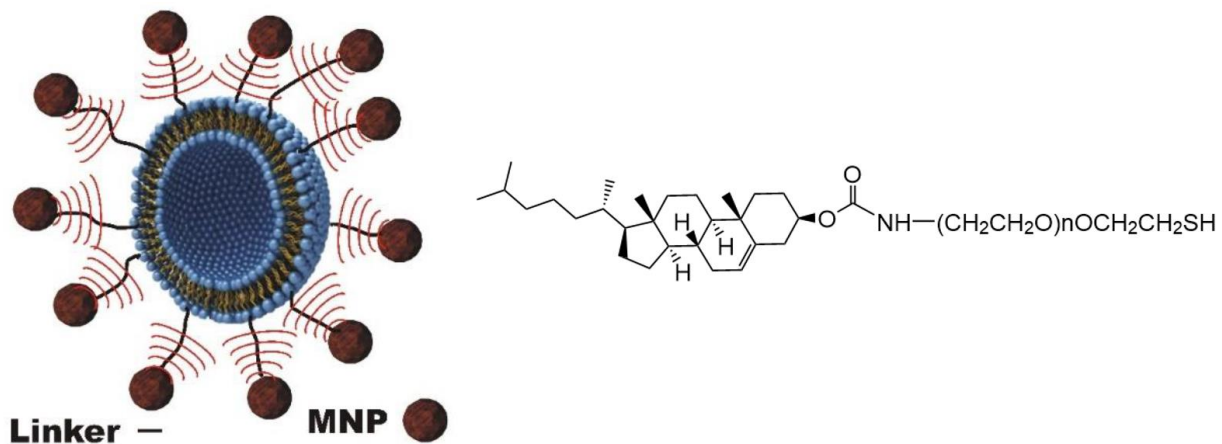
Figure 2.2 (Left) Schematic representation of surface-modified magnetoliposomes using chemical linkers (PEG) to attach magnetic nanoparticles to the liposomal membrane. (Right) Molecular structure of Cholesterol-PEG-SH ligands to link nanoparticles with liposomes.

2.1.2   Liposomes with hydrophilic magnetic nanoparticles at the core

To load the hydrophilic magnetic nanoparticles at the aqueous core, the required magnetic nanoparticles are added during the hydration step of liposomes synthesis along with dye/drug molecules with all other steps remaining the same as described in **section 2.1** above. In our work, 0.5 mL each of dextran-coated iron oxide nanoparticles solution and CF solution (100mM) are added to the thin lipid during hydration step such that a ratio of the number of liposomes to the number of MNPs in average is 1:1. In another sample, the concentration of magnetic particles was increased by four times the original concentration with slow evaporation such that 2mL of nanoparticles solution was reduced to 0.5 mL. Then 0.5 mL of concentrated NPs solution is added along with 0.5 mL of 100 mM CF solution during the hydration step. This results in an approximately 1:4 ratio of a number of liposomes to nanoparticles (at the core) on average. Control samples lack nanoparticles. The four types of samples formed are named control, core (1:1), core (1:4) and bilayer and used in the entire text and graphs in **Chapter 4**.

2.1.3   Liposomes with lipophilic magnetic nanoparticles at the lipid bilayer

For the magnetoliposomes with hydrophobic (lipophilic) magnetic nanoparticles loaded in between the lipid bilayers, the calculated amount of nanoparticles is added in the initial step of liposomes preparation along with chloroform solutions of lipids and cholesterol. The iron oxide nanoparticles (350 µL) dispersed in toluene (i.e., lipophilic MNPs), were added to the phospholipid-cholesterol mixture. This mixture is then heated in a water bath at 55 ℃ to remove the organic solvents for over 3 hours. After the removal of the excess of organic solvent, the vial containing the residual solid is transferred to a vacuum chamber and it is then kept in a vacuum for about an hour to obtain a thin lipid dry film. The lipid film is then hydrated with 1 mL of 50mM CF solution in PBS. The remaining steps for the preparation of liposome sample is same as described in **section 2.1** above.

2.2   Synthesis of Iron-Oxide Core/ Gold shell Nanoparticles

As discussed in section 1.4.1, iron oxide nanoparticles, are the most widely used magnetic nanoparticles in drug carrier systems. From the literature, it is evident that iron oxide nanoparticles synthesized in both organic and aqueous phases can be used as a base material for synthesizing gold-coated NPs.[111, 112] However, the nanoparticles produced in organic phases require further conversion to aqueous phase via phase transfer reactions. For the magneto-liposomes where gold-coated MNPs are directly added to the aqueous surroundings of liposomes and attached to their surface through gold-thiol interactions, it is more suitable to synthesize iron oxide nanoparticles directly in an aqueous phase. Iron oxide nanoparticles are then coated with gold onto their surfaces at room temperature.

2.2.1 Method I: Gold Coating on Commercial Iron Oxide Nanoparticles

Gold coating provides a binding surface for the thiol groups to attach the nanoparticles to the liposomes. The preparation of the gold-coated particles is as follows from commercial iron oxide nanoparticles:- Hydroxylamine hydrochloride ($NH_2OH.HCl$), chloroauric acid trihydrate ($HAuCl_4.3H_2O$), and sodium citrate were purchased from Sigma Aldrich. The coating of the iron oxide nanoparticles was carried out as described by Lyon *et.al.*,[112] with slight modifications. The reaction took place at room temperature by mixing reagents. Commercial iron oxide NPs (Fe_3O_4, 99.5+%, 15–20 nm, 20% W in water) were diluted to the concentration of 4.1675 g/L. For gold coating, the iron oxide NPs and sodium citrate solutions were taken in a 2:1 volume ratio, i.e., 11.7 mL of diluted iron oxide NPs and 5.35 mL of 0.1 M sodium citrate solution were mixed. The mixture was diluted by adding 100 mL of water and stirred for 15 min. Then 535 µL of 0.2 M $NH_2OH.HCl$ and 445 µL of 0.127 M $HAuCl_4.3H_2O$ were added and stirred. The gradual change in the color of the solution to pink indicated the presence of reduced gold (**Figure 2.3 A**).

2.2.2   Method II: Gold Coating on Lab Synthesized Iron Oxide Nanoparticles

(A) Synthesis of iron oxide nanoparticles

Chemicals required for the synthesis, hexahydrate ferric chloride ($FeCl_3.6H_2O$), tetrahydrate ferrous chloride ($FeCl_2.4H_2O$), sodium hydroxide (NaOH), hydrochloric acid (HCl), nitric acid (HNO_3), and tetramethylammonium hydroxide (TMAOH) were purchased from Sigma Aldrich and used without further purifications. The Fe_3O_4 nanoparticles (cores) were prepared by co-precipitation of Fe (II) and Fe (III) chlorides (Fe(II)/Fe(III) ratio is 0.5) in an alkaline solution by the method of Lyon *et.al.*,[112] with modifications. Briefly, 4.595 g of Fe (III) chloride and 1.71 g of Fe (II) chloride were dissolved in 20 mL of distilled water in the presence of 100 mL of 2M HCl.

The solution was then vigorously stirred until the dissolution of Fe salts. Subsequent dropwise addition of a solution of 2M NaOH into the mixture with vigorous stirring, resulted in a pale-yellow solution which changed to brown and finally to dark black over time. The black precipitate was collected on a 3000 Gauss permanent magnet, washed twice with H_2O and once with 0.1M TMAOH then isolated via centrifugation. The precipitate from above was washed in 0.01M HNO_3 to obtain oxidized Fe_3O_4 nanoparticles. The particles were then dissolved in 0.01M HNO_3 and heated at 65 °C with stirring until the solution developed a brown color. The oxidized Fe_3O_4 nanoparticles were suspended in 0.1M TMAOH after washing with distilled water.

(B) Preparation of Au-Fe oxide composite nanoparticles

Au-shell was coated on the iron oxide nanoparticles according to the boiling citrate seeding procedure reported by Brown *et al.*,[113] with slight modifications. First, 3 mL of the 0.212 mM $N(CH_3)_4$-stabilized, oxidized Fe_3O_4 stock solution was diluted with 6 mL of 0.01M sodium citrate and stirred for 30 min to exchange absorbed OH^- with citrate ions to make the final working magnetic-core solution. Again, 1 mL of this solution was diluted with 3 mL of 0.01 M sodium citrate solution. The reaction solution containing magnetic cores and reduction agent was first sonicated for 15 min and then heated to 65 °C while vigorously stirring the solution. One milliliter of the solution of $HAuCl_4$ was added as soon as the solution reached 65 °C, and after 15 min of addition of Au^{3+} salts (10 mM solution of $HAuCl_4$), the heating was stopped. However, stirring was continued till the solution cooled to room temperature. At this stage, a dark red/purple solution of gold-coated iron oxide nanoparticles was obtained (**Figure 2.3 B**).
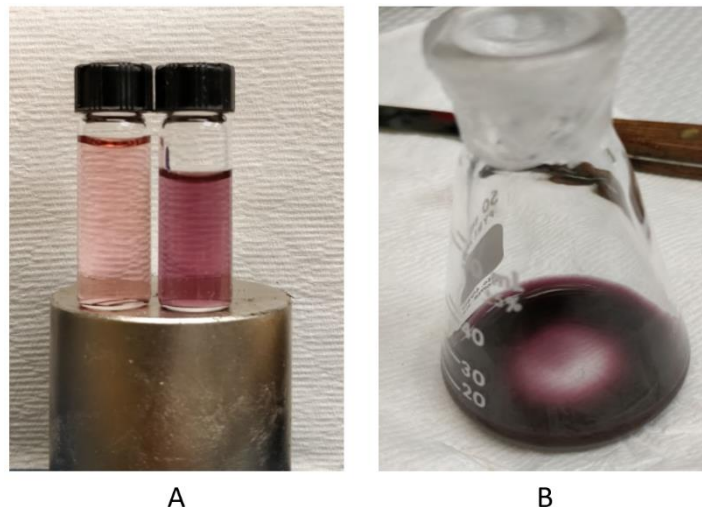
Figure 2.3. *(A) The gold coating on commercial Iron oxide nanoparticles. (B) Gold-coated sample of lab synthesized iron oxide nanoparticles.*

2.3 Preparation of rattle-type Fe$_3$O$_4$@SiO$_2$ hollow microspheres:

The samples of non-magnetic (uncalcined) Fe$_2$O$_3$@*SiO$_2$* samples were obtained from our collaborator Dr. Yongqiang Wang at Henan University, China. The Rattle-type Fe$_3$O$_4$@SiO$_2$ hollow microspheres can be prepared by the method described by L. Cheng *et al.*[114] Here, a template etching route is used to synthesize the rattle-type Fe$_3$O$_4$@SiO$_2$ hollow microspheres with desired shell thickness and void space, where uniform Fe$_2$O$_3$ microspheres are used as a template. The synthesis involves the following scheme:
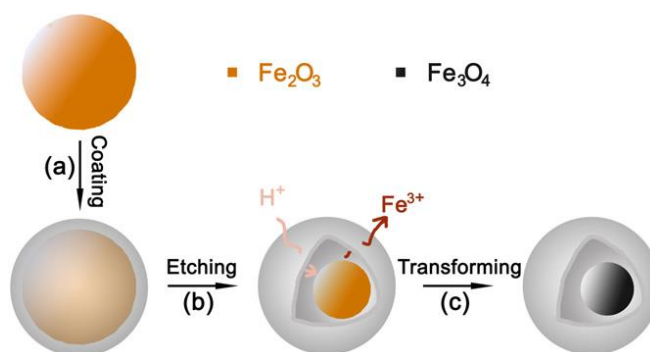
Figure 2.4. *Schematic illustration of the template-etching route for uniform rattle-type Fe$_3$O$_4$@SiO$_2$ hollow microspheres. [From Reference 114]*

31

First, *Fe₂O₃* microspheres were prepared through a hydrothermal reaction. Using these microspheres as a template, the mesoporous silica shell was coated through a sol-gel method using tetraethyl orthosilicate precursor to form *Fe₂O₃@SiO₂*. After that, *Fe₂O₃@SiO₂* core-shell microspheres were etched by HCl solution. Etching with the acid solution created a void between a core and the shell and rattle-type *Fe₂O₃@SiO₂* core-shell particles are obtained. It has to be noted that etching time and concentration control the core size. Finally, rattle-type $Fe_3O_4@SiO_2$ hollow microspheres were obtained after heating the particles (rattle-type *Fe₂O₃@SiO₂* core-shell particles obtained from our collaborator) in reducing atmospheres. For this, the sample when calcined in 4% H_2/92% N_2 at 400 °C for 4 hours, black powder was obtained as a final product which was finally collected by a magnet. In our work, four samples of rattle-type silica shells have been synthesized with different effective volumes, magnetic core sizes, and shell thickness. High-Resolution TEM was used to determine the size and morphology of synthesized rattle-type silica shell samples with varying core sizes. The detail of the work is discussed in **Chapter 5**.

2.4   Homogeneous and Inhomogeneous magnetic fields

There are two main types of magnets constructed for the experiments to explore the use of inhomogeneous and homogeneous magnetic fields for drug delivery (**Figure 2.5**). While both magnets produce inhomogeneous and homogeneous magnetic fields in different amounts, which allows testing drug delivery efficiencies how they depend on the various magnetic field types when combined with magnetic field calculations. First, the Helmholtz coil consists of a pair of coils arranged in a way that the magnetic field is additive resulting in a quasi-homogeneous magnetic field at the center of the magnet. The length of the magnet is 48 mm with an 8 mm spacer in the middle. The electromagnetic coil consists of a notched copper disc laser cut from its material

combined with insulator discs and stacked together to produce a helical coil similar to the construction of bitter coils used at the National High Magnetic Field facility. This arrangement facilitates efficient transfer of high-frequency current with minimal heating and mechanical problems.
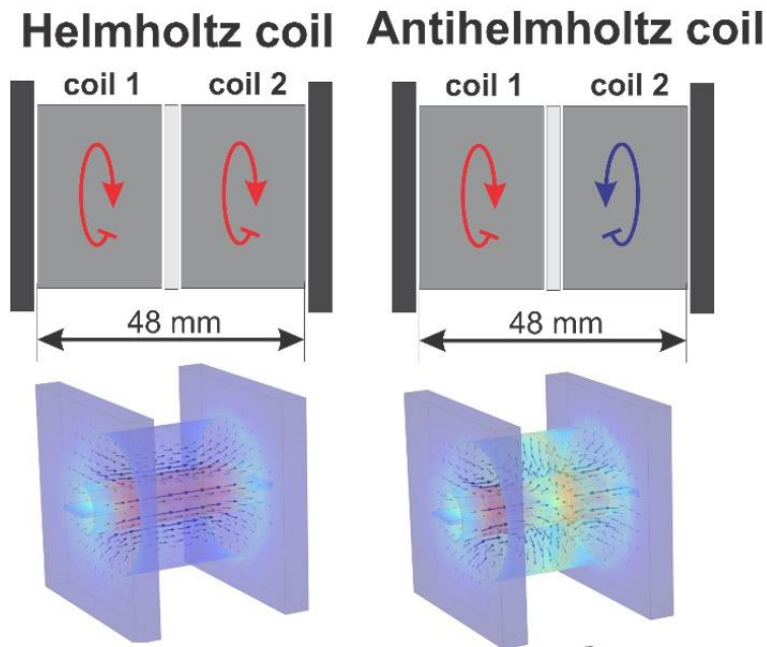
Figure 2.5. Types of coils used in the generation of the pulsed magnetic fields.

Time-varying current on the order of a few tens of thousands of amperes is passed through the coil resulting in time-dependent magnetic pulses, which are delivered to the magnet every 20 seconds from the power source. The current is controlled by the size of capacitor and the voltage charge on the capacitor. In the Anti-Helmholtz coil, the direction of the coil pair is opposing so the magnetic fields in the individual coils oppose each other resulting in the large spatial variation of the magnetic field inside the coil. As the COMSOL calculation shows the B field distribution inside the coil at its peak current level (**Figure 2.6**), the main difference is that the Helmholtz coil produces an intense magnetic field in the center of the coil without too much magnetic field

gradient, while the Anti-Helmholtz coil produces intense magnetic field gradient with minimal peak magnetic fields due to cancellation of the magnetic field components from the coil pair. Please, note that both coil types have a strong magnetic field gradient at the edge of the coils. Product of magnetic field and magnetic field gradient values (**Figure 2.6 C**) is maximum at the edges and minimum at the center of the Helmholtz coil. However, this is different in case of anti-Helmholtz coil where the values are minimum at the center, maximum at near 10 mm from center and again minimum at 16 mm from the center of coil (**Figure 2.6 (C)** red curve).

(A)   **B Field**

(B)   **B Field Gradient**

(C) Product of B Field and B Field Gradient
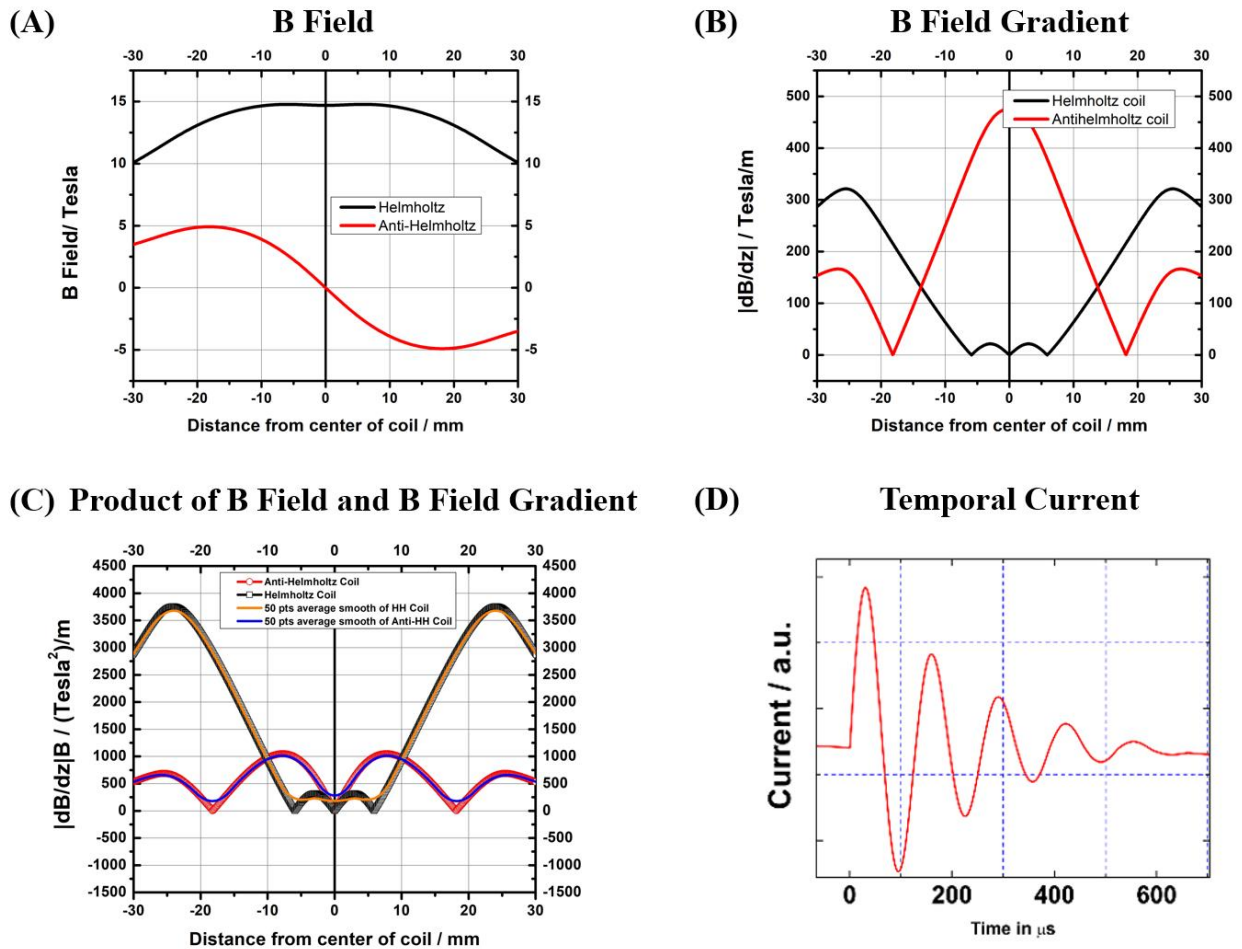
(D)   **Temporal Current**

Figure 2.6 *Graphical representation of (A) B-Field,(B) B-Gradient, (C) Product of B-Field and its gradient and (D) Temporal current in Helmholtz and Anti-Helmholtz coils inside the coil.*

2.5 Description of pulsed magnetic field for ultrasound generation

The pulsed magnetic field was generated as described in detail by Podaru *et. al.*[106] Briefly, the inhomogeneous magnetic field was generated with the help of a pulsed power delivery system, which can produce approximately 40,000 amps current in an external circuit in a short amount of time. The current source when turned on with the help of a triggering switch, resulted in an oscillating current in the RLC circuit (circuit consisting of a resistor, an inductor, and a capacitor) producing approximately 200 μsec inhomogeneous magnetic pulses inside the anti-Helmholtz coil. Inside the coil, the off-center measured peak magnetic field amplitude was approximately 5 Tesla. The magnetic pulses were applied every 20 s which allowed recharging of the capacitor. The arrangement of a couple of coils in an anti-Helmholtz coil allows the production of opposing magnetic fields in each coil so that a large magnetic field gradient (~800 T/m) can be produced at the center of the coil, but zero magnetic field amplitude. This magnetic field gradient is responsible for creating translational motion of the iron oxide nanoparticles in the magneto liposomes, which results in the generation of ultrasonic waves. The inhomogeneous magnetic field is used in the experiment, as the homogeneous magnetic field generating ultrasound via magnetostriction is less efficient. The magnet was integrated with an automatic sample handling system to lower the small amount of sample into the magnet and to then transfer the sample to a temperature-controlled metal block integrated with a fluorescence probe (**Figure 2.7**). This automatic delivery system provided excellent repeatability in the experiments. This device allowed us to obtain photoluminescence (PL) measurements and expose the sample to inhomogeneous magnetic pulses with excellent reproducibility.
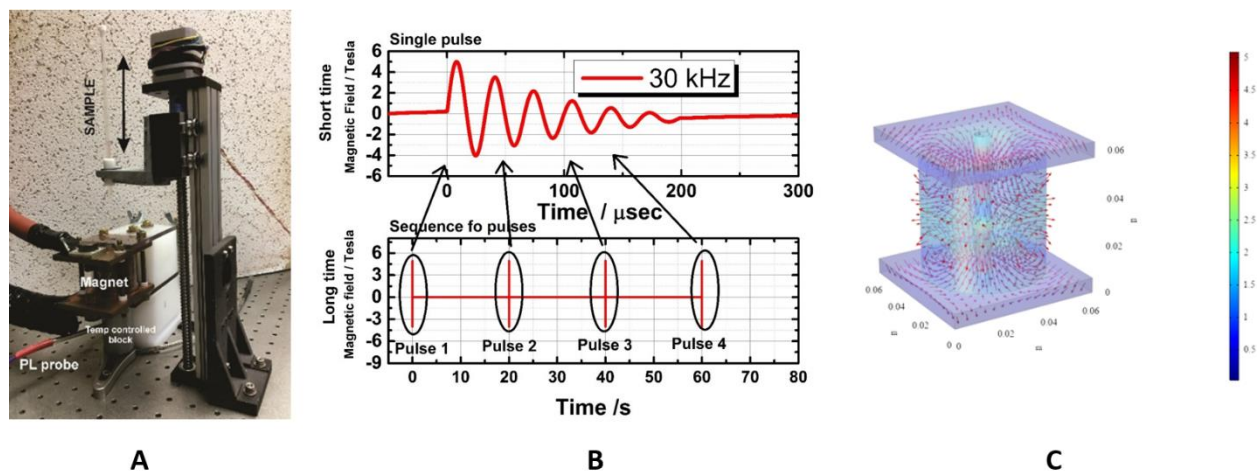
Figure 2.7. *Integrated pulsed magnetic field and temperature-dependent PL measurement system. (**A**) For magnetic field exposure, the sample was lowered into a temperature-controlled metal block. PL was monitored with the help of a Raman fluorescence probe. (**B**) The upper graph shows the magnetic pulse in one of the coils of the anti-Helmholtz coil pair and the graph below shows the sequence of the magnetic pulses as they are applied. (**C**) The magnetic vector field inside the coil modeled with COMSOL multi-physics software. The scale bar shows the intensity of the magnetic field in Tesla. The sample was placed in the center of this magnet where the magnetic field was zero, but the magnetic field gradient was large (~800 Tesla/m) The sample with a small sample volume was placed in the center of the coil for the experiments.*

2.6 Carboxyfluorescein permeability assay

The encapsulated carboxyfluorescein (CF) dye from the liposomal core was monitored by fluorescence measurement. When carboxyfluorescein is strongly packed inside the liposomes, the fluorescence of this dye is self-quenched, resulting in little fluorescence. Once the dye has been released from the liposomes, its fluorescence strongly increases, which can be used to characterize the amount of drug released from liposomes. A fraction of the liposome sample obtained from a column separation was diluted 10 times from the original (200 µL diluted to the total volume of 2 mL), with distilled water (*see Appendix A, supporting information for the concentration of liposomes per sample*). In the next step, magnetic nanoparticles were added to the diluted liposome

solution. Then 200 µL of the sample was taken in an NMR tube and kept in a cylindrical hollow loop, as shown in **Figure 2.7 (A)** above. The delay stage helps to raise and lower the sample tube as needed and is controlled by LabVIEW software written for this purpose. Initially, the background fluorescence of the sample was measured, before applying magnetic pulses. The sample tube was then raised to the center of anti-Helmholtz coils where the magnetic field gradient was maximal. Exactly 20 pulses were applied to the sample and the sample was then lowered to measure the fluorescence. After measuring post magnetic pulse fluorescence, the sample was subjected to a thermal cycle, where temperature gradually increased at the rate of 0.1 °C/10 sec, with the help of a metal jacket connected to the temperature controller. Fluorescence data were recorded after the completion of a thermal cycle (increased from initial 25 °C to 65 °C and cooled back to 25 °C). Liposomes were fully lysed when heated to 65 °C, thereby releasing all the dyes enclosed at the core. Figures A1 and A2 in the supporting information (Appendix A) show that all the samples have fairly comparable CF encapsulation and release. This provides strong evidence of the reproducibility of the CF permeability assay described here. The CF release is measured as a factor of,

$$\text{Release factor of CF (fmax)} = \frac{\text{total fluorescence after thermal cycle}}{\text{initial background fluorescence}} \qquad \ldots\ldots\ldots\ldots \textbf{Equation 2.1}$$

For photoluminescence intensity percentage change,

$$\%\text{PL intensity change} = 100\frac{f_d/f_i - 1}{f_{max} - 1} \qquad \ldots\ldots\ldots\ldots.. \textbf{Equation 2.2}$$

Where,

    f_d = fluorescence data points

    f_i = initial background fluorescence data points

    f_{max} = maximum value of fluorescence release factor

1st fluorescence data point/initial background fluorescence = 1 (normalized).

Once the % PL intensity change is measured at each temperature from 25 °C to 65 °C range, a

plot for CF permeability assay looks like the figure below (**Figure 2.8**).
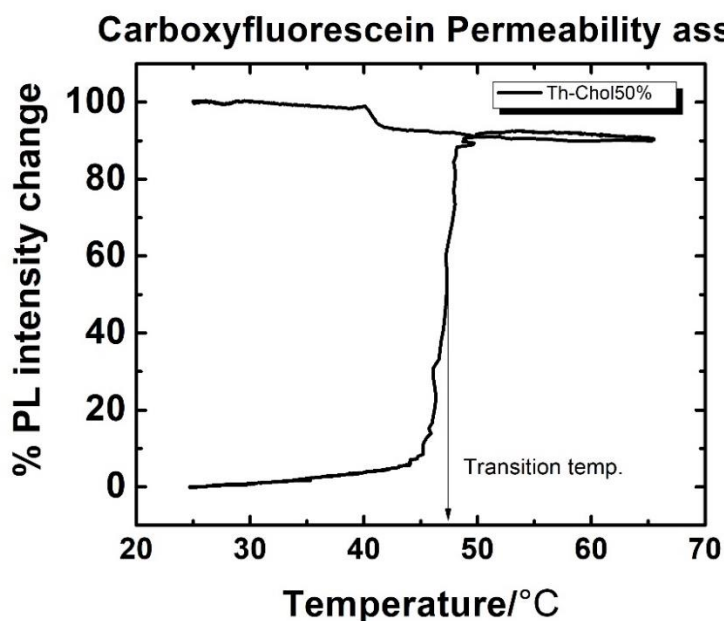
Figure 2.8. Typical PL curve of the liposomes loaded with CF. The PL slowly increases with temperature as the CF starts leaking out from the liposomes. When the temperature reaches the transition temperature of the liposomes, it releases its load. When the heated sample undergoes cooling, the PL will gradually increase till room temperature is reached again. The initial and final PL provides the measuring stick for the amount of drug released from the liposomes!

2.7 Doxorubicin loading and release assay from rattle type silica shell

Doxorubicin is loaded in the rattle-type silica shell structures, following the method described by

L. Cheng *et al*.,[114] with slight modifications. Briefly, 0.2 mg/mL aqueous solution of Doxorubicin

was prepared, and the rattle-type silica shell sample was added to the solution in a ratio of 1 mg

sample per mL DOX solution in a glass vial. The mixture was then kept in a shaker (OS-20) for

24 hours in dark conditions. The DOX-loaded silica shell samples were collected by a magnet, washed three times with deionized water to remove the unloaded drug molecules, and finally dried at room temperature.

For release, the sample was first added into the PBS solution in an NMR tube. The change in fluorescence intensity of doxorubicin was measured using a Raman probe. The background fluorescence of a sample was measured and then a pulsed magnetic field was applied for several cycles at 37 °C. The release of doxorubicin (after application of pulses) was measured until no significant change in fluorescence intensity of the solution was observed. When the release curve saturated signifying no further release, the fluorescence intensity at this point was taken as maximum release to calculate the percentage DOX release. During the experiment, three different sets of measurements were carried out for each sample; first without any pulses (control) to observe passive release, second; set of 10 pulses each hour up to 6 hours, and third, 60 pulses at the beginning.

It is important to note that though the pulses applied are very short (microsecond scale) the observed release of the drug molecules from silica shells take a longer time. This is not because the pulses are less efficient instead the diffusion of drug molecules throughout the supernatant solution take considerably longer time. Once the magnetic pulses are applied, the drug molecules are pushed outward through mesoporous channels of the silica shells. To measure the fluorescence of doxorubicin released, the doxorubicin molecules have to be homogeneously dispersed throughout the PBS solution (**Figure 2.9**). This requirement results in the significant increase in the time for observed release. The actual release time from the samples is however much shorter.
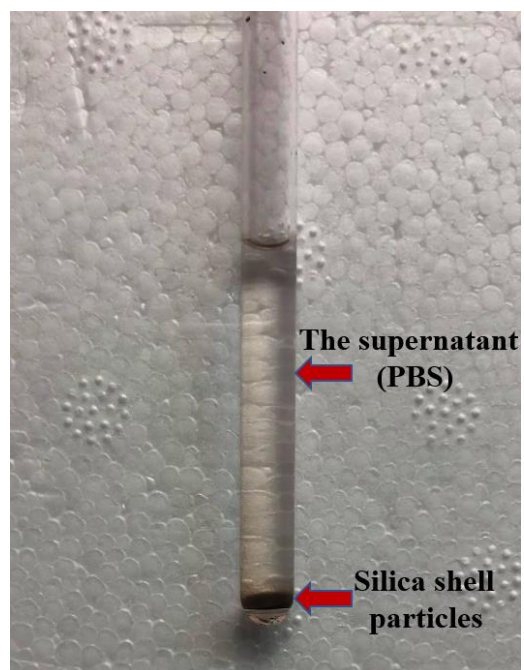
Figure 2.9*. The tube with silica shell samples settled at the bottom. Doxorubicin released after the application of magnetic pulses need to be dispersed throughout the supernatant above the samples.*

Chapter 3 - Pulsed magnetic fields induced drug release from gold-coated magnetic nanoparticles decorated liposomes.

3.1 Introduction

Liposomes are widely established, clinically approved, nano-sized lipid vesicles used as drug delivery agents.[115, 116] Their flexibility in size and composition,[117] biocompatibility, suitability for both hydrophilic and hydrophobic drugs, and more stability than other lipid vesicles, make them applicable in biomedical research fields.[64, 115-118] Compared to other lipid vesicles, the use of liposomes is more advantageous due to their ability to load hydrophilic molecules in their aqueous cores[119, 120] and hydrophobic ones in their bilayers.[118, 121] In addition, the bilayer permeability does not allow the dissolved hydrophilic molecules at aqueous lumen to easily pass through the bilayer, which makes it an efficient drug carrier.[118-121] The liposomes release drug/payload via passive or active stimuli.[55, 121, 122] Several active stimuli such as changes in temperature[122-124] magnetic fields,[55] pH,[124, 125] light,[126] ultrasound,[44] and radiofrequency[127] have been used to trigger liposomes.

The incorporation of magnetic nanoparticles (MNPs) like iron-oxide nanoparticles (IONPs) adds a new dimension to the drug release process, allowing remote control via magnetic fields.[55] In most cases, MNPs are encapsulated in an aqueous core along with drug molecules, and the entire magneto-liposomal system is exposed to an alternating magnetic field (AMF),[63, 69] which triggers the drug release by the process of magnetic hyperthermia.[128] Under the action of an AMF,

MNPs like IONPs generate heat which elevates the temperature of the liposomes above the transition temperatures (Tm) of the constituent lipids.[63, 123, 128] This phenomenon not only facilitates the thermal disruption of the lipid bilayer to release the payload at the desired site but also eliminates unhealthy tissues through a thermal ablation.[55, 63, 123, 128, 129] The challenge is that the magnetic hyperthermia triggered delivery is slow concerning some important physiological processes (blood circulation) or to the lifetime of some thermo-sensitive drug molecules. Faster triggering could benefit this field by expanding the applications of liposomal drug delivery systems. Considering liposome preparation, the lipid composition can be chosen so that its transition temperature is near to 37 °C (normal human body temperature), but it may lead to the leakage of the drug before reaching its target site. On the other hand, the release is slow and inefficient if the transition temperature of the liposome is higher than the body temperature.[55, 64, 123, 128] The requirement of using strong, continuous, high-frequency magnetic fields make this approach challenging in the biomedical field.[129-131]

Liposomal drug delivery systems when induced ultrasonically, provide a faster drug release mechanism.[132] Studies focused on ultrasound triggering have revealed that pressure waves involved in ultrasound mechanically disrupt the lipid bilayer that increases the permeability of liposomal membrane leading to the drug release.[132, 133] This methodology is non-invasive, and ultrasound has a reasonable penetration depth of soft tissue, making it a powerful tool for triggered drug release.[134] Studies have revealed that low-frequency ultrasound imparts only the mechanical effect which is connected with cavitation while high-frequency ultrasound can induce both thermal and mechanical effects.[132-134] To elevate the system at an appropriate temperature, high-frequency ultrasound requires a very high intensity of ultrasound power (1–100 W/cm^2) that may not only impact liposomal drug delivery vehicles but healthy tissue as well.[132, 134]

In the presence of high-frequency inhomogeneous magnetic fields, colloidal magnetic nanoparticles can emit ultrasonic waves.[135] The magnetic nanoparticles used as sonosensitizers for ultrasound generation have significantly enhanced their effectiveness for sonodynamic applications,[106, 135, 136] due to the high penetration depths of inhomogeneous magnetic fields compared to that of conventional ultrasound applications. In effect, the combination of a magnetic field and the use of magnetic nanoparticles allows spatial focusing by concentrating the ultrasound at the nanoscale. In liposomal drug delivery systems, mechanical disruption of the lipid bilayer via pulsed magnetic field-generated ultrasound has been proven effective for rapid (microseconds and milliseconds) and controlled release over traditional thermal (seconds and minutes) disruption of the bilayer of the liposomes. Ultrasound generation from MNPs in inhomogeneous magnetic fields is more effective than a generation from homogeneous magnetic fields because the latter has an additional effect called the magnetostriction effect.[106, 110, 137] Please, note that diamagnetic materials (liposomes, water, drugs) also respond to magnetic fields but to a lesser extent so the use and location of magnetic nanoparticles are critical to magnifying the impact of the mechanical waves in biological applications.

In the previous works,[63, 69, 70, 121, 128] the magnetic nanoparticles were loaded at the interior (either at the core or within the bilayer) of the liposomal drug delivery systems. Though this approach provides a fairly simple and robust way to combine the drug and the trigger, a competition between the drug and the triggering nanoparticles (NPs) for the space inside the liposome is its major drawback. The present work has two important novelties to enhance the efficiency of drug release. First, the magnetic nanoparticles have been moved outside the liposomes in their vicinity by using a chemical linker (**Figure 3.1 A**; the chemical linker used here is a PEGylated cholesterol with one end modified with a thiol (-SH) group) instead of

encapsulating them at the aqueous cores of liposomes or in the bilayers of the respective liposomes. The relocation of the triggering particles provides more volume for drug encapsulation and the lack of competition between drug molecules and MNPs increases the drug release efficiency. A second less obvious advantage is that the drug release efficiency/trigger will be larger for a typical liposome (≈200 nm in diameter). Based on geometric factors, with calculations, one can show that the theoretical drug release would be higher per nanoparticle for a typical liposome, drug, NP formulation (200 nm, 1 nm, 20 nm), as shown in **Figure 3.1 B**. To provide a stable interaction of the liposome and magnetic NPs, a thin gold coating is applied on the iron oxide nanoparticles which adds the versatility of magneto-liposomes. Here, iron oxide NPs are used as the source for ultrasound generation on exposure to a pulsed magnetic field while a gold coating provides efficient linking with the thiol (–SH) group present in the liposomal surface as sulfur–gold bond enthalpy is approximately 200 KJ/mol.[138]
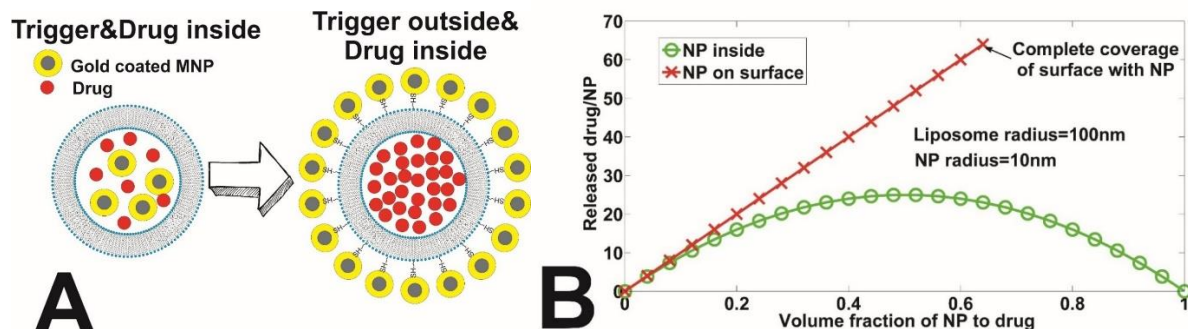
Figure 3.1. (A) Cholesterol–PEG–SH ligands to link nanoparticles with liposomes. (B) Calculated drug delivery efficiency as a fraction of Nanoparticle (NP) to the drug for the two different compositions shown in (A). In this calculation, the triggering magnetic NP is assumed to be 10 nm in radius and the liposome as a radius of 100 nm.

3.1.1 The Role of Magnetic Field Duration in Triggering Magnetic Fields in Magneto-liposome Experiments

In the past few decades, several magneto liposome formulations and experimental approaches have been used, which makes a comparison of these experiments difficult from the basic physical

chemistry standpoint. **Table 3.1** provides a comparison of the various experimental data from the literature. To provide a new perspective on existing data of magneto liposome experiments, the drug release efficiencies were normalized to the duration of magnetic fields used. First, one can define the duty cycle of the magnet which will serve as a normalization factor for **Table 3.1**. A duty cycle D is a fraction of a period during which a signal remains active. It is mathematically expressed in percentage or a ratio by,

$$D = \frac{\text{Pulse Width (PW)}}{\text{Total period of signal (T)}} * 100\%$$ …………. **Equation 3.1**

Table 3.1. *Comparison of normalized efficiencies of magneto liposomal drug delivery systems from literature. The data show that pulsed magnetic field-induced release is more effective than other techniques when the unit time release is concerned.*

Ref.	Liposome/NP formulation	Trigger Location	Max. Release(%)	Application time (min)	Duty cycle	Magnetic field(mT)	Unit time (%Release/s)
121	PC/CoFe$_2$O$_4$	Bilayer	90	50	100	330	0.03
55	DSPC/PEG/IONPS	Bilayer	180	30	100	-	0.1
128	MPPC/SPION	Bilayer	90	6	100	94.5	0.25
69	HSPC/Fe$_3$O$_4$	Core	20	180	9.77	1.5	0.00185
70	DPPC/FePt	Core	8.4	3.3E-5	0.001	3000	248,000

In magnetic pulses applications, D varies from lower values (<1%) in pulsed magnetic fields to as high as 100% for alternating current magnetic fields (AC-MF). The key reason is purely

technological, which makes it easily produce transient intense magnetic fields or lower amplitude continuous magnetic fields. Alternating current magnetic fields (AC-MF) typically have 100% duty cycles, whereas in a pulsed magnetic field, pulses are triggered in an interval of a few seconds and the time of each pulse oscillation is in the microsecond range. In this work, magnetic pulses are triggered in every 20 seconds, and each pulse has a 200 µs oscillation time which gives a 0.001% duty cycle, becoming 10,000 times more efficient than normal AC-MF. Since the time of application in pulsed MF is in order of microseconds compared to minutes in AC-MF hyperthermia processes, pulsed MF is far more advantageous than AC-MF. In addition, the field intensity in pulsed MF is in Tesla compared to the milli-Tesla scale in AC-MF.

3.2 Materials and Methods

3.2.1 Chemicals

The lipids and the regular cholesterol required for the liposome preparation were purchased from Avanti Polar Lipids (Alabaster, AL). Lipids used in the liposome preparation were I) 1,2-dipalmitoyl-sn-glycero-3-phosphocholine (DPPC, MW = 734.05) and II) 1,2-distearoyl-sn-glycero-3-phosphocholine (DSPC, MW = 790.16). Two different types of cholesterol were used in the experiments: regular cholesterol and cholesterol–PEG–SH. The latter was purchased from Nanocs Inc. (New York, NY, USA). Other chemicals and gold nanoparticles (40 nm gold NPs and 50 nm magnetic gold NPS were purchased from Sigma Aldrich). Commercial iron oxide NP (Fe_3O_4, 99.5 + %, 15–20 nm, 20% W in water) samples were purchased from US Research Nanomaterials Inc. (Houston, TX, USA). Syringes required for the extrusion of liposomes (1 mL, Model 1001 TLL SYR) were purchased from Hamilton Robotics (Reno, NV, USA). Polycarbonate filters (25 mm diameter, 0.2 µm pore size) were purchased from Spi Supplies (West Chester, PA, USA).

3.2.2 Preparation of liposomes, synthesis of Iron oxide core/gold shell nanoparticles, generation of pulsed magnetic field and carboxyfluorescein permeability assay

The method of liposomes preparation is given in **section 2.1** of this dissertation. *Figure B1 in supporting information (Appendix B)* shows the graph for the size distribution of liposomes, obtained from DLS measurement. The average diameter of liposomes was 192.5 nm and the polydispersity index, PDI, was 0.139.

The details of iron oxide nanoparticles synthesis and procedure of gold coating to form Iron oxide core/ Au-shell magnetic nanoparticles are given in **section 2.2 (Chapter 2)**.

In **section 2.5** (**Chapter 2**) of this dissertation, a description of the method for a pulsed magnetic field generation is provided.

Also, a method for release study i.e., Carboxyfluorescein permeability assay is discussed in **section 2.6 (Chapter 2).**

3.3 Results

3.3.1 Characterization of Nanoparticles

Elemental analysis of samples of nanoparticles shows that the synthesized iron oxide nanoparticles (Table 3.2) have a percentage ratio of atoms Fe:O equal to 1:1.64 which is nearly 1.5. That suggests the particles formed are possibly Fe_2O_3 nanoparticles. However, the EDX alone cannot confirm the formation of Fe_2O_3. Based on the procedure discussed in the methods section, the particles are further oxidized so they can also be Fe_3O_4. Nevertheless, the particles are iron oxide, as revealed by EDX data. The presence of carbon in Table 3.2 and a carbon peak in *Figure B2 (see the supporting information, Appendix B)*, is due to the tetramethylammonium hydroxide (TMAOH) used as a suspension medium for synthesized iron oxide nanoparticles.

Table 3.2. *Elemental analysis of synthesized iron oxide nanoparticles.*

Element	Weight %	Atomic %	Uncertainty %	Detector Correction
C	77.87	90.10	1.32	0.28
O	7.08	6.15	0.33	0.51
Fe	15.04	3.74	0.33	0.99

The elemental analysis of gold-coated samples in Tables 3.3 and 3.4 show that the gold coating on commercial iron oxide nanoparticles has smaller Au ratios to gold-coated on synthesized iron oxide nanoparticles. The lesser the ratio of gold, the lesser the dead mass for a magnetic particle. This is supported by the percentage release data shown in Tables 3.5 and 3.6, which reveals that gold-coated commercial iron oxide samples are more efficient at carboxy-fluorescein (CF) release. The EDX spectrum images of different types of nanoparticles are included in supporting information *(see Figures B3&B4, Appendix B).*

Table 3.3. *Elemental analysis of gold-coated synthetic iron-oxide nanoparticles.*

Element	Weight %	Atomic %	Uncertainty %	Detector Correction
O	22.60	76.61	2.73	0.51
Fe	2.98	2.89	1.38	0.99
Au	74.41	20.48	5.78	0.99

Table 3.4. *Elemental analysis of gold-coated commercial iron-oxide nanoparticles.*

Element	Weight %	Atomic %	Uncertainty %	Detector Correction
O	23.36	75.79	1.10	0.51
Fe	6.02	5.59	0.50	0.99
Au	70.60	18.60	2.40	0.99

The transmission electron microscopy (TEM) images of the nanoparticles used in this work are shown in Figure 3.2. Figure 3.2A has TEM images for commercial iron oxide nanoparticles (Fe_3O_4) obtained from the website of US Research Nanomaterials Inc. The size of the particles is

between 15 and 20 nm as mentioned on the website of the manufacturer. Figure 3.2B shows the

distribution of synthetic iron oxide nanoparticles. Figure 3.2 C&D represents the gold-coated

samples for commercial and synthesized iron oxide nanoparticles, respectively. The TEM images

show the homogeneity and uniformity in size of "in-house made" nanoparticles.
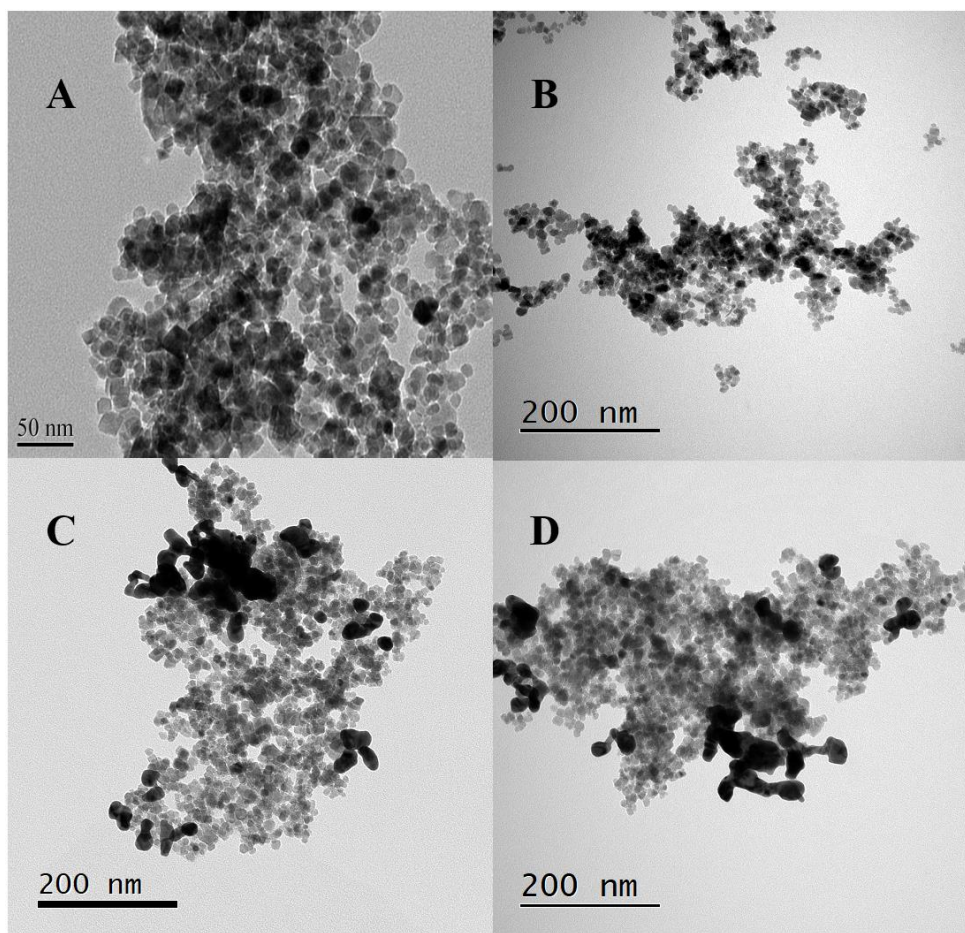
Figure 3.2. TEM images. (A) Commercial iron oxide nanoparticles (image from www.usnano.com). (B) Synthetic iron oxide nanoparticles. (C) The gold-coated commercial iron oxide nanoparticles (D). The gold-coated synthetic iron oxide nanoparticles. (See Appendix B, Figure B5 A–C for more TEM images).

3.3.2 Characterization of liposomes-Nanoparticles composite

The TEM images (Figure 3.3), provide evidence for the interaction between thiolated liposomes

and gold-coated iron oxide nanoparticles. The images in Figure 3.3 show that thiolated liposomes

have a greater affinity towards the gold-coated magnetic nanoparticles compared to the regular liposomes without thiol groups. The concentration of nanoparticles at the interface of liposomes, in Figure 3.3A–C, strongly indicates that the proposed formulation of magneto-liposomes was accomplished. In Figure 3.3D the lesser nanoparticles around the liposomes are as per our expectation because the regular liposomes lack thiol groups to bind the gold coated MNPs. The negative staining method was used for TEM images *(see Appendix B, the supporting information for the details of the negative staining method).*
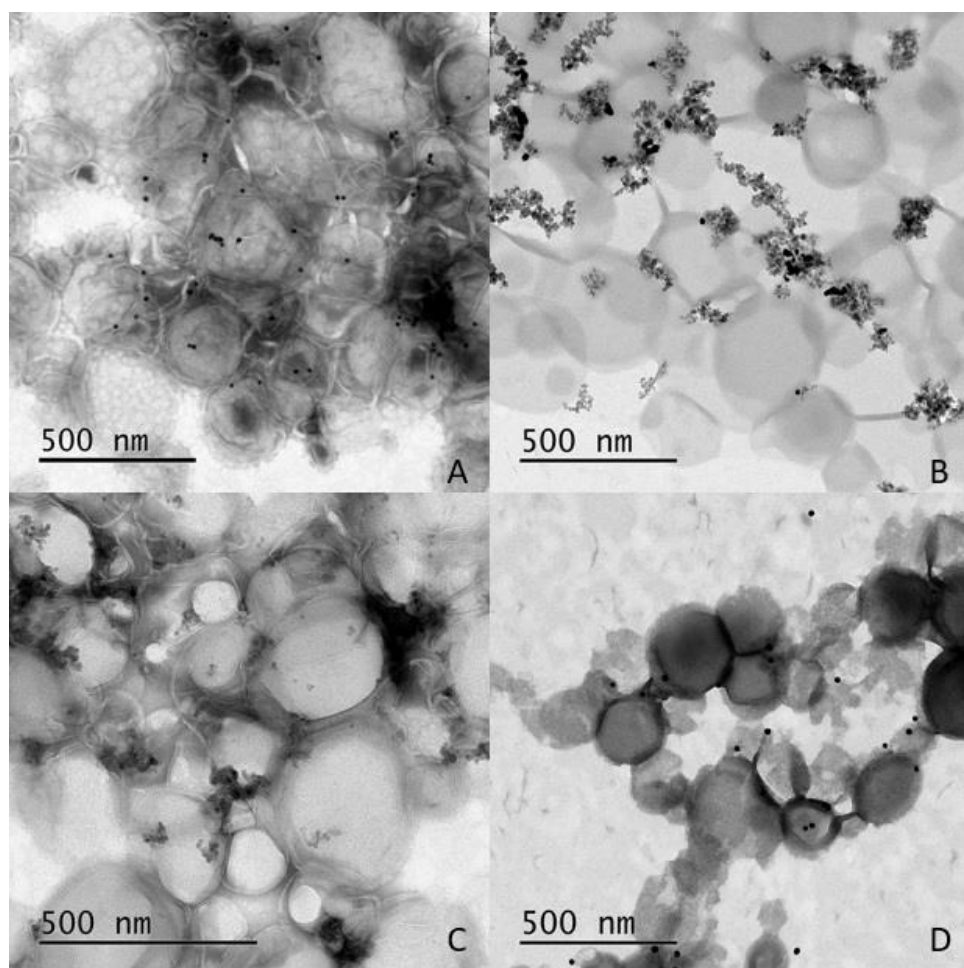
Figure 3.3 TEM images. (*A*, *B*) Thiolated liposomes with gold-coated synthetic iron oxide NPs. (*C*) Thiolated liposomes with gold-coated commercial iron oxide NPs. (*D*) Regular liposomes with gold-coated commercial iron oxide NPs. The images exhibit the chemisorption of gold-coated MNPs on the liposomal surface by gold–thiol bonds. See Appendix B, B6 A&B for more images.

50

3.3.3 Changes in the transition temperature of the liposomes on NPs addition

Two different types of liposome samples (regular liposomes with no thiol groups and thiolated liposomes with 50% Th-CHOL) are allowed to interact with different types of nanoparticles. The percentage photoluminescence (PL) intensity Vs. temperature graphs (Figure 3.4A, B) show that the addition of nanoparticles results in a change of transition temperature of liposomes. For the regular liposomes without thiol groups (Figure 3.4A), the change in transition temperature (concerning a sample without nanoparticles) is negligibly small upon addition of the iron oxide NPs and gold nanoparticles (AuNPs 40 nm size), while there is a small change (decrease by approximately 3 °C) when interacting with 50 nm in size gold-coated iron oxide NPs. These indicate that there is no significant interaction between the liposomes and nanoparticles. However, for the thiolated sample (Th-Chol 50%) in Figure 3.4B, the interaction with nanoparticles is such that the transition temperature changes by 3 to 8 °C.
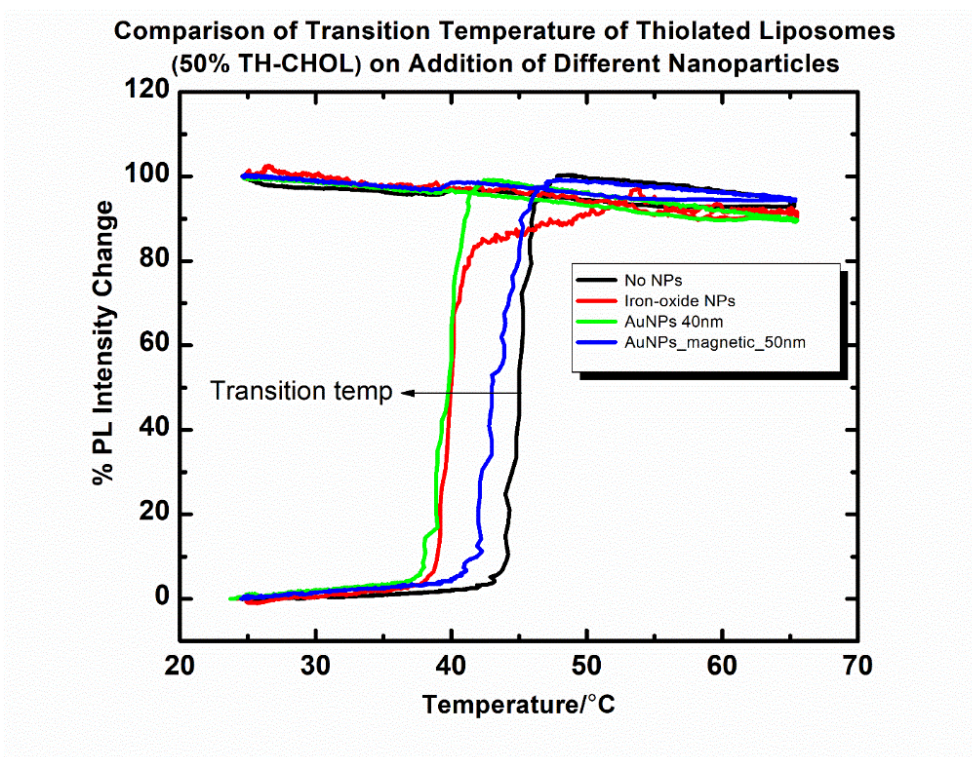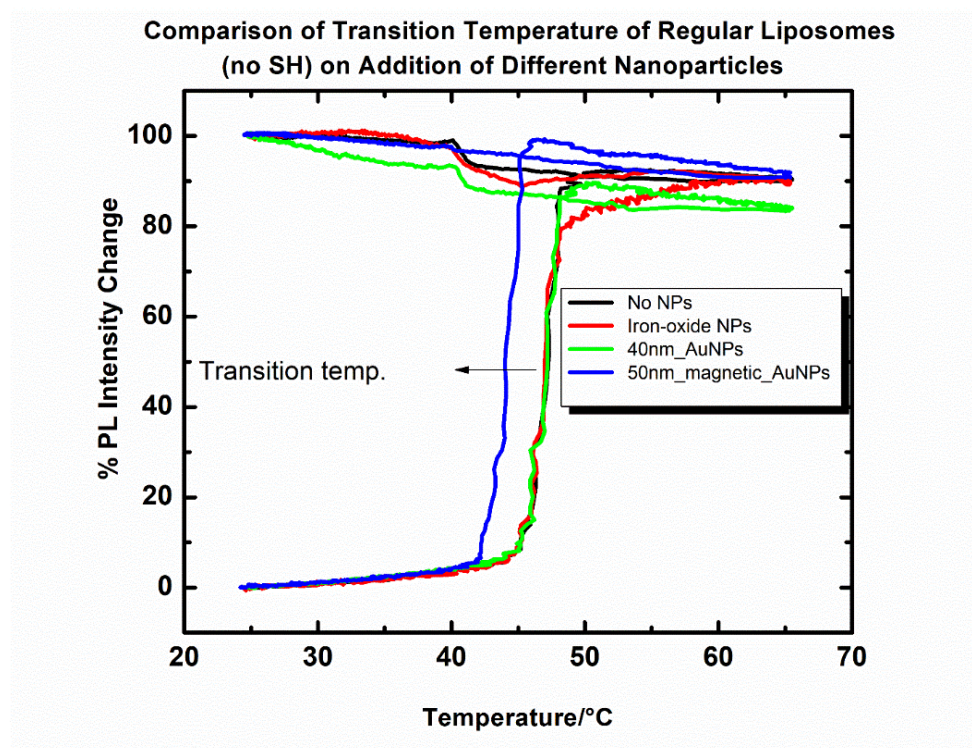
Figure 3.4 *Comparison of transition temperatures (Tm) of (**A**) regular (non-thiolated) liposomes (**B**) thiolated (with 50% Thiolated cholesterol) liposomes, with various nanoparticles (see text for detail). Please, note that the PL intensity is normalized to 0–100% at 25 °C for comparison.*

The data show that the formation of the liposome/NP complexes takes place on a relatively slow timescale. To investigate the kinetics of interactions of magnetic Au NPs (50 nm) with regular and thiolated liposome samples, a separate experiment was carried out. In Figure 3.5 A & B, the data show that when magnetic Au-NPs interact with liposomes, interaction is evidenced by the change in transition temperature. The transition temperature exhibits the time-dependence of this interaction and varies with the liposome composition. For the regular liposome sample, the change in transition temperature seems to be over in a relatively short amount of time (5 min) and for the Th-Chol 50% sample, the transition temperature continues to shift lower over longer periods. In addition, the absolute value of transition temperature change is larger than in the case of regular liposomes. Please, note that the slow kinetics can be observed since the heating curve takes about an hour to obtain in this particular experimental setup.

Comparison of Transition Temperature of Regular Liposomes (no SH) on Addition of Nanoparticles (Kinetic Study)

(A)
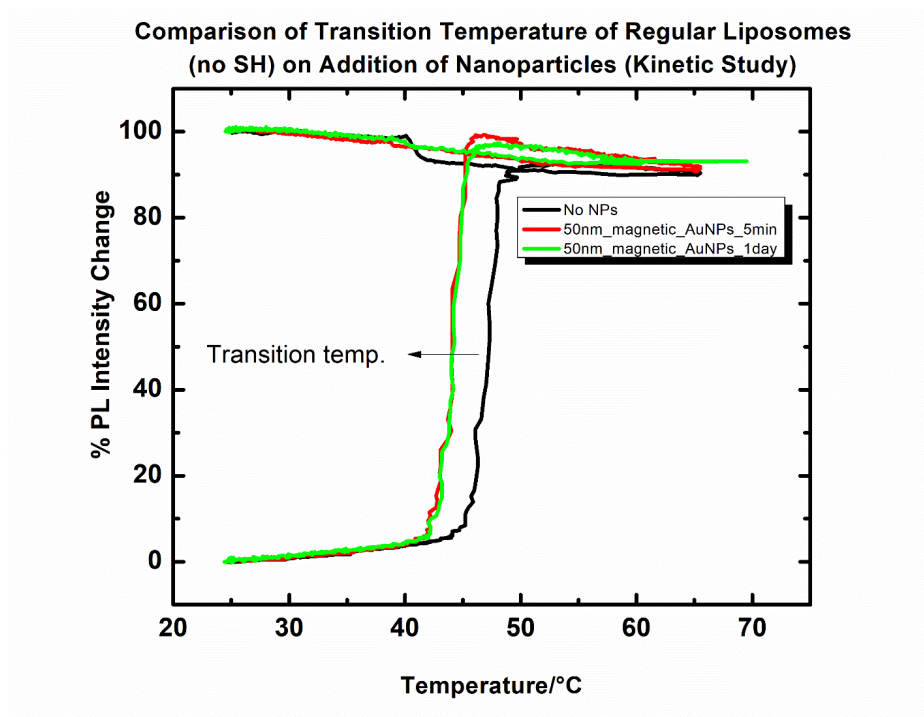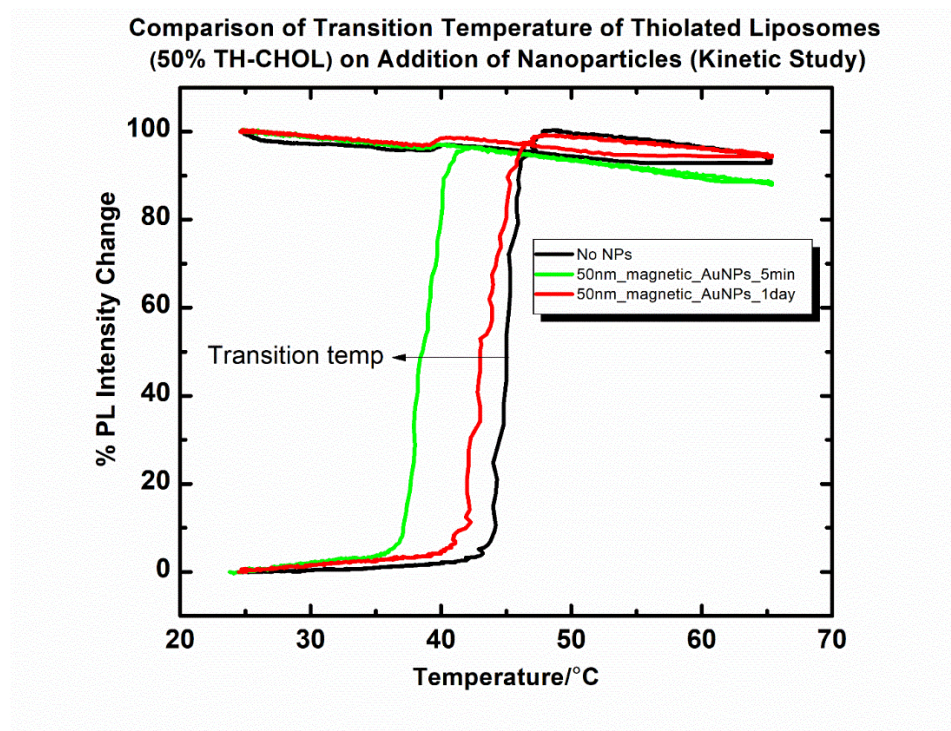
(B)

*Figure 3.5 Kinetics of interactions of 50 nm magnetic AuNPs with (**A**) regular liposomes (**B**) thiolated liposomes (Th-Chol 50%).*

3.3.4 Pulsed magnetic field triggered drug release from MNP-coated liposomes: The impact of dilution (Osmotic Pressure)

Osmotic pressure can build up if the chemical potentials of the solvent are different on the two sides of a membrane. One might anticipate that osmotic pressure may have a significant impact on liposomal stability. The build-up from the osmotic pressure could also lead to "pressure priming" the liposomes to accelerate drug release upon triggering. We investigated the release of CF from thiolated, and regular liposomes combined with synthetic iron oxide nanoparticles under the pulsed magnetic field under various dilution conditions. For this, two different dilution media, distilled water, and PBS solution were used. Dilution of liposome samples would result in larger osmotic pressure in the case of distilled water. To minimize the impact of the gold–thiol bond interaction under different dilution conditions, bare iron oxide MNPs were chosen. The concentration of the

iron oxide nanoparticle solution was 170 g/L, and the iron oxide nanoparticles were added to a 2 mL diluted solution of liposomes, and after 5 min, the release study was carried out. The data are presented in Figure 3.6 A&B exhibiting the release of CF dye under different conditions and with increasing numbers of pulses. The graph in Figure 3.6A shows that the thiolated liposomes diluted with water as dilution media exhibit a higher percentage of the release of CF dye compared to PBS as dilution medium, under the same number of magnetic pulses (20 pulses) in the whole series of different volumes of nanoparticles used. Even the 40 magnetic pulses in PBS dilution media have lower release than with 20 pulses in water media (except in 6 and 8 µL). The graph in Figure 3.6B shows similar studies for the regular liposomes with different dilution media under magnetic pulses. The release percentage is almost double when liposomes are diluted in distilled water as compared to dilution in a PBS solution. In conclusion, while liposomal drug delivery systems utilize buffers to stabilize the liposomes, dilution will impact the drug release efficiency and the stability of the liposomes. Even the liposomes that have no NPs show noticeable release after applications of 20 magnetic pulses; therefore, in the next step, the experiments were carried out in distilled water as dilution media.

(A)

(B)
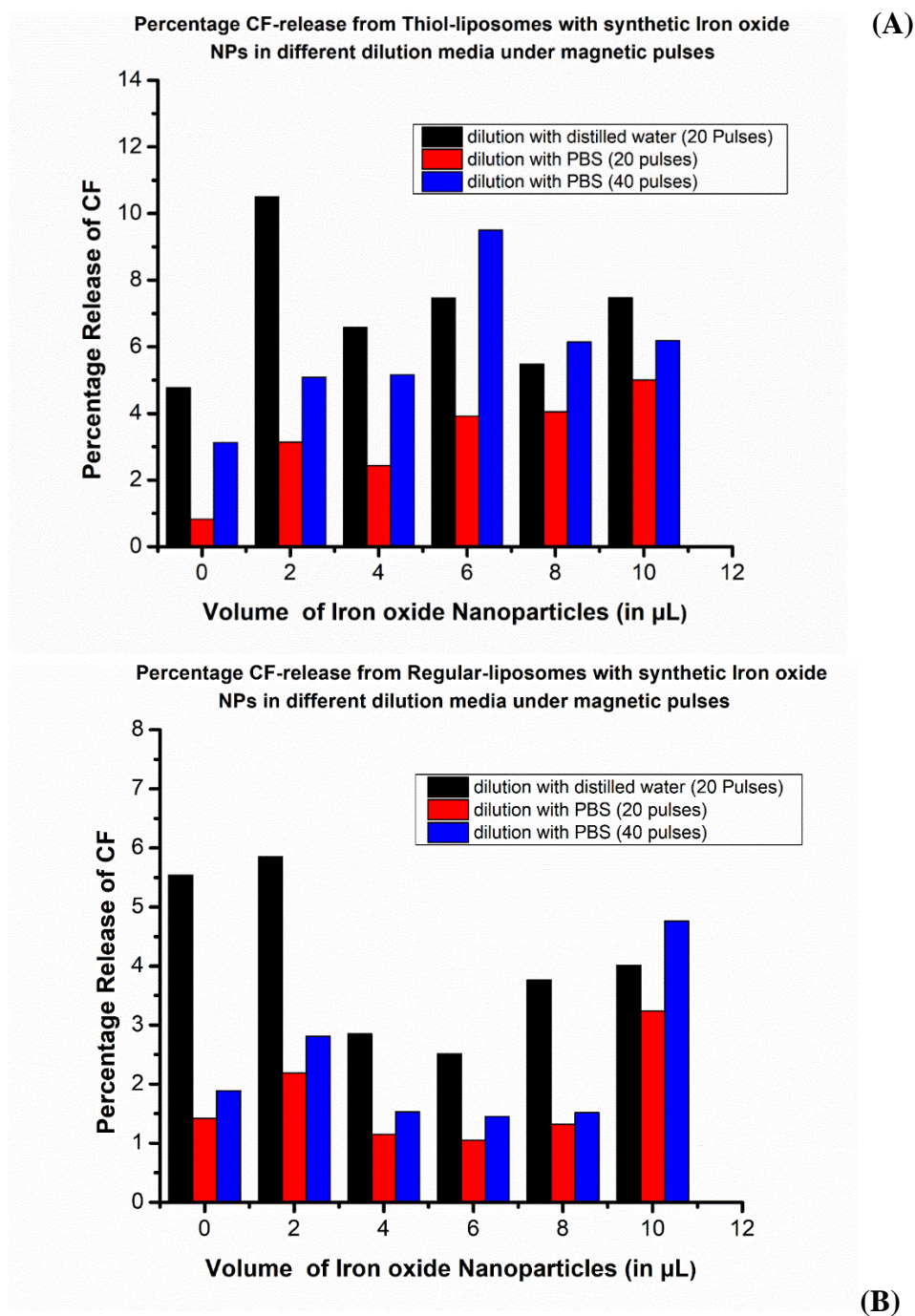
Figure 3.6. (A) Effect of dilution media on the thiolated liposome-iron oxide NP system under a pulsed magnet. (B) Effect of dilution media on the regular liposome-iron oxide NP system under a pulsed magnet.

3.3.5 Pulsed magnetic field triggered drug release from MNPs decorated liposomes

The goal of utilizing gold-coated magnetic particles and covering the surfaces of liposomes with –SH bonds is to localize ultrasound close to the lipid membrane for an effective drug delivery system. In this study, we investigated the percentage release of carboxyfluorescein liposome/NP complexes consisting of the regular and thiolated phospholipids under the pulsed magnetic fields. The types of magnetic nanoparticles used in the experiments were: commercial iron oxide NPs, gold-coated commercial iron oxide NPs, synthetic iron oxide NPs, and gold-coated synthetic iron oxide NPs. All the nanoparticle solutions were normalized to the concentration of commercial iron oxide nanoparticles (170 g/L) and the nanoparticle solution was added at different volumes in each experiment ranging from 0 to 10 µL onto the liposome samples (2 mL)**.** The results of percentage release of CF dye for regular and thiolated liposomes with distilled water as dilution media are summarized in **Tables 3.5** and **3.6**. As shown in the data, the release efficiencies after the application of 20 magnetic pulses varied from 1% to 20%. Overall, the gold-coated commercial iron oxide particles combined with thiolated liposomes exhibited the best drug release efficiencies.

Table 3.5. Percentage release of CF on the interaction of regular liposomes with different nanoparticles under a pulsed magnetic field.

Volumes of NPs (µL)	Commercial Iron Oxide NPs	Gold coated Commercial IONPs	Synthetic Iron Oxide	Gold Coated Synthetic IONPs
0	5.5%	5.2%	5.0%	5.4%
2	2.1%	3.4%	5.8%	2.7%
4	2.6%	10.8%	2.9%	3.0%
6	1.2%	9.8%	2.5%	5.8%
8	1.3%	9.3%	3.7%	2.8%
10	0.9%	6.3%	4.0%	3.6%

Table 3.6. *Percentage release of CF on the interaction of 50% Thiolated Cholesterol (Th-Chol) liposomes with different nanoparticles under pulsed magnetic field.*

Volumes of NPs (µL)	Commercial Iron Oxide NPs	Gold coated Commercial IO NPs	Synthetic Iron Oxide	Gold Coated Synthetic IO NPs
0	4.8%	4.5%	4.7%	4.6%
2	5.0%	7.5%	10.5%	6.5%
4	3.6%	14.2%	6.6%	7.5%
6	9.5%	17.6%	7.5%	9.9%
8	3.9%	20.5%	5.6%	7.6%
10	3.8%	14.6%	7.4%	6.8%

3.4 Discussion

3.4.1 Effect of nanoparticles on the transition temperature of liposomes

In the previous works,[63, 69, 121, 128, 139] the magnetic nanoparticles were loaded either at the hydrophilic cores or the lipid bilayers of liposomes. Hydrophilic MNPs disperse in the aqueous core, whereas hydrophobic MNPs can interact with bilayers. These binding interactions are mainly electrostatic; however, binding can take place under non-favorable electrostatic contributions that involve van der Waal forces.[140] It has been found that the incorporation of hydrophilic gold nanoparticles at the liposomal lipid bilayer results in membrane softening relative to pure liposomes, manifested by reducing bending modulus. The membrane softening phenomenon is both size and concentration-dependent.[141] Some investigations include perturbation of lipid properties upon nanoparticle adsorption, based on atomistic simulations. It has also been observed that nanoparticles penetrate shallowly into the bilayer, leading to local membrane thinning and bending.[142]

In this work, the nanoparticles were added outside the liposomes where the interaction was based on physisorption in the case of regular liposomes. However, the interaction was based on

chemisorption, in the case of thiolated liposomes. It is clear from the graph in Figure 3.4B that there is a change in the transition temperature of liposomes only when the nanoparticles are added. Thus, it is the nanoparticles that cause some interaction with lipid bilayer resulting in the shift in Tm. The type of interaction is yet to be explored in detail. Further, the kinetic studies (Figure 3.5A, B) for the interaction of nanoparticles and liposomes suggest that the interaction of the thiol group with gold-coated MNPs is time-dependent. More experiments based on time-dependent interactions are required to explore the detailed mechanism.

3.4.2 Effect of Osmotic pressure on CF release

As depicted by the graphs in Figure 3.6A, B the CF release is enhanced upon dilution with distilled water compared to the PBS mediated dilution, under a pulsed magnetic field. The overall increase in the release can be explained based on the osmotic pressure effect on liposomal stability. The aqueous core of liposomes contained CF dye dissolved in PBS. When liposomes are diluted with distilled water, the concentration of ions is higher at the core compared to the surroundings of liposomes. Hence, osmotic behavior aids the liposomal bilayer disruption under magnetic pulse. However, dilution with PBS makes an isotonic environment at both the core and the surroundings so that the magnetic pulses solely contribute towards bilayer disruption; thus, the overall percentage release of the dye is lesser compared to the release under dilution with distilled water.

3.4.3 Comparative CF release study from Thiolated and Regular liposomes with MNPs coating under Pulsed magnetic field applications

The release of CF (4.5%–5.5%) was observed for both types of liposomes even in the absence of nanoparticles (i.e., 0 µL in Tables 3.5 and 3.6). This is probably due to the diamagnetic behavior of water that assists the release under the high magnetic field of about 5 T and the distortion leading

to leakage in the bilayer of the liposomes under these conditions.[143-145] Among the different types of nanoparticles employed, the gold-coated commercial iron oxide nanoparticles provide a greater release (as high as 20.5%) of CF dyes from thiolated liposomes and about 10.8% release from regular liposomes. This is potentially due to the bigger size (15–20 nm magnetic core) of these particles than the "in-house" synthesized nanoparticles samples (8–12 nm magnetic core). It is obvious that the bigger magnetic particles possess greater magnetic moments under the application of a magnetic field, and hence ultrasound generation is more effective. In a similar study with cells, the iron oxide nanoparticles (25 nm diameter) were found to induce microporation within cells under pulsed magnetic field application.[146] Thus, we anticipate that magnetic nanoparticles can trigger the drug release by the microporation of the lipid bilayer of liposomes, triggered by a pulsed magnetic field. Both commercial and synthetic iron oxide nanoparticles contribute release as high as 9.5–10.5% with thiolated liposomes, while with regular liposomes, the release is limited to below 6%. The iron oxide nanoparticles still contribute to less overall release than gold-coated samples, which is to be expected as these particles do not reside closer to liposomes. The gold-coated synthetic iron oxide nanoparticles exhibit the release in the range of 5% to 10% depending on the volumes of nanoparticles added. From the results in Tables 3.5 and 3.6, it was revealed that gold-coated nanoparticles contribute towards greater release than bare iron oxide nanoparticles. This was expected, as gold-coated samples tend to reside in the close vicinity of liposomes due to gold–thiol (Au–SH) bonds, which are absent in the case of bare iron oxide nanoparticles. Additionally, the thiolated liposomes are more efficient towards release than simple, regular liposomes that lack thiol (-SH) groups.

3.5 Conclusions

The change in transition temperature of liposomes in presence of nanoparticles indicates the interaction of the liposomes with gold-coated magnetic nanoparticles. In addition, it has been found that thiolated liposomes show greater interaction, as compared to regular liposomes with gold-coated nanoparticles. The interactions between liposomes (with thiolated and regular samples) and the gold-coated magnetic nanoparticles show that the thiolated sample has a significant shift in transition temperature due to gold–thiol interaction over time. Interestingly, the liposomes examined in this work show a tendency to release more CF when the dilution media is distilled water instead of PBS. We have concluded that this behavior is due to the osmotic effect on liposomal stability under different dilution media. Distilled water makes the surroundings of liposomes more dilute than the liposomal core (which contains CF solution in PBS). The increase in the release of CF before and after the addition of magnetic NPs shows that there is a strong interaction of magnetic NPs with liposomes under the application of magnetic pulses. Though the bare iron oxide NPs only attach to the liposomes via physisorption, they can still disrupt the liposomal bilayer when magnetic pulses are applied. The gold-coated iron oxide NP with thiolated liposome samples exhibit increased release of CF due to the strong binding of NPs onto the surfaces of the liposomes by gold–thiol bonds. The bonded NPs are nearer to the bare iron oxide NPs, and hence under magnetic pulses, they can rupture the lipid bilayer more efficiently, enhancing the release of CF. Furthermore, the liposomes under the influence of pulsed magnetic fields produce very efficient CF releases in a unit time compared to the literature values of previous work.

Chapter 4 - Pulsed Magnetic Field Assisted Drug Release from Magneto-liposomal Systems: Functional role of Hydrophilic and Lipophilic Magnetic Nanoparticles for triggering.

4.1 Introduction

The encapsulated drugs can spontaneously diffuse through the lipid membrane in the liposomal systems but to enhance the rate of drug release, a variety of external stimuli can be used.[11, 122-126, 139] These external stimuli greatly vary in many respects such as how powerful is the applicator device, how rapid they can initiate drug delivery, and how deep they can penetrate in living tissue. Among these external stimuli, external magnetic fields can provide an efficient route towards a fast drug release[11, 121, 139] because the magnetic fields not only have great penetration depth but also be applied slowly and fast as well. Under the application of external alternating or rotating magnetic fields, encapsulated magnetic nanoparticles inside the liposomes, a combined system known as 'magneto-liposomes' can offer an enhanced release of drugs.[11, 64, 147, 148] Magnetic nanoparticles as a triggering agent can play important role in the process of drug delivery. To maximize the drug delivery efficacy, the location of the magnetic nanoparticle in a drug delivery system is decisive. Magnetic nanoparticles can be integrated with liposomes at the core (aqueous lumen),[69, 119] at the lipid bilayer,[55, 128] or the external surface[149, 150] of liposomal membranes to govern the drug release. Depending upon the location of MNPs and the types and strength of magnetic fields,[69, 139, 149] the nanoparticles can induce both mechanical and/or thermal effects on the liposomal systems to increase the rate of drug release.[55, 128, 148, 151, 152]

Through the process known as magnetic hyperthermia, the superparamagnetic nanoparticles encapsulated inside liposomes can generate local heating under a high frequency alternating magnetic field (HF-AMF/ 10-1000 kHz).[61, 63, 153, 154] During the process, the temperature of liposomes increases above the transition temperature (T_m) of constituent lipids, and the bilayer permeability increases resulting in the enhancement of the drug diffusion.[61, 128] Besides, excess heat generated from the particles can result in the thermal ablation of unhealthy tissues. At low-frequency alternating magnetic field (LF-AMF), 0.01-10 kHz the magnetoliposomes can release drugs, through the contribution of the mechanical effect of magnetic fields on NPs while minimizing the hyperthermia effect.[64, 119] Alternatively, short intense magnetic pulses[69, 70] can be used to generate ultrasound from magnetic nanoparticles enclosed in liposomes, which disrupts the lipid bilayer to release a significant quantity of cargo rapidly.[70, 150]

Lipophilic magnetic nanoparticles entrapped in between the lipid bilayer can directly actuate liposomal membrane both thermally and mechanically[55, 121] so that the diffusion barrier between the interior and exterior of the liposomal systems is directly affected. Efficient nanoparticle loading at the bilayer is a challenging task and the presence of nanoparticles can potentially lead to bilayer instability thereby contributing to the passive release.[55, 155] To fit within the lipid bilayer dimensions, the size of nanoparticles should be small enough (<6.5 nm).[57, 58] This diminishes the ability of magnetic nanoparticles to respond towards magnetic fields as the magnetic moment scales with the volume of the magnetic nanoparticle.[156] In addition, clustering of the nanoparticles at the bilayer can reduce the effectiveness of the drug delivery system.[56] Homogeneous dispersion of magnetic nanoparticles at bilayer to produce highly efficient magneto-liposomal system has been demonstrated via tuning of liposomal composition and structure.[55, 128, 157, 158] Besides the approaches mentioned above, the magneto-liposomal system with hydrophilic

magnetic nanoparticles attached to the external surface of liposomes through chemisorption have been designed. The gold-thiol interaction through surface modifications of the liposomal membrane has been facilitated to attach the gold-coated magnetic nanoparticles on the liposomal surface.[150] This approach eliminates the competition of the drug and nanoparticles for the space at the interior of liposomes thus increasing the drug loading capacity in the liposomal drug delivery system. In this study, an intense short magnetic field is used to create nano/micropores on the lipid membrane through the generation of ultrasound from oscillating nanoparticles.[146, 150]

The goal of the present work is to explore the location of the magnetic nanoparticle in a variety of positions around the liposomes while using short magnetic pulses for drug release. This study includes the hydrophilic magnetic nanoparticles encapsulation at the aqueous core or entrapment of lipophilic magnetic nanoparticles at the lipid bilayer of liposomes. A short time release over the maximum release from magnetoliposomes is the motivation of the present work. The application of very short magnetic pulses (with 200 μsec of oscillation time) in an interval of 20 seconds, makes the active time of the magnetic field much less compared to typical alternating magnetic fields or pulsed magnetic fields used in literature.[55, 64, 69, 128, 139] Compared to 100% duty cycle in AMF and few percentages in other PMF systems,[69] the duty cycle of a pulsed magnetic field is 0.001% which potentially facilitates fast kinetic release. In this study, 20 short magnetic pulses are used such that the total time required does not exceed 10 minutes and the actual application time of the magnetic field is only ~4 ms.

4.2 Experimental methods

4.2.1 Chemicals and Materials

Lipid (DPPC, MW = 734.05) and Cholesterol (ovine, >98%, MW = 386.654) used in the preparation of liposomes are purchased from Avanti Polar Lipids (Alabaster, AL). Syringes (1 mL, Model 1001 TLL SYR) for the extrusion of liposomes were purchased from Hamilton Robotics (Reno, NV, USA) while polycarbonate filter membranes (25 mm diameter, 0.2 µm pore size) were purchased from Spi Supplies (West Chester, PA, USA). Magnetic nanoparticles (Dextran coated, 25-30 nm) are purchased from NANOCS (Boston, MA, USA). Magnetic nanoparticles (Iron oxide magnetic nanoparticles in toluene, 5nm) and a model drug 5,6- Carboxyfluorescein (CF) are purchased from Sigma-Aldrich (St. Louis, MO, USA). Sephadex G-50 Medium for column preparation in size exclusion chromatography is purchased from GE Healthcare Bio-sciences AB (Uppsala, Sweden).

4.2.2 Preparation of magneto-liposomes

The liposomes samples are prepared with the method described in the sections 2.1, 2.1.1 and 2.1.2 (**Chapter 2**).

4.2.3 Generation of pulsed magnetic field

The details of PMF generation are described in sections 2.4 and 2.5 (**Chapter 2)** above. In the present work, two different capacitors with capacitance 7µF and 77µF, have been used for magnetic field generation. The change in capacitor affects the magnetic pulses mainly in their magnitude of amplitude and to some degree in the frequency as shown in **Figure 4.1**. Please note that while the amplitude of the magnetic field is increased (red curve) the frequency of oscillation

decreases. With the decrease in frequency of oscillation of magnetic field, intensity of ultrasound generated is expected to decrease. However, the increase in amplitude of magnetic field oscillation tends to increase the intensity if ultrasonic waves generated. The combination of the two factors can greatly determine the release of carboxyfluorescein from magnetoliposomes. In this work, the magnetic field with higher amplitude of magnetic field is referred as *higher magnetic field* (red curve) and one with lower amplitude is referred to as *lower magnetic field* (blue curve). It is not trivial to control the amplitude and frequency of magnetic field oscillation simultaneously hence in this work, capacitors with capacitance of 7µF and 77µF (that have different amplitudes and frequencies) have been used in this work. Two different magnetic fields from different capacitors are then used to investigate the role of variation in the magnetic field on the extent of drug release from the magneto-liposomal drug delivery system.
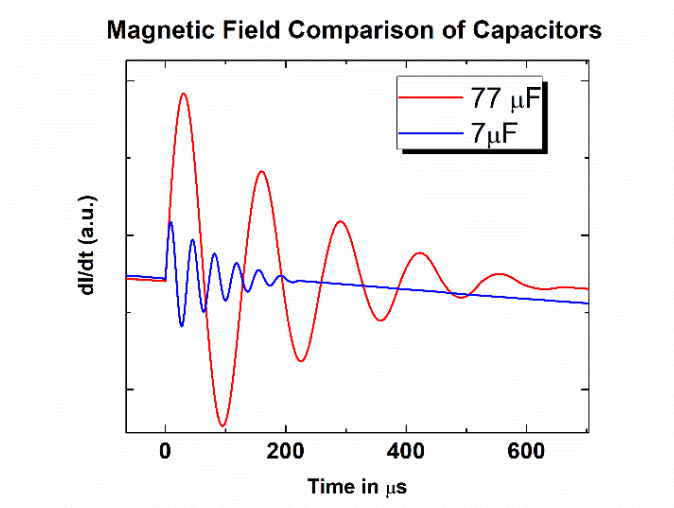
Figure 4.1. *Magnetic Field comparison of Capacitors; HMF and LMF corresponding to 77µF and 7µF respectively.*

4.3 Results and Discussion

4.3.1 Characterization of magneto-liposomes

A. *Magnetoliposomes with MNPs at the core: Hydrophilic MNPs*

The low-resolution TEM images of magnetoliposomes with MNPs at the core with a ratio of liposomes to average nanoparticles per liposomes equal to 1:1 (Fig A, B) and 1:4 (Fig C, D) show that the magnetic nanoparticles are entrapped inside the liposomes to form magnetoliposomes.
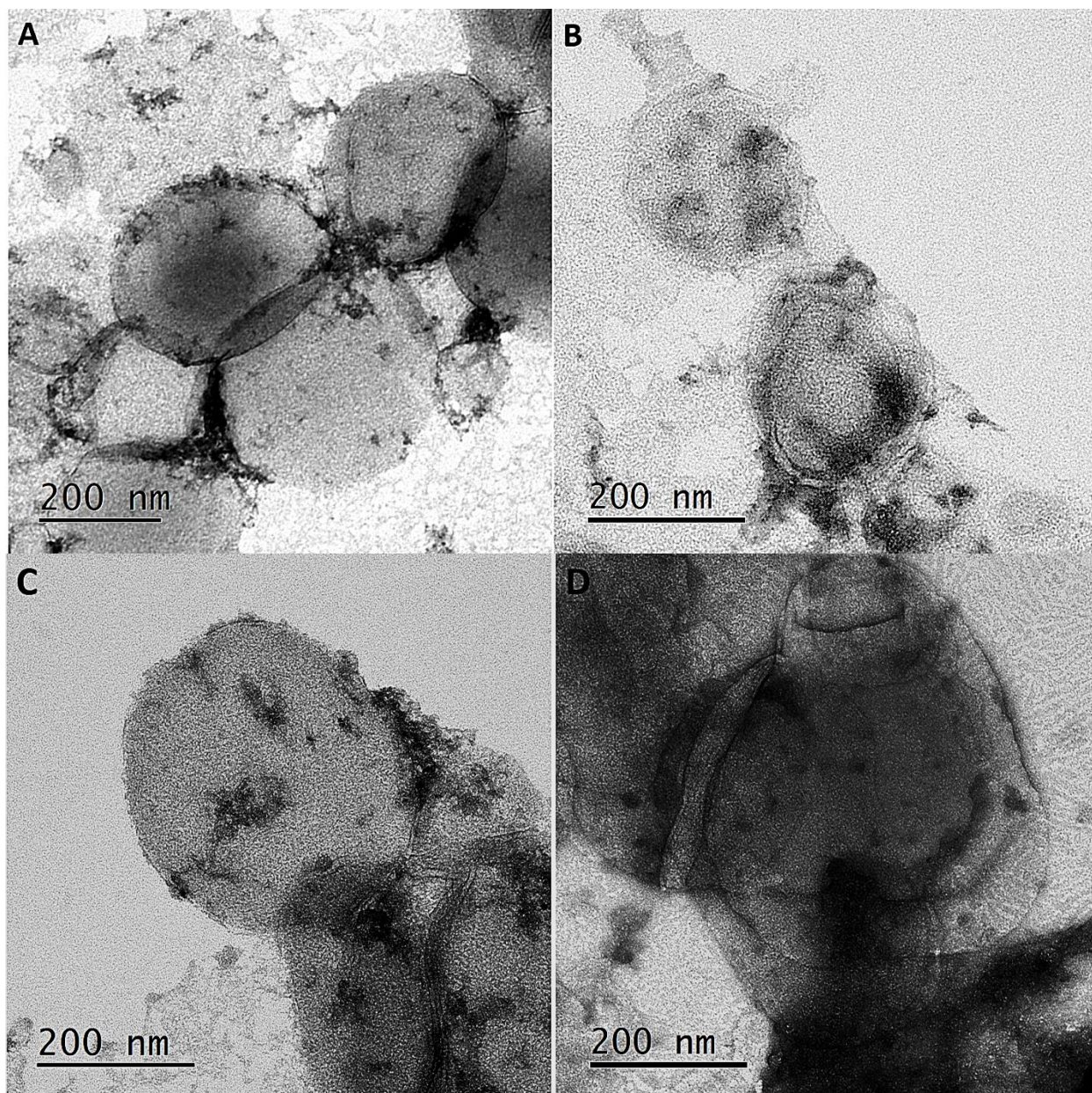
Figure 4.2 TEM images of magnetoliposomes with MNPs at the core with the ratio of a number of liposomes to the average number of nanoparticles per liposome (**A, B**) 1:1 and (**C, D**) 1:4.

As the dispersion medium of original MNPs is water, they reside in the aqueous core. Also, free MNPs are separated by gel column, the presence of nanoparticles is due to those encapsulated at the liposomal core. EDX analysis data in Tables 4.1 and 4.2 provide additional evidence of magnetoliposomes formation. The presence of iron in each of those samples is due to the loaded magnetic nanoparticles. The EDX spectra are included in *supporting information (Appendix C, C1 and C2).*

Table 4.1. *Elemental analysis of magnetoliposomes with magnetic nanoparticles at the core (1:1)*

Elements	Weight %	Atomic %
C	76.75	83.07
O	19.55	15.88
Fe	2.72	0.63

Table 4.2. *Elemental analysis of magnetoliposomes with magnetic nanoparticles at the core (1:4)*

Elements	Weight %	Atomic %
C	68.39	81.41
O	16.62	14.85
Fe	2.39	0.61

B. Magnetoliposomes with MNPs at bilayer: lipophilic MNPs

TEM images in Figure 4.3 A and B show the magnetoliposomes with MNPs at liposomal bilayer. The original nanoparticles are stabilized in organic solvent hence during the liposome formation, the MNPs are preferably entrapped at lipid bilayer. The unencapsulated MNPs are separated during column separation. The EDX spectrum is included in *supporting information (Appendix C, C3).*

Table 4.3. *Elemental analysis of magnetoliposomes with magnetic nanoparticles at the bilayer*

Elements	Weight %	Atomic %
C	66.77	83.76
O	11.06	10.42
Fe	2.73	0.73

The EDX analysis of magnetoliposomes with lipophilic MNPs in Table 4.3 provides additional evidence of successful preparation of the magnetoliposomal system. The data in the table reveal the percentage of Fe almost in the same value as in samples with hydrophilic MNPs. The average iron content per liposome in both lipophilic and hydrophilic magnetoliposomes is

essential for the comparable resultant magnetic field effect. Provided the content of Fe in magnetoliposomes remains constant, the dependence of CF release from lipophilic and hydrophilic magnetoliposome systems under pulsed MF can be explored well.
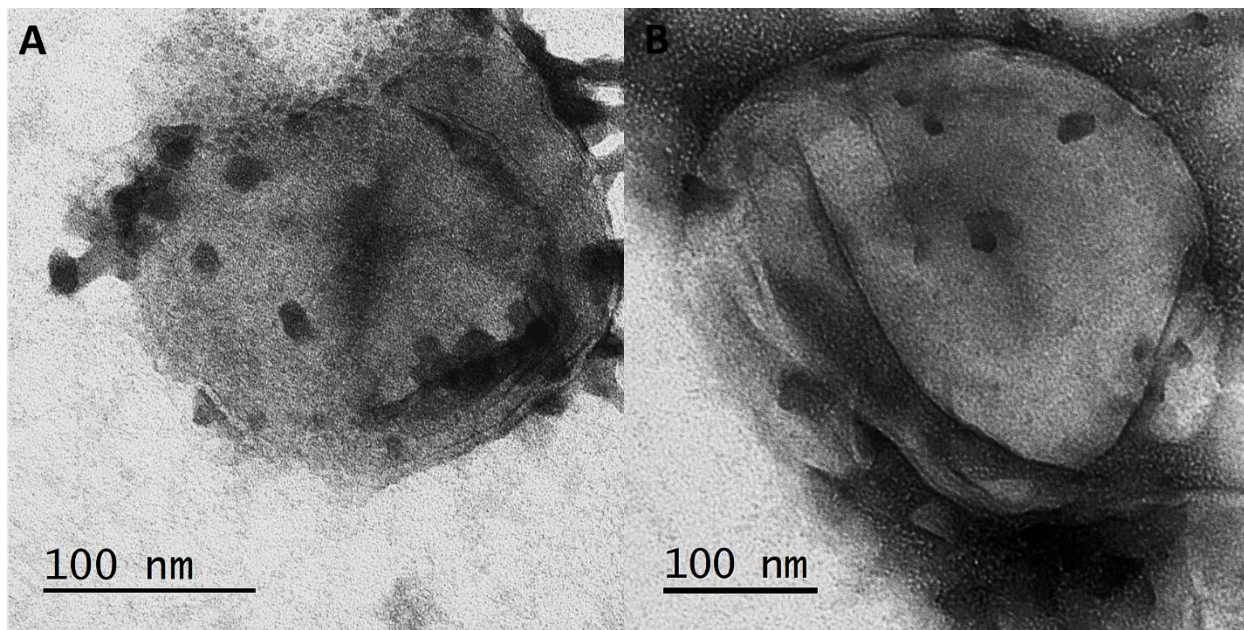
Figure 4.3 (A, B)*: TEM images of magnetoliposomes with magnetic nanoparticles at bilayer.*

4.3.2 Transition temperature of liposomes with magnetic nanoparticles

To investigate the change in lipid properties with the different types of magnetic nanoparticles entrapped, the temperature profile of magnetoliposomes samples with lipophilic and hydrophilic magnetic nanoparticles, ranging from room temperature (25 ℃) to 65 ℃ (where liposomes are completely lysed giving maximum CF release) is compared as shown in Figure 4.4. The graph clearly shows that the samples with hydrophilic MNPs (at the core) including the control sample (one lacking any MNPs) have similar profiles. The transition starts at around 40℃ which corresponds to the transition temperature of constituent lipid DPPC (T_m = 41℃). On the other hand, the magnetoliposomes with MNPs at bilayer have a different thermal profile which starts

earlier than other samples. This difference can be attributed to the difference in the location of magnetic nanoparticles in those samples. As the MNPs remain at aqueous volume at the core, the samples with hydrophilic particles have similar properties to the control sample without disturbing the phase transition of the lipid bilayer. But, lipophilic MNPs loaded between the lipid bilayer has a significant effect on the phase transition of lipid which gives important information regarding the presence of MNPs loading at the bilayer.
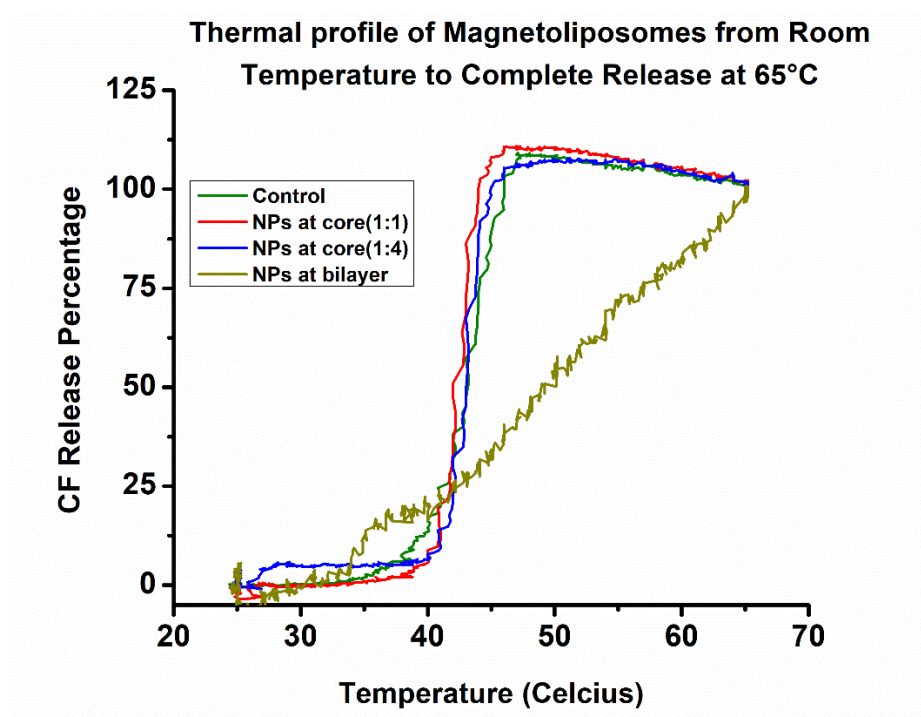
Figure 4.4. Comparison between thermal profiles of magnetoliposomes samples with hydrophilic and lipophilic magnetic nanoparticles ranging from 25 ºC (room temperature) to 65 ºC (destruction of liposomes for total release).

4.3.3. CF release from magnetoliposomes at different positions of the magnet

To explore the impact of the homogeneous and inhomogeneous magnetic pulses for releasing drugs from the magneto liposomal drug delivery system, an experiment was designed where the

release of carboxyfluorescein from magnetoliposomes was investigated at different positions of the magnets (**Figure 4.5**).
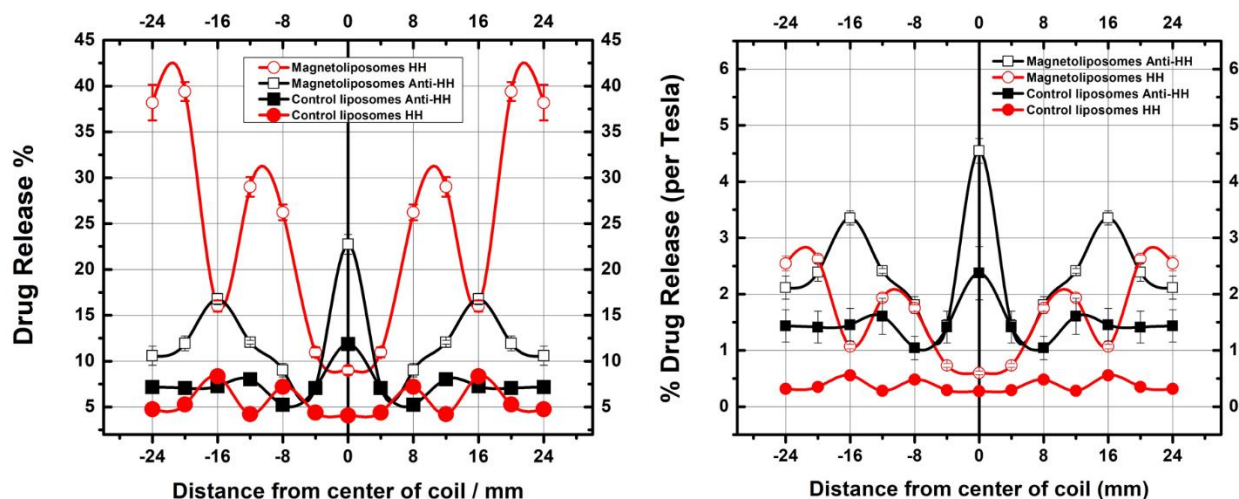
*Figure 4.5. (**Left**) Percentage CF release from magneto-liposome at different positions of a magnet under pulsed magnetic field using both Helmholtz and Ani-Helmholtz coils. (**Right**) Percentage CF release normalized (per Tesla) for the graph on the left.*

Clearly, the largest release is observed at the regions in these magnets where the magnetic field gradient is highest. Magnetic field gradient is higher at the edges of both Helmholtz and anti-Helmholtz coils and note that the magnetic field gradients are different in the two different coils as shown in **Figure 4.5 (Left)** . Also, the magnetic field gradient is at its minimum at the center for Helmholtz coils though the magnetic field itself is maximum. The release observed in the center of the Anti-Helmholtz coil and the edge of the Helmholtz coil is mainly due to the generation of ultrasound from the magnetic particles in the presence of time-dependent inhomogeneous magnetic fields. While the magnetic field alone does not contribute to efficient drug release, a combination with the strong magnetic field gradient has an additive effect. The enhancement in release in presence of field gradient has multiple possible reasons. First, some level of ultrasound is generated from the homogeneous magnetic fields due to the magnetostriction effect. The

combination of ultrasound due to magnetostriction and that from the homogeneous magnetic field could account for the ~38% drug release from magneto-liposomes. In addition, the possibility of other collective effects that can destabilize the liposomal systems has to be considered. The lipid bilayer can be polarized under strong magnetic fields resulting in drug leakage and the MNPs-liposomes together could lead to an aggregation which can wear out liposomes yielding additional drug release. At about ± 16 mm from the center of the magnet of the Helmholtz coil, there is a large drop in release percentage while in the case of the anti-Helmholtz coil at this point, a big jump in the release is seen. We anticipate that this point corresponds to a region where there is a change in direction of magnetic field gradient and more ultrasound is produced. The graph on the **Figure 4.5 (Right)** shows per Tesla release of CF from magnetoliposomes at different position of magnets. Though the graph on the right shows that the maximum release is observed at the edges of Helmholtz coils, it is important to note that the Helmholtz coil used in this work produces three times more magnetic field than the anti-Helmholtz coil. On normalization, the release per Tesla provides a better comparison for the release of CF at different positions of Helmholtz and anti-Helmholtz coils. The result of this experiment provides proof of concept how the various composition of liposome samples was affected under the influence of different types of magnetic fields. These results will help construct practical devices for efficient drug release.

The result from the above graph agrees with the variation of product of magnetic field gradient and magnetic field along the length of Helmholtz coil (**Figure 2.6 C**). The product of magnetic field and its gradient determines the magnetic force acting on the magnetic nanoparticles in an external magnetic field (**Equation 1.1**). This value is maximum at the edges and minimum at the center of Helmholtz coil and the CF release is also maximum when magnetoliposomes are placed at the edges of Helmholtz coils and minimum when placed at center of coil respectively.

However, for anti-Helmholtz coils, the result in graph (**Figure 4.5**) is not in a complete agreement with the graph from **Figure 2.6 C**. Though the product of magnetic field and its gradient (and hence the magnetic force acting on particles) is minimum at the center, the release of CF is maximum. Also, the magnetic force is minimum at around 16 mm from the center of anti-Helmholtz coil, but the CF release is significantly higher (~ 15%). While the mechanism of CF release is unclear, we anticipate that this contradiction is due to the polarization effects of magnetic fields on liposomal bilayer. To explain the mechanism of release at different positions of magnet, further investigation is required.

4.3.4. Carboxyfluorescein release assay from magnetoliposomes

The CF release assay was carried out in a way described in Chapter 2 of this dissertation. In addition, a difference between the release after applying 20 magnetic pulses in a row at the beginning and the release after each magnetic pulse was investigated under both lower and higher magnetic fields (LMF and HMF) conditions. Our goal was to explore how detailed information on the measurement of percentage CF release after each pulse provides greater insight into the optimization of pulse magnetic field application on magnetoliposomes to achieve rapid drug release. Also, both approaches should have more or less similar percentage release from magnetoliposomes for the total 20 magnetic pulses.

A. The Percentage CF release after 20 magnetic pulses applied in a row

The percentage CF release calculated from each magnetoliposomes sample under application of 20 consecutive magnetic pulses using lower and higher magnetic fields are shown in figure 4.6 below.
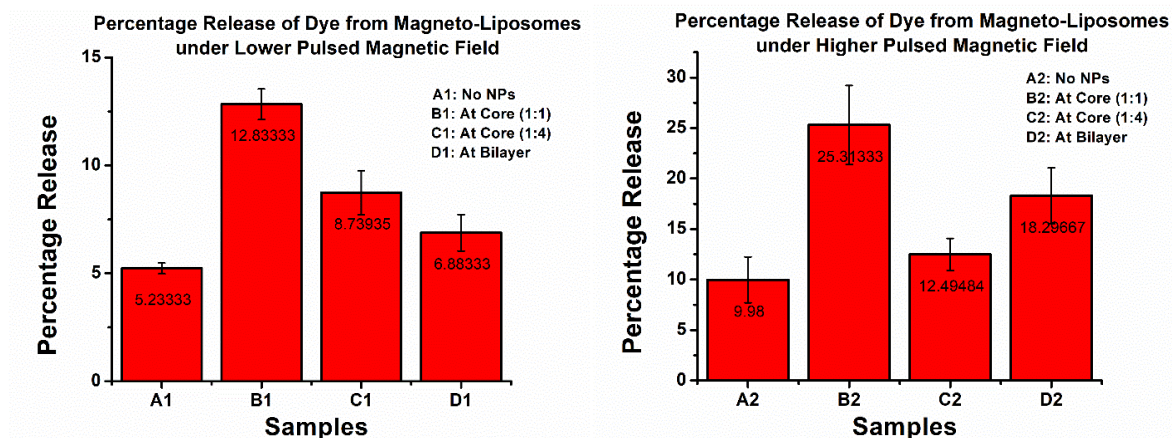
Figure 4.6. *Percentage CF release from different magneto-liposome samples under application of 20 magnetic pulses in a row in the presence of (LEFT) lower (RIGHT) higher pulsed magnetic fields.*

The control samples have significant releases even in absence of magnetic nanoparticles. It has been reported that a magnetic field can change both the physical and chemical properties of water.[159-161] Hence the release from the control samples can be attributed to the diamagnetic response of water in strong magnetic fields. It is important to note that the release from the control sample is nearly doubled in a higher magnetic field compared to the release from a lower magnetic field. For the sample with nanoparticles at the core (1:1), there is nearly 13% release under lower magnetic field which is again doubled to about 26% under higher magnetic fields. The release from samples with NPs at the core (1:4) surprisingly has a lower release compared to samples with NPs at the core (1:1) in both types of magnetic fields. We assume that this could be due to the lesser CF loading when nanoparticles concentration is increased. The release is still more in higher

magnetic fields compared to the lower magnetic fields for samples with NPs at the core (1:4). Finally, for the samples with nanoparticles embedded into the lipid bilayer, the release is approximately tripled in a higher magnetic field compared to release in lower magnetic field conditions. This is possibly due to better enhancement in membrane permeability under a higher magnetic field when nanoparticles are closer to the lipid membrane. Please note that the release from samples with NPs at the core (1:1) is still greater than samples with NPs at the bilayer in both types of magnetic fields. This could be due to two possible reasons. First, the bigger magnetic nanoparticles at the core (25-30 nm) can respond better towards strong magnetic fields compared to tiny magnetic nanoparticles at the bilayer.[156] Second, the nanoparticle loading is easier at the core with greater volume than at the lipid bilayer. The overall greater release in presence of a higher magnetic field from all liposome samples compared to that in the lower magnetic field proves that MNPs response increases with magnetic field strength and hence increase membrane permeability due to more effective ultrasound generation at higher magnetic field condition.

B. The percentage CF release measurement after each magnetic pulse

Under lower pulsed magnetic field (LMF), the percentage release of CF measured after each pulse to a total of 20 magnetic pulses from different samples of magnetoliposomes is shown in ***Figure 4.7 (Left)***. For each type of liposomes sample, release continuously increases for 10-12 initial pulses and then the curve attains a plateau. The control sample has released nearly 5% at saturation. The sample with magnetic nanoparticles at the core (1:1), has about 11% release compared to the sample with a 1:4 ratio which has only about 8% release. For the samples with magnetic nanoparticles at bilayer, the release is around 10%. The percentage release for each type of liposome sample at saturation agrees with the release obtained when pulses are applied in a row (***Figure 4.6-Left***). For similar studies in presence of a higher magnetic field (***Figure 4.7-Right***), it

is observed that the percentage release gets enhanced for each type of liposome sample. The result provides evidence for an increase in release with an increase in a magnetic field. The observed increase in CF release is due to an increase in ultrasound generation from magnetic nanoparticles under a higher magnetic field which in turn increases the liposomal permeability thereby providing a path for drug release.
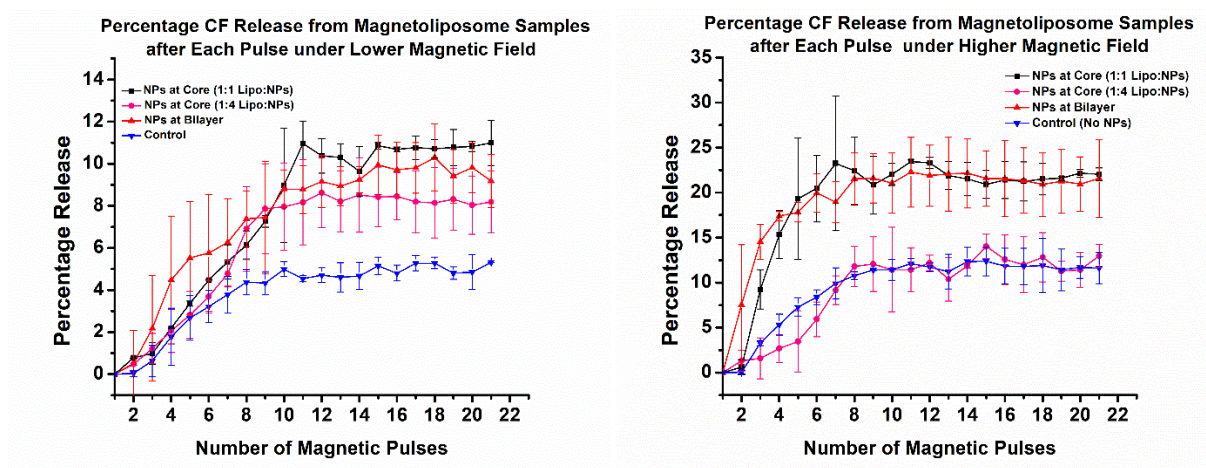
Figure 4.7. *Percentage CF release measurement after each magnetic pulse from different types of magneto-liposomal systems under lower (LEFT) and higher (RIGHT) pulsed magnetic fields.*

Though the reason behind the saturation observed in the graph is unclear and demands further investigations, it has an important implication that even 10-12 pulses are sufficient for the release of payload from magneto-liposomes. Nevertheless, our target for short time release is achieved which merely requires 3-4 minutes for 20-25% (MNPs both at the core at bilayer) and release of drug from magneto-liposomal systems.

4.4 Conclusions

The results presented exhibit that the pulsed magnetic fields can enhance the drug release from liposomal systems with magnetic particles loaded at the core or the bilayer. The substantial release from control samples is an interesting as well as important result and can be described with the diamagnetic response of water in stronger magnetic fields used in our study. The release from all liposomal samples increases with an increase in magnetic field strength. This provides a field dependence of release phenomenon from liposomes. The significant drug release from magneto-liposomes in a short duration (3-4 minutes) opens a path for therapeutic applications of the pulsed magnetic field designed in this work. Further investigation is however required to address the drug release saturation observed during measurement after each pulse. Also, the exploration of additional reasons behind the release from control samples will help to extend the scope of this method.

Chapter 5: Pulsed Magnetic Field Activated Doxorubicin Release from Rattle-type Mesoporous Silica Shells.

5.1 Introduction

Due to the numerous advantageous properties, mesoporous silica nanoparticles have been extensively used as a drug delivery system.[76, 79-83] Among different types of magnetic silica composites, the rattle-type magnetic core mesoporous silica shell spheres possess ideal properties like low density and high specific area which make them an excellent candidate for the drug carrier system. It provides not only enough void space for the drug loading but also furnishes the platform to functionalize the desired organic groups favorable for drug loading, targeting, and delivery. In addition, the shell provides protection that reduces drug toxicity, enhances the colloidal stability of nanoparticles, and avoids the possible drug degradation simultaneously.[73, 91, 100-102] Unlike organic drug carriers like liposomes and micelles, mesoporous silica systems have inherent chemical and mechanical stability.[72, 73] Along with magnetic core, mesoporous silica systems can be used for controlled targeted drug delivery purposes.[83, 86, 89, 90] Under the exposure of external stimuli like magnetic fields, ultrasound, and mechanical forces, the rattle-type magnetic core silica shell system can release the contents in a controlled manner.[31, 72, 73] Apart from magnetic hyperthermia applications, magnetic fields can also be used to generate particle motion. Both alternating magnetic fields and pulsed magnetic fields can be used for the conversion of the magnetic field into translational motion of the particles, the field gradient required for the conversion is higher in the case of a pulsed magnetic field.[105, 106] The other advantage of using the pulsed magnetic field is that it can be used for the ultrasound generation by the oscillatory motion of nanoparticles under magnetic field gradient.[70, 106, 135]

5.2 Strategy

In this work, the design of magneto-mechanical (**Figure 5.1**) and mechano-acoustic (**Figure 5.2**) nano pumps have been proposed for the drug release study. The magnetic core in the rattle type silica shell system when placed in the inhomogeneous magnetic field, the magnetic field gradient at the junction of anti-Helmholtz coils is strong enough to produce the translational motion on the core particle.[105, 106] As the magnetic core is surrounded by the pool of drug (doxorubicin) solution, we aim to accelerate the release of drugs through the pores towards the exterior of the silica shell.
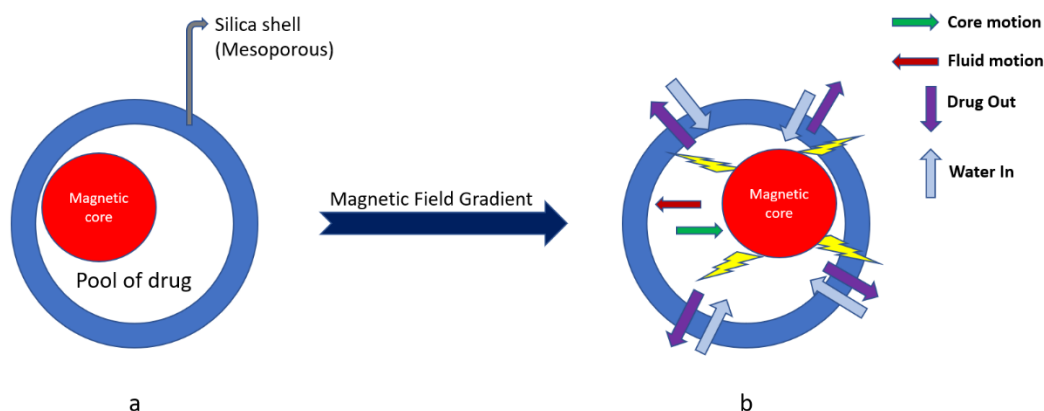
Figure 5.1. (a) Mesoporous rattle-type Silica shell with drug and magnetic core, (b) drug pushed outward, and water pushed inwards through mesopores due to motion of magnetic core under an influence of magnetic field gradient.

The translational motion of the core now can act as the 'nano pump' which can squeeze out the drug molecules. The target here is to achieve a short time release over the maximum release and since the duty cycle of the pulsed magnetic field is much higher this system can prove itself an efficient route for drug release through a silica shell system. The back-and-forth motion of the magnetic core under the pulsatile mechanism behaves as a magneto-mechanical pump. Where the

regular diffusion process takes several hours for significant release, this system is expected to perform the task in a lesser time.

In addition, the magnetic core under an inhomogeneous magnetic field can generate ultrasound through oscillation.[106, 135] The ultrasound produces sonic pressure towards the solution of drug present in its surrounding thereby pushing the drug molecules out through the mesopores. This mechano-acoustic pump at the core of a rattle-type mesoporous silica shell can thus behave as an extraordinary drug delivery system.
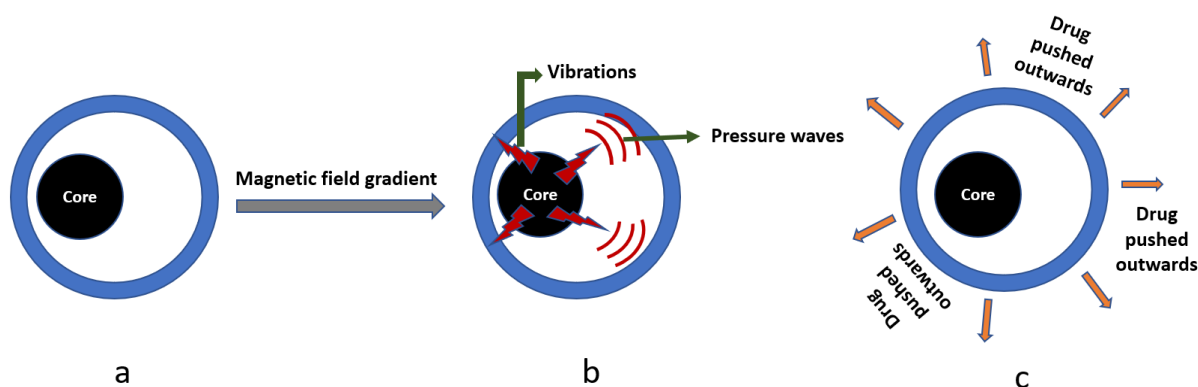
Figure 5.2. (a) The rattle-type silica shell with magnetic core (b) under magnetic field gradient magnetic core particle generates ultrasound due to vibrations (c) Drug pushed outwards through mesopores due to pressure waves of ultrasound propagating through a pool of drug solution.

Figure 5.2 illustrates the possible mechanism for the magnetic field-assisted drug release from the ultrasound-generated pressure waves. Hence, mechanical vibrations are transformed into acoustic (ultrasonic) waves that trigger drug release. The efficiency of such nano-pump potentially depends on different physical parameters like the size of the magnetic core, shell thickness, and volume available for drug loading. It is expected that the proposed hypothesis helps to develop an

efficient method for the drug release study and in turn, enhances the suitability of rattle-type mesoporous silica systems as efficient drug carriers.

5.3 Experimental Methods

The details of the experimental set-up for pulsed magnetic field and ultrasound generation are given in **sections 2.4** and **2.5** (**Chapter 2**). Similarly, the materials and methods to prepare rattle-type silica shell structures are discussed in **section 2.3**, doxorubicin loading, and release studies are described in **section *2.7*** of **Chapter 2**.

5.4 Results and Discussion

5.4.1 Characterization of samples

The HR-TEM images of four different samples of rattle-type Silica shell structures are given in Figure 5.3. The images clearly show that they have different core sizes (magnetic core), shell thickness, and overall size. Though all the samples have an overall comparable size in a range of 275nm to 315 nm, the core size for sample D (128 nm) lies between the core sizes of sample C (97nm) and samples A & B. The shell thickness for samples A and B is between 50-60 nm while that for samples C and D is comparatively thinner in a range of 22-30 nm. The calculation of the effective volume between the magnetic core and silica shell is more in samples C and D compared to samples A and B. When the larger effective volume provides higher drug loading, the core size and shell thickness have an important role during the drug release. All these physical parameters have been tabulated in **Table 5.1**.

Table 5.1. *The dimensions of rattle-type mesoporous silica shells*

Samples	Overall Size (nm)	Core-diameter (nm)	Shell Thickness (nm)	Effective Volume (nm^3) (percentage)
A	304.8±11.28	146.0±22.64	54.4±6.02	2.3129*10^6 *(58.67%)*
B	301.2±9.98	150.8±7.78	57.2±3.79	1.6173*10^6 *(47.39%)*
C	274.4±24.16	97.6±12.24	26.8±4.63	5.1495*10^6 *(91.35%)*
D	315.6±16.16	128.8±16.63	25.2±3.29	8.6472*10^6 *(88.54%)*
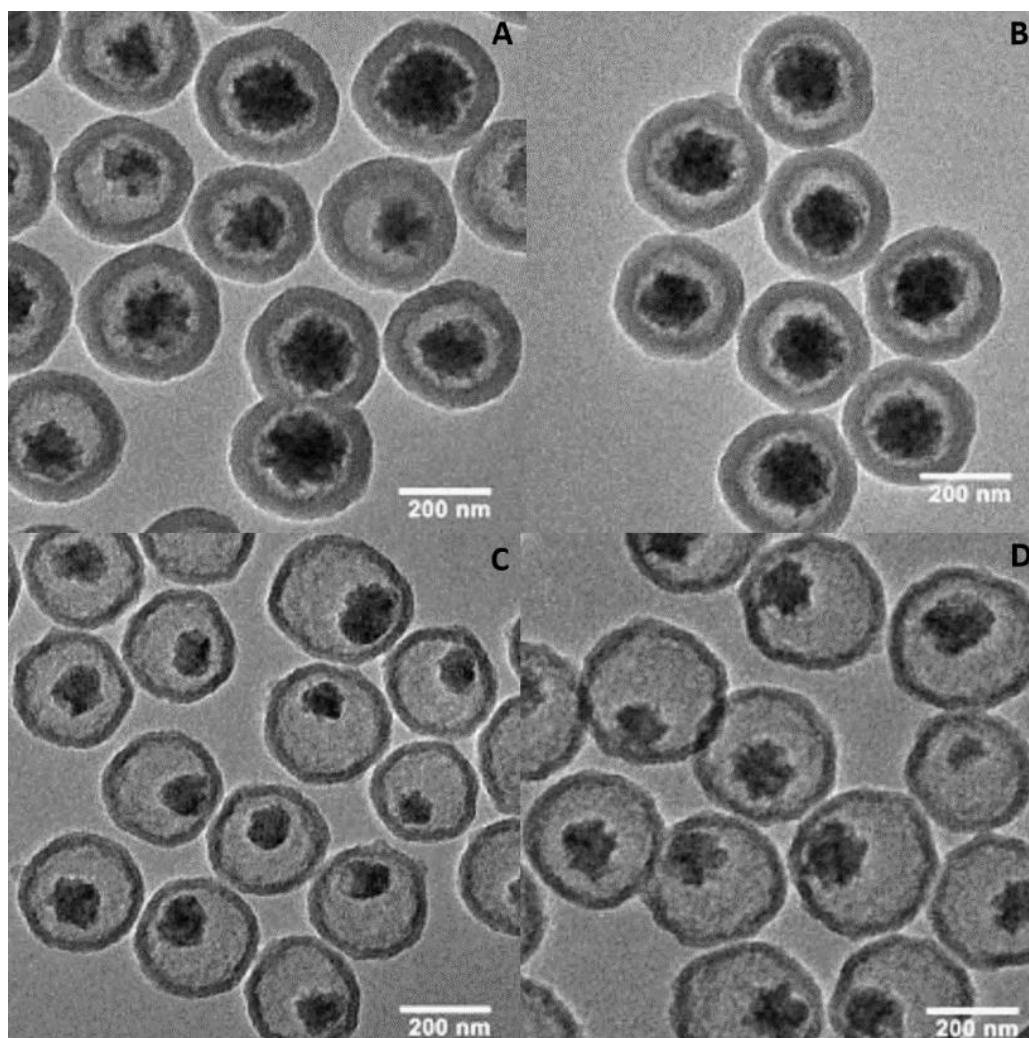
Figure 5.3. *HR-TEM images of rattle-type silica shell sample A, B, C, and D.*

5.4.2   The Doxorubicin release studies under magnetic pulses

In this study, the relation between the size of a magnetic core, shell thickness, and effective volume of rattle-cage silica systems with the doxorubicin release was investigated. Among four samples, samples A and B have the relatively lesser passive release of near 25% at the end of 10 hours while samples C and D have relatively higher passive release ~60% in the same period. This can be attributed to the difference in shell thickness of those samples. As samples A&B have greater shell thickness (50-60 nm), the passive release from these samples is lesser than that of samples C&D with relatively thinner shells (25-30 nm).
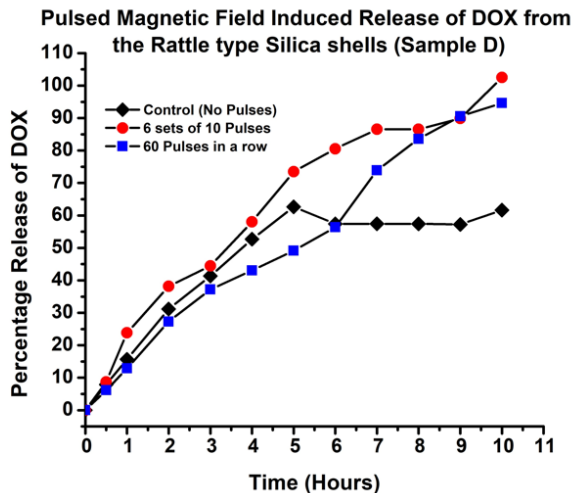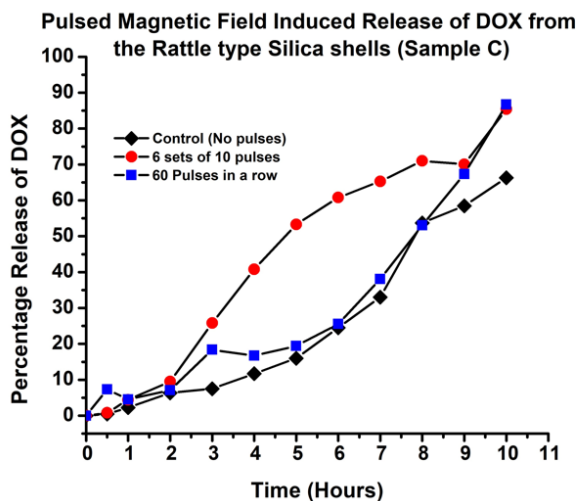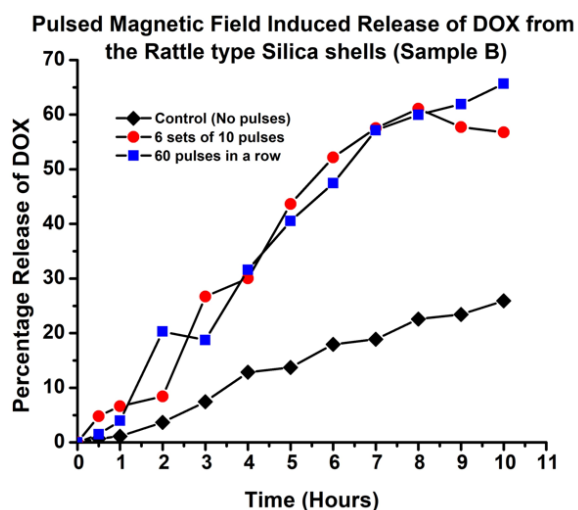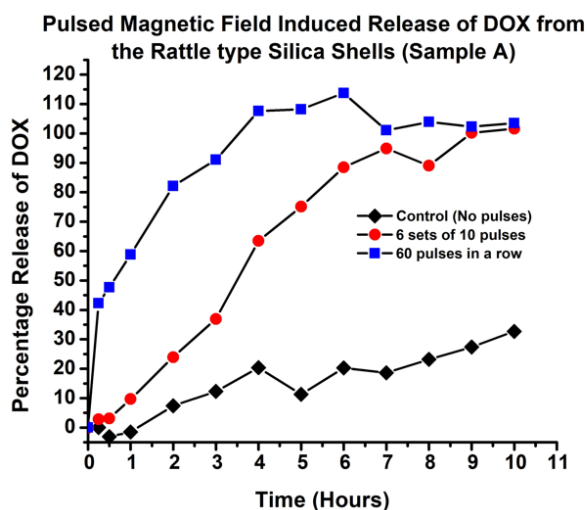
Figure 5.4. Percentage doxorubicin release from different silica shell samples. und no pulses (black solid rhombus), 60 pulses in a row at the beginning (blue solid squares), and with 6 sets of 10 magnetic pulses applied each hour up to initial 6 hours (red solid circles).

When 6 sets of 10 magnetic pulses are applied (10 pulses each hour up to the initial 6 hours), the release percentage is quite interesting (as shown by solid red circles). All the samples have a more or less similar trend in doxorubicin release. Though there is a kind of saturation in release at the end of 10 hours from all those samples, sample A has maximum release ~100% while samples C and D have nearly 90% release and sample B has only about 60% release. Despite similar shell thickness, overall size, and core size for samples A and B, the significant difference is seen in total release at the end of 10 hours. This could be because sample B has minimum effective volume among all 4 samples which leads to lesser drug loading in it.

When 60 magnetic pulses are applied in a row at the beginning of the experiment, there is a difference in the release profile for these samples. Except for sample A, the percentage release for all other samples is less effective than when sets of pulses were applied every hour. For sample A, 60% of its content is released within 1 hour and 100% release is obtained in 4 hours. The kinetics of release is significantly enhanced when consecutive pulses are applied to the sample and it attains a saturation much faster than the application of 10 pulses each hour. The difference in a release from the samples can be described based on the sizes of the magnetic core. As per our hypothesis, the smaller magnetic core is less efficient towards the action of 'nano-pump' and its efficiency enhances with a gradual increase in its size. Sample C has the smallest core size and hence a lesser release rate (blue solid squares) than sample D (with intermediate core size) and still lesser than sample A (larger core size).

Nevertheless, the percentage release of doxorubicin from all four samples is much faster in pulsed magnetic field applications than in other magnetic field systems. Thus the combination

of rattle-type core/silica shell structures with pulsed magnetic field makes an efficient drug carrier system.

5.5 Conclusions

A route for the synthesis of rattle-type core/silica shell drug delivery systems with different core sizes, shell thickness, and effective volume for drug loading has been successfully presented. The release measurements show that the release of doxorubicin is significantly enhanced in the presence of magnetic pulses compared to passive release in absence of pulses. The effective volume present for drug loading plays an important role in the release rate. It has also been observed that passive release increases with thinner shell systems. The action of the nano-pump proposed in the study significantly depends on the size of the magnetic core as it requires to be big enough to push the drug molecules out of shells through mechanical and/or ultrasonic pressure waves. However, it requires further investigation to optimize all three parameters that govern the drug release from these systems.

Chapter 6: Triggering Passive Molecular Transport into Cells with a Combination of Inhomogeneous Magnetic Fields and Magnetic Nanoparticles.

Chapter 6, in full, is a summary of the materials from *ACS Appl. Nano Mater.* 2020, 3, 3, 2414–2420. https://doi.org/10.1021/acsanm.9b02537.

6.1 Introduction

In living cells, the increase in passive transport of macromolecules across the membranes is possible through a process of microporation which involves the changes in cellular membrane permeability under exposure to external stimuli like magnetic, electrical, or mechanical forces.[162-164] The molecules of drugs, genes, and various cell nutrients are not available to the cells easily so this methodology can help transport them to cells actively.[163, 164] While electroporation can create micropores in cells through the application of high voltage electric fields (thereby polarizing the cell membrane),[165] magnetoporation involves the application of homogeneous static or pulsed magnetic fields to create such pores.[166] Please, note that both techniques can lead to irreversible microporation through the mechanism of membrane polarization.[165, 166] Besides, the use of ultrasonic sound waves has also been reported to alter the cell membrane permeability.[167]

In this work, we aim to increase the transport of small molecules into cells through a combination of inhomogeneous pulsed magnetic fields with iron oxide magnetic nanoparticles. As discussed earlier in this dissertation, magnetic nanoparticles can generate ultrasound in an inhomogeneous magnetic field.[106] Briefly, in an inhomogeneous magnetic field, the magnetic nanoparticles oscillate due to the translational motion of those particles. This particle oscillation leads to the generation of ultrasound which can create pores within the cell membrane.[106, 135] Since

the direct use of ultrasound waves suffers attenuation in biological systems, the use of magnetic nanoparticles as sonosensitizers is beneficial as magnetic fields do not experience attenuation to the same extent as sound waves.[168] Also, the magnetic nanoparticles can be modified with specific ligands which facilitate the targeted microporation techniques. The microporation induced by magnetic nanoparticles in cell membrane under pulsed magnetic field can foster the molecular transportation into cells. This strategy involves three steps as given below:

1. Nanoparticle uptake into the cell by incubating dextran-coated iron oxide nanoparticles with cancer cell lines (U-937).
2. The application of a pulsed magnetic field to the cancer cells in the presence of small molecules (Doxorubicin).
3. Increase in uptake and accumulation of small molecules through microporation into the cells.

6.2 Methods

In this study, the cancerous lymphocytic leukemia cell lines U-937, dextran-coated iron oxide nanoparticles (Dex-IONPs), and anticancer drug Doxorubicin (small molecule) were taken. The inhomogeneous magnetic field was generated using anti-Helmholtz coil pairs as described in **section 2.4** (**Chapter 2**). The doxorubicin transport into the cells was evaluated by measurement of cell viability and HPLC. The dextran-coated magnetic nanoparticles are selected in this study to maximize their uptake into the cells via glucose receptor-mediated endocytosis.[169-171]

6.3 Results and discussion

6.3.1 Optimization of Dex-IONPs concentration and Visualization of Dex-IONPs into Cells

On investigating the effects of Dex-IONPs in U-937 cells, the concentration of Dex-IONPs is optimized to be 0.0025 mg/mL hence in all remaining experiments, this concentration of Dex-IONPs is used. In the next step, a visualization was performed to ensure the loading of Dex-IONPs within the cell lines. On incubating the U-937 cells in presence of 0.0025 mg/mL of Dex-IONPs followed by isolation, washing with PBS, and subsequent removal of unloaded nanoparticles, the cells were fixed by cold methanol. Further incubation in presence of Prussian blue and counterstaining with Nuclear Fast Red, the bright field transmission visualization showed that Dex-IONPs were successfully loaded into the cell lines as shown in Figure 6.1. The control sample has no nanoparticles (Figure 6.1 A & B) while nanoparticle uptake is visible in samples incubated with nanoparticles (Figure 6.1 C & D). The Dex-IONPs uptake into the cells is further confirmed by TEM images (Figure 6.1 E, F & G) and EDX analysis (Figure 6.1H).
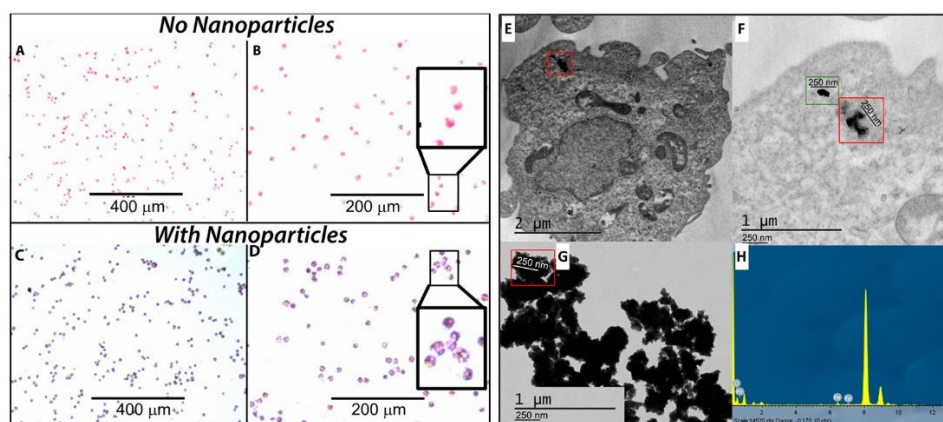
Figure 6.1. *Visualization showing the uptake of dextrin coated nanoparticles in U-937 human cancer cell line. (A, B) control–absence of nanoparticles; (C, D) uptake; the insets within panels B and D are zoomed in areas for uptake comparison. TEM images and spectrum for U-937 cells incubated with Dex-IONPs (E–H): U-937 cell (E), red box enlarged showing two nanoparticle clusters (F). TEM of the Dex-IONPs individually (G), and the spectrum (H).*

6.3.2 Effects of Dex-IONPs, doxorubicin and the application of magnetic pulses

In this experiment, the percentage of cell death was measured to determine the effects of Dex-IONPs, Doxorubicin, and the application and quantity of magnetic pulses on U-937 cells (**Figure 6.2**). In absence of both Dex-IONPs and doxorubicin, the application of pulses had no significant effect on cell death. When nanoparticles were included in absence of doxorubicin, the application of pulses still had no significant increase in cell death. However, when doxorubicin was administered, the cell death increased to about 50% even in absence of Dex-IONPs and in presence of 0, 20, and 50 pulses. Finally, when both doxorubicin and nanoparticles were present, there was no increase in cell death in absence of magnetic pulses. However, on applying 20 pulses, there was a nearly 15% rise in cell death to a system compared to the similar system with 20 pulses in presence of doxorubicin and absence of Dex-IONPs. It implies that a 15% increase in cell death is due to nanoparticles indued microporation of cells under magnetic field and thus the increase in doxorubicin uptake into cells. The application of 50 pulses further increased the percentage of cell death, in a non-linear fashion.
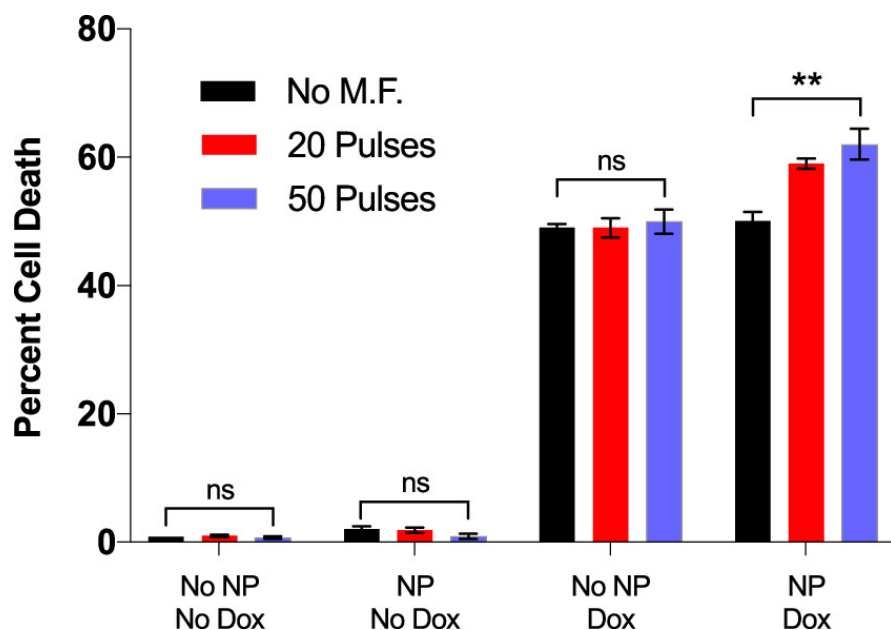
Figure 6.2. *Percentage of U-937 (human cancer cell line) cell death in combinational treatments in the presence or absence of dextrin-coated nanoparticles, doxorubicin, and or 0, 20, or 50 magnetic pulses applied. For each data set: 0.0025 mg/mL of dextrin-coated nanoparticles used, 48 h period after magnetic field application.*

6.3.3. Individual and combined effects of long-term cell viability of Dex-IONPs & PMF

To determine whether or not the Dex-IONPs and/or magnetic pulses have any long-term effects on cell viability, two sets of experiments were performed. First, to investigate the effect of Dex-IONPs, U-937 cells were either incubated with Dex-IONPs or an equivalent amount of media, for 72 hours. There was no significant difference between the cells incubated with various concentrations of Dex-IONPs compared to those incubated with media only (Figure 6.3 A). We anticipate that a 15% increase in cell death observed earlier (Figure 6.2) was not due to the long-term exposure of the nanoparticles. In a second experiment, U-937 cells when treated with 20 magnetic pulses and incubated for 72 hours, there was negligible change in cell viability (Figure 6.3 B). In the presence of both Dex-IONPs and 20 magnetic pulses, there was still no significant change in cell viability after 72 hours of incubation. Based on the result, we assume that there is no individual or combined effect of Dex-IONPs and magnetic pulses on cell viability on long-term exposure to U-937 cells. Hence, the observed 15% increase in cell death (Figure 6.2) is due to the enhanced doxorubicin transport into U-937 cells facilitated by microporation effects.
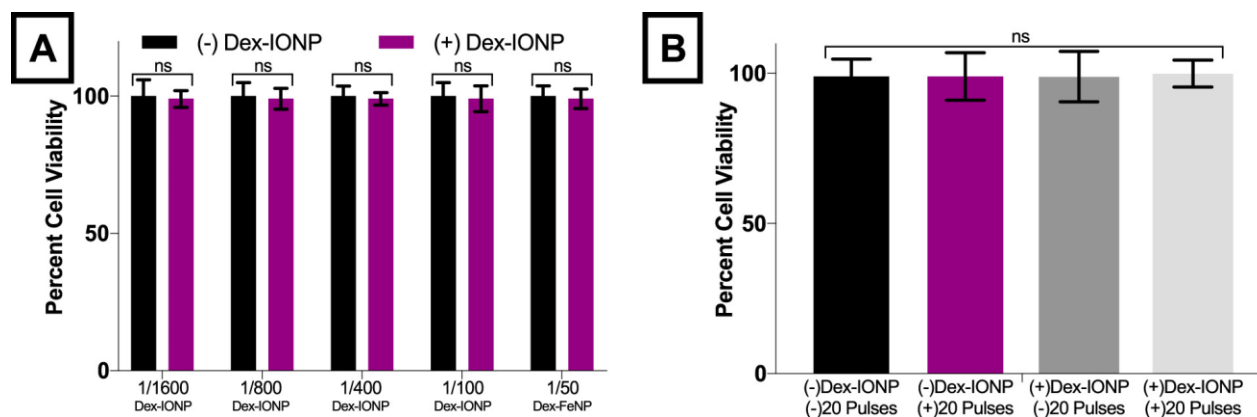
Figure 6.3. *Investigations into the possible individual and combined effects of long-term cell viability of Dex-IONPs (A), and magnetic and combinational application (B) within U-937 cells. (A) Effects upon cell viability with the exposure of various concentrations of Dex-IONPs over a 72-h period. (B) Cell viability effect 72 h after 20 magnetic field pulses applied to U-937 cells and combinational effects of both Dex-IONPs and pulses.*

6.3.4 Quantification of doxorubicin within cells

Here, quantification of doxorubicin within cell lines was performed in the absence and presence of magnetic pulses to determine whether or not the 15% increase in cellular death was due to an increase in doxorubicin uptake. Under the same experimental conditions used for the analysis of cell death, doxorubicin quantification was obtained using HPLC. It was observed through HPLC measurement within U-937 cells that the presence of magnetic pulses causes a 75.2% increase of doxorubicin uptake into the cells compared to those in absence of magnetic pulses (Figure 6.4).
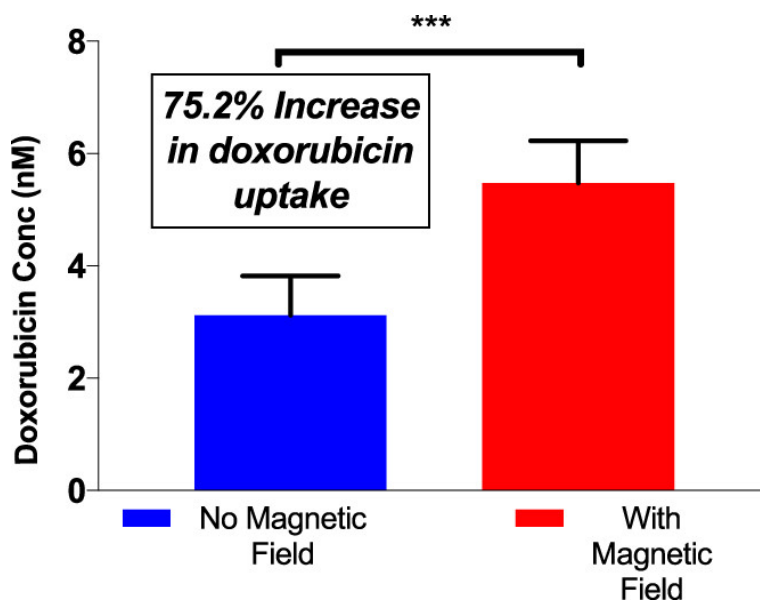
Figure 6.4. Quantification via HPLC of doxorubicin uptake within U-937 human cancer cells in the presence of 0.0025 mg/mL of dextran-coated IONPs, 20 magnetic pulses; over 2 h.

6.3.5 Effect of magnetic field on overall drug effectiveness

To determine the overall effectiveness of the drug in this combinational strategy, an investigation was made which revealed that in the presence of 0.0025 mg/mL concentration of Dex-IONPs, the

IC_{50} of doxorubicin dropped from 289 nM to 169 nM when the magnetic field was applied (Figure 6.5). Thus, the combination of magnetic nanoparticles with a magnetic field is beneficial.
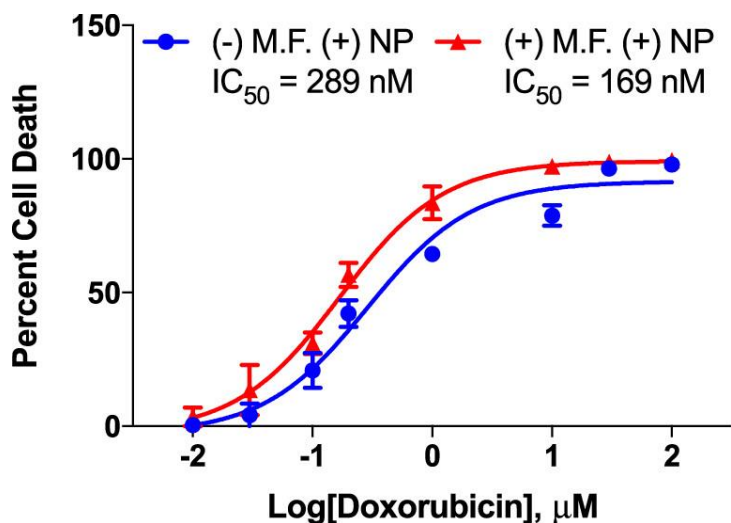
Figure 6.5. *Nanoparticle facilitated by magnetic field effects upon doxorubicin IC_{50} in U-937 human cancer cells. Cells were incubated with nanoparticles at 0.0025 mg/mL for 24 h, drug/blank added along with 20 magnetic pulses applied, incubated for 48 h.*

6.4 Conclusion

The magnetic nanoparticles under the application of inhomogeneous magnetic field pulses can increase the drug efficiency of anticancer drugs like doxorubicin. It is observed that each of three components, nanoparticles, drugs, and magnetic pulses are futile when acting independently. However, the pulsed magnetic field can enhance the cytotoxicity of the drug (Doxorubicin) in presence of Dex-IONPs. This rise is predicted to be due to a 75.2% increase in cellular uptake and accumulation of doxorubicin with the combinational approach used in this study. Also, the enhancement of doxorubicin uptake is due to an increase in molecular transport through the microporation within the cells, induced by magnetic nanoparticles under pulsed magnetic field application.

Chapter 7: Summary

The work in this dissertation demonstrated a faster drug release methodology for both flexible and rigid drug carrier systems under an inhomogeneous pulsed magnetic field. Preparation and characterization of liposomes, efficient drug loading and incorporation of magnetic nanoparticles in liposomal systems at different location are discussed in chapters 2, 3 and 4. Under the application of magnetic pulses generated from the inhomogeneous magnetic fields, the liposomes and magnetoliposomes would efficiently release the drug (carboxyfluorescein) in a short time. The gold-coated nanoparticles are synthesized in the lab and attached to the surface-modified (PEGylated) liposomes which released 20% of their content with the application of 20 magnetic pulses in mere ~7 minutes. The effect of dilution media on CF release efficiency and the effect of nanoparticle addition on the transition temperature of liposomal systems are explored. The encapsulation of hydrophilic magnetic nanoparticles at the core and hydrophobic nanoparticles at the lipid bilayer of liposomes has been demonstrated. For these magneto-liposomal formulations, the release under lower and higher inhomogeneous pulsed magnetic fields has been discussed in chapter 4. The release as high as 25% can be achieved from the liposomes with magnetic nanoparticles at the core and nearly 20% release can be obtained from liposomal systems with magnetic nanoparticles at the bilayer. Also, measurement of CF release after each magnetic pulse from both magneto-liposomal formulations has revealed that 10-12 magnetic pulses are sufficient to achieve the 20-25% of CF release, and this requires only about 4 minutes. Hence our goal of short time release has been well achieved. Further investigations are required to address the reason behind the saturation in CF release after 10-12 pulses.

Besides liposomal systems, a rigid drug carrier system; rattle-type core/silica shells are synthesized and loaded with doxorubicin. The release of doxorubicin from these carriers under a pulsed magnetic field has been investigated. The experimental results show that the release is dependent on the size of the magnetic core, the shell thickness through which the drug diffuses, and also on the effective volume available for the drug loading. The fast release from silica-based drug carriers has been successfully achieved. However, a more experimental investigation is required to explore the role of all physical parameters to make strong scientific deductions.

In addition, the application of a pulsed magnetic field in combination with magnetic nanoparticles to trigger a passive molecular transport into the cells is well explored. The results have shown that the combinational strategy of utilizing magnetic nanoparticles and an inhomogeneous magnetic field is efficient to enhance the uptake and accumulation of small molecules into the cells through microporation within cells. In addition, the effectiveness of the drug molecules is found to increase with this strategy. This study opens up a new pathway to explore cancerous cell treatment.

Overall, an inhomogeneous pulsed magnetic field has been proven to be an efficient triggering technique to enhance the release of payload drug carrier systems and we anticipate that this technique is not limited to liposomal and silica shell systems, but equally efficient in more drug carriers systems. This technique is equally efficient in small molecule transport and has potential applications in therapeutic applications.

References

1.   Beija, M.; Salvayre, R.; Lauth-de Viguerie, N.; Marty, J. D., Colloidal systems for drug delivery: from design to therapy. *Trends Biotechnol* **2012,** *30* (9), 485-96.

2.   Trucillo, P., Drug Carriers: Classification, Administration, Release Profiles, and Industrial Approach. *Processes* **2021,** *9* (3), 470.

3.   Küçüktürkmen, B.; Bozkır, A., A new approach for drug targeting to the central nervous system. In *Nanoarchitectonics in Biomedicine*, 2019; pp 335-369.

4.   Patra, J. K.; Das, G.; Fraceto, L. F.; Campos, E. V. R.; Rodriguez-Torres, M. D. P.; Acosta-Torres, L. S.; Diaz-Torres, L. A.; Grillo, R.; Swamy, M. K.; Sharma, S.; Habtemariam, S.; Shin, H. S., Nano based drug delivery systems: recent developments and future prospects. *J Nanobiotechnology* **2018,** *16* (1), 71.

5.   Devadasu, V. R.; Bhardwaj, V.; Kumar, M. N. V. R., Can Controversial Nanotechnology Promise Drug Delivery? *Chemical Reviews* **2013,** *113* (3), 1686-1735.

6.   Hoang, N.; Nimjee, S. M., Central Nervous System Drug Delivery After Ischemic or Hemorrhagic Stroke. In *Nervous System Drug Delivery*, 2019; pp 473-500.

7.   Mody, N.; Tekade, R. K.; Mehra, N. K.; Chopdey, P.; Jain, N. K., Dendrimer, liposomes, carbon nanotubes and PLGA nanoparticles: one platform assessment of drug delivery potential. *AAPS PharmSciTech* **2014,** *15* (2), 388-99.

8.   Monteiro, N.; Martins, A.; Reis, R. L.; Neves, N. M., Liposomes in tissue engineering and regenerative medicine. *J R Soc Interface* **2014,** *11* (101), 20140459.

9.   Goel, H.; Siddiqui, L.; Mahtab, A.; Talegaonkar, S., Fabrication design, process technologies, and convolutions in the scale-up of nanotherapeutic delivery systems. In *Nanoparticle Therapeutics*, 2022; pp 47-131.

10.   Rodrigues, F. C.; Devi, N. G.; Thakur, G., Role of targeted drug delivery in cancer therapeutics. In *Advances and Challenges in Pharmaceutical Technology*, 2021; pp 327-354.

11.   Pattni, B. S.; Chupin, V. V.; Torchilin, V. P., New Developments in Liposomal Drug Delivery. *Chem Rev* **2015,** *115* (19), 10938-66.

12.   Sercombe, L.; Veerati, T.; Moheimani, F.; Wu, S. Y.; Sood, A. K.; Hua, S., Advances and Challenges of Liposome Assisted Drug Delivery. *Front Pharmacol* **2015,** *6*, 286.

13.   Demetzos, C., Application of Nanotechnology in Drug Delivery and Targeting. In *Pharmaceutical Nanotechnology*, 2016; pp 77-145.

14.   Kamps, J. A. A. M.; Scherphof, G. L., Biodistribution and Uptake of Liposomes In Vivo. In *Liposomes, Part D*, 2004; pp 257-266.

15.   Knop, K.; Hoogenboom, R.; Fischer, D.; Schubert, U. S., Poly(ethylene glycol) in drug delivery: pros and cons as well as potential alternatives. *Angew Chem Int Ed Engl* **2010,** *49* (36), 6288-308.

16.   Sharma, A.; Sharma, U. S., Liposomes in drug delivery: Progress and limitations. *International Journal of Pharmaceutics* **1997,** *154* (2), 123-140.

17.   Vemuri, S.; Rhodes, C. T., Preparation and characterization of liposomes as therapeutic delivery systems: a review. *Pharmaceutica Acta Helvetiae* **1995,** *70* (2), 95-111.

18.   Yadav, D.; Sandeep, K.; Pandey, D.; Dutta, R. K., Liposomes for Drug Delivery. *Journal of Biotechnology & Biomaterials* **2017,** *07* (04).

19.   Kraft, J. C.; Freeling, J. P.; Wang, Z.; Ho, R. J., Emerging research and clinical development trends of liposome and lipid nanoparticle drug delivery systems. *J Pharm Sci* **2014,** *103* (1), 29-52.

20.   Polaka, S.; Katrajkar, K.; Siva Reddy, D. V.; Shukla, H.; Arafat, B.; Tekade, R. K., Factors affecting the pharmacokinetics of the liposomal drugs. In *Biopharmaceutics and Pharmacokinetics Considerations*, 2021; pp 567-599.

21.   Nakhaei, P.; Margiana, R.; Bokov, D. O.; Abdelbasset, W. K.; Jadidi Kouhbanani, M. A.; Varma, R. S.; Marofi, F.; Jarahian, M.; Beheshtkhoo, N., Liposomes: Structure, Biomedical Applications, and Stability Parameters With Emphasis on Cholesterol. *Front Bioeng Biotechnol* **2021,** *9*, 705886.

22.   de Kruyff, B.; Demel, R. A.; dan Deenen, L. L. M., The effect of cholesterol and epicholesterol incorporation on the permeability and on the phase transition of intact Acholeplasma laidlawii cell membranes and derived liposomes. *Biochimica et Biophysica Acta (BBA) - Biomembranes* **1972,** *255* (1), 331-347.

23.   Lasic, D. D.; Martin, F. J.; Gabizon, A.; Huang, S. K.; Papahadjopoulos, D., Sterically stabilized liposomes: a hypothesis on the molecular origin of the extended circulation times. *Biochimica et Biophysica Acta (BBA) - Biomembranes* **1991,** *1070* (1), 187-192.

24.   Allen Theresa, M.; Cullis Pieter, R., Drug Delivery Systems: Entering the Mainstream. *Science* **2004,** *303* (5665), 1818-1822.

25.   Papisov, M. I., Theoretical considerations of RES-avoiding liposomes: Molecular mechanics and chemistry of liposome interactions. *Advanced Drug Delivery Reviews* **1998,** *32* (1), 119-138.

26.   Senior, J.; Delgado, C.; Fisher, D.; Tilcock, C.; Gregoriadis, G., Influence of surface hydrophilicity of liposomes on their interaction with plasma protein and clearance from the circulation: Studies with poly(ethylene glycol)-coated vesicles. *Biochimica et Biophysica Acta (BBA) - Biomembranes* **1991,** *1062* (1), 77-82.

27.   Kirpotin, D.; Park, J. W.; Hong, K.; Zalipsky, S.; Li, W.-L.; Carter, P.; Benz, C. C.; Papahadjopoulos, D., Sterically Stabilized Anti-HER2 Immunoliposomes: Design and Targeting to Human Breast Cancer Cells in Vitro. *Biochemistry* **1997,** *36* (1), 66-75.

28.   Maruyama, K.; Takizawa, T.; Yuda, T.; Kennel, S. J.; Huang, L.; Iwatsuru, M., Targetability of novel immunoliposomes modified with amphipathic poly(ethylene glycol) s conjugated at their distal terminals to monoclonal antibodies. *Biochimica et Biophysica Acta (BBA) - Biomembranes* **1995,** *1234* (1), 74-80.

29.   Kapoor, M.; Lee, S. L.; Tyner, K. M., Liposomal Drug Product Development and Quality: Current US Experience and Perspective. *The AAPS Journal* **2017,** *19* (3), 632-641.

30.   Chen, W.; Cheng, C.-A.; Zink, J. I., Spatial, Temporal, and Dose Control of Drug Delivery using Noninvasive Magnetic Stimulation. *ACS Nano* **2019,** *13* (2), 1292-1308.

31.   Karimi, M.; Sahandi Zangabad, P.; Ghasemi, A.; Amiri, M.; Bahrami, M.; Malekzad, H.; Ghahramanzadeh Asl, H.; Mahdieh, Z.; Bozorgomid, M.; Ghasemi, A.; Rahmani Taji Boyuk, M. R.; Hamblin, M. R., Temperature-Responsive Smart Nanocarriers for Delivery Of Therapeutic Agents: Applications and Recent Advances. *ACS Applied Materials & Interfaces* **2016,** *8* (33), 21107-21133.

32.   Franco, M. S.; Gomes, E. R.; Roque, M. C.; Oliveira, M. C., Triggered Drug Release From Liposomes: Exploiting the Outer and Inner Tumor Environment. *Front Oncol* **2021,** *11*, 623760-623760.

33.   Soares, D. C. F.; de Oliveira, M. C.; dos Santos, R. G.; Andrade, M. S.; Vilela, J. M. C.; Cardoso, V. N.; Ramaldes, G. A., Liposomes radiolabeled with 159Gd-DTPA-BMA: Preparation, physicochemical characterization, release profile and in vitro cytotoxic evaluation. *European Journal of Pharmaceutical Sciences* **2011,** *42* (5), 462-469.

34.   Torchilin, V. P., Multifunctional, stimuli-sensitive nanoparticulate systems for drug delivery. *Nat Rev Drug Discov* **2014,** *13* (11), 813-27.

35.   Andreev, O. A.; Engelman, D. M.; Reshetnyak, Y. K., Targeting acidic diseased tissue: New technology based on use of the pH (Low) Insertion Peptide (pHLIP). *Chim Oggi* **2009,** *27* (2), 34-37.

36.   Yao, L.; Daniels, J.; Wijesinghe, D.; Andreev, O. A.; Reshetnyak, Y. K., pHLIP®-mediated delivery of PEGylated liposomes to cancer cells. *Journal of Controlled Release* **2013,** *167* (3), 228-237.

37.   Shchegravina, E. S.; Tretiakova, D. S.; Alekseeva, A. S.; Galimzyanov, T. R.; Utkin, Y. N.; Ermakov, Y. A.; Svirshchevskaya, E. V.; Negrebetsky, V. V.; Karpechenko, N. Y.; Chernikov, V. P.; Onishchenko, N. R.; Vodovozova, E. L.; Fedorov, A. Y.; Boldyrev, I. A., Phospholipidic Colchicinoids as Promising Prodrugs

Incorporated into Enzyme-Responsive Liposomes: Chemical, Biophysical, and Enzymological Aspects. *Bioconjugate Chemistry* **2019,** *30* (4), 1098-1113.

38.   Lee, Y.; Thompson, D. H., Stimuli-responsive liposomes for drug delivery. *Wiley Interdiscip Rev Nanomed Nanobiotechnol* **2017,** *9* (5).

39.   Chen, K.-J.; Chaung, E.-Y.; Wey, S.-P.; Lin, K.-J.; Cheng, F.; Lin, C.-C.; Liu, H.-L.; Tseng, H.-W.; Liu, C.-P.; Wei, M.-C.; Liu, C.-M.; Sung, H.-W., Hyperthermia-Mediated Local Drug Delivery by a Bubble-Generating Liposomal System for Tumor-Specific Chemotherapy. *ACS Nano* **2014,** *8* (5), 5105-5115.

40.   Shim, G.; Ko, S.; Kim, D.; Le, Q.-V.; Park, G. T.; Lee, J.; Kwon, T.; Choi, H.-G.; Kim, Y. B.; Oh, Y.-K., Light-switchable systems for remotely controlled drug delivery. *Journal of Controlled Release* **2017,** *267*, 67-79.

41.   Miranda, D.; Lovell, J. F., Mechanisms of Light-induced Liposome Permeabilization. *Bioeng Transl Med* **2016,** *1* (3), 267-276.

42.   Mathiyazhakan, M.; Wiraja, C.; Xu, C., A Concise Review of Gold Nanoparticles-Based Photo-Responsive Liposomes for Controlled Drug Delivery. *Nanomicro Lett* **2018,** *10* (1), 10-10.

43.   Sirsi, S. R.; Borden, M. A., State-of-the-art materials for ultrasound-triggered drug delivery. *Advanced Drug Delivery Reviews* **2014,** *72*, 3-14.

44.   Schroeder, A.; Kost, J.; Barenholz, Y., Ultrasound, liposomes, and drug delivery: principles for using ultrasound to control the release of drugs from liposomes. *Chemistry and Physics of Lipids* **2009,** *162* (1), 1-16.

45.   Nunez-Magos, L.; Lira-Escobedo, J.; Rodriguez-Lopez, R.; Munoz-Navia, M.; Castillo-Rivera, F.; Viveros-Mendez, P. X.; Araujo, E.; Encinas, A.; Saucedo-Anaya, S. A.; Aranda-Espinoza, S., Effects of DC Magnetic Fields on Magnetoliposomes. *Front Mol Biosci* **2021,** *8*, 703417.

46.   Guo, T.; Lin, M.; Huang, J.; Zhou, C.; Tian, W.; Yu, H.; Jiang, X.; Ye, J.; Shi, Y.; Xiao, Y.; Bian, X.; Feng, X., The Recent Advances of Magnetic Nanoparticles in Medicine. *Journal of Nanomaterials* **2018,** *2018*, 7805147.

47.   Bucak, S.; Yavuzturk, B.; Demir, A., Magnetic Nanoparticles: Synthesis, Surface Modifications and Application in Drug Delivery. In *Recent Advances in Novel Drug Carrier Systems*, 2012.

48.   Bonini, M.; Berti, D.; Baglioni, P., Nanostructures for magnetically triggered release of drugs and biomolecules. *Current Opinion in Colloid & Interface Science* **2013,** *18*, 459–467.

49.   Hegyi, G.; Szigeti, G. P.; Szász, A., Hyperthermia versus Oncothermia: Cellular Effects in Complementary Cancer Therapy. *Evid Based Complement Alternat Med* **2013,** *2013*, 672873-672873.

50.   Klibanov, A. L.; Hossack, J. A., Ultrasound in Radiology: From Anatomic, Functional, Molecular Imaging to Drug Delivery and Image-Guided Therapy. *Invest Radiol* **2015,** *50* (9), 657-670.

51.   Hegewisch-Becker, S.; Braun, K.; Otte, M.; Corovic, A.; Atanackovic, D.; Nierhaus, A.; Hossfeld, D. K.; Pantel, K., Effects of Whole Body Hyperthermia (41.8°C) on the Frequency of Tumor Cells in the Peripheral Blood of Patients with Advanced Malignancies1. *Clinical Cancer Research* **2003,** *9* (6), 2079-2084.

52.   Thomas, C. R.; Ferris, D. P.; Lee, J.-H.; Choi, E.; Cho, M. H.; Kim, E. S.; Stoddart, J. F.; Shin, J.-S.; Cheon, J.; Zink, J. I., Noninvasive Remote-Controlled Release of Drug Molecules in Vitro Using Magnetic Actuation of Mechanized Nanoparticles. *Journal of the American Chemical Society* **2010,** *132* (31), 10623-10625.

53.   Riedinger, A.; Guardia, P.; Curcio, A.; Garcia, M. A.; Cingolani, R.; Manna, L.; Pellegrino, T., Subnanometer Local Temperature Probing and Remotely Controlled Drug Release Based on Azo-Functionalized Iron Oxide Nanoparticles. *Nano Letters* **2013,** *13* (6), 2399-2406.

54.   Moros, M.; Idiago-Lopez, J.; Asin, L.; Moreno-Antolin, E.; Beola, L.; Grazu, V.; Fratila, R. M.; Gutierrez, L.; de la Fuente, J. M., Triggering antitumoural drug release and gene expression by magnetic hyperthermia. *Adv Drug Deliv Rev* **2019,** *138*, 326-343.

55. Amstad, E.; Kohlbrecher, J.; Müller, E.; Schweizer, T.; Textor, M.; Reimhult, E., Triggered Release from Liposomes through Magnetic Actuation of Iron Oxide Nanoparticle Containing Membranes. *Nano Letters* **2011,** *11* (4), 1664-1670.

56. Bonnaud, C.; Monnier, C. A.; Demurtas, D.; Jud, C.; Vanhecke, D.; Montet, X.; Hovius, R.; Lattuada, M.; Rothen-Rutishauser, B.; Petri-Fink, A., Insertion of Nanoparticle Clusters into Vesicle Bilayers. *ACS Nano* **2014,** *8* (4), 3451-3460.

57. Ginzburg, V. V.; Balijepalli, S., Modeling the Thermodynamics of the Interaction of Nanoparticles with Cell Membranes. *Nano Letters* **2007,** *7* (12), 3716-3722.

58. Bixner, O.; Reimhult, E., Controlled magnetosomes: Embedding of magnetic nanoparticles into membranes of monodisperse lipid vesicles. *Journal of Colloid and Interface Science* **2016,** *466*, 62-71.

59. Sub Wi, H.; Lee, K.; Kyu Pak, H., Interfacial energy consideration in the organization of a quantum dot–lipid mixed system. *Journal of Physics: Condensed Matter* **2008,** *20* (49).

60. Deatsch, A. E.; Evans, B. A., Heating efficiency in magnetic nanoparticle hyperthermia. *Journal of Magnetism and Magnetic Materials* **2014,** *354*, 163-172.

61. Babincová, M.; Čičmanec, P.; Altanerová, V.; Altaner, Č.; Babinec, P., AC-magnetic field controlled drug release from magnetoliposomes: design of a method for site-specific chemotherapy. *Bioelectrochemistry* **2002,** *55* (1), 17-19.

62. Nobuto, H.; Sugita, T.; Kubo, T.; Shimose, S.; Yasunaga, Y.; Murakami, T.; Ochi, M., Evaluation of systemic chemotherapy with magnetic liposomal doxorubicin and a dipole external electromagnet. *International Journal of Cancer* **2004,** *109* (4), 627-635.

63. Tai, L. A.; Tsai, P. J.; Wang, Y. C.; Wang, Y. J.; Lo, L. W.; Yang, C. S., Thermosensitive liposomes entrapping iron oxide nanoparticles for controllable drug release. *Nanotechnology* **2009,** *20* (13), 135101.

64. Nappini, S.; Bombelli, F. B.; Bonini, M.; Nordèn, B.; Baglioni, P., Magnetoliposomes for controlled drug release in the presence of low-frequency magnetic field. *Soft Matter* **2010,** *6* (1), 154-162.

65. Salvatore, A.; Montis, C.; Berti, D.; Baglioni, P., Multifunctional Magnetoliposomes for Sequential Controlled Release. *ACS Nano* **2016,** *10* (8), 7749-7760.

66. Sparreboom, A.; Kehrer, D. F.; Mathijssen, R. H.; Xie, R.; de Jonge, M. J.; de Bruijn, P.; Planting, A. S.; Eskens, F. A.; Verheij, C.; de Heus, G.; Klaren, A.; Zhang, S.; Verhaeghe, T.; Palmer, P. A.; Verweij, J., Phase I and pharmacokinetic study of irinotecan in combination with R115777, a farnesyl protein transferase inhibitor. *Br J Cancer* **2004,** *90* (8), 1508-15.

67. Rozners, E., ChemInform Abstract: NonIonic RNA Analogues: Stereoselective Synthesis, Biophysical Properties, and Biological Relevance. *Cheminform* **2008,** *39*.

68. Guo, H.; Chen, W.; Sun, X.; Liu, Y. N.; Li, J.; Wang, J., Theranostic magnetoliposomes coated by carboxymethyl dextran with controlled release by low-frequency alternating magnetic field. *Carbohydr Polym* **2015,** *118*, 209-17.

69. Nardoni, M.; Della Valle, E.; Liberti, M.; Relucenti, M.; Casadei, M. A.; Paolicelli, P.; Apollonio, F.; Petralito, S., Can Pulsed Electromagnetic Fields Trigger On-Demand Drug Release from High-Tm Magnetoliposomes? *Nanomaterials* **2018,** *8* (4).

70. Podaru, G.; Ogden, S.; Baxter, A.; Shrestha, T.; Ren, S.; Thapa, P.; Dani, R. K.; Wang, H.; Basel, M. T.; Prakash, P.; Bossmann, S. H.; Chikan, V., Pulsed Magnetic Field Induced Fast Drug Release from Magneto Liposomes via Ultrasound Generation. *The Journal of Physical Chemistry B* **2014,** *118* (40), 11715-11722.

71. Arruebo, M.; Fernández-Pacheco, R.; Ibarra, M. R.; Santamaría, J., Magnetic nanoparticles for drug delivery. *Nano Today* **2007,** *2* (3), 22-32.

72. Li, X.; Xie, C.; Xia, H.; Wang, Z., pH and Ultrasound Dual-Responsive Polydopamine-Coated Mesoporous Silica Nanoparticles for Controlled Drug Delivery. *Langmuir* **2018,** *34* (34), 9974-9981.

73.   Zhu, J.; Niu, Y.; Li, Y.; Gong, Y.; Shi, H.; Huo, Q.; Liu, Y.; Xu, Q., Stimuli-responsive delivery vehicles based on mesoporous silica nanoparticles: recent advances and challenges. *J Mater Chem B* **2017,** *5* (7), 1339-1352.

74.   Sing, K., Reporting physisorption data for gas/solid systems with special reference to the determination of surface area and porosity (Recommendations 1984). *Pure and Applied Chemistry* **1985,** *57*, 603.

75.   Kresge, C. T.; Leonowicz, M. E.; Roth, W. J.; Vartuli, J. C.; Beck, J. S., Ordered mesoporous molecular sieves synthesized by a liquid-crystal template mechanism. *Nature* **1992,** *359* (6397), 710-712.

76.   Vallet-Regi, M.; Rámila, A.; del Real, R. P.; Pérez-Pariente, J., A New Property of MCM-41: Drug Delivery System. *Chemistry of Materials* **2001,** *13* (2), 308-311.

77.   Vallet-Regí, M., Ordered Mesoporous Materials in the Context of Drug Delivery Systems and Bone Tissue Engineering. *Chemistry – A European Journal* **2006,** *12* (23), 5934-5943.

78.   Zhu, M.; Wang, H.; Liu, J.; He, H.; Hua, X.; He, Q.; Zhang, L.; Ye, X.; Shi, J., A mesoporous silica nanoparticulate/β-TCP/BG composite drug delivery system for osteoarticular tuberculosis therapy. *Biomaterials* **2011,** *32* (7), 1986-1995.

79.   Zhu, Y.; Shi, J.; Shen, W.; Dong, X.; Feng, J.; Ruan, M.; Li, Y., Stimuli-responsive controlled drug release from a hollow mesoporous silica sphere/polyelectrolyte multilayer core-shell structure. *Angew Chem Int Ed Engl* **2005,** *44* (32), 5083-7.

80.   Lai, C.-Y.; Trewyn, B. G.; Jeftinija, D. M.; Jeftinija, K.; Xu, S.; Jeftinija, S.; Lin, V. S. Y., A Mesoporous Silica Nanosphere-Based Carrier System with Chemically Removable CdS Nanoparticle Caps for Stimuli-Responsive Controlled Release of Neurotransmitters and Drug Molecules. *Journal of the American Chemical Society* **2003,** *125* (15), 4451-4459.

81.   Vallet-Regi, M.; Balas, F.; Arcos, D., Mesoporous materials for drug delivery. *Angew Chem Int Ed Engl* **2007,** *46* (40), 7548-58.

82.   Zhu, Y.-f.; Shi, J.-l.; Li, Y.-s.; Chen, H.-r.; Shen, W.-h.; Dong, X.-p., Storage and release of ibuprofen drug molecules in hollow mesoporous silica spheres with modified pore surface. *Microporous and Mesoporous Materials* **2005,** *85* (1), 75-81.

83.   Zhu, Y.; Fang, Y.; Borchardt, L.; Kaskel, S., PEGylated hollow mesoporous silica nanoparticles as potential drug delivery vehicles. *Microporous and Mesoporous Materials* **2011,** *141* (1-3), 199-206.

84.   Knezevic, N. Z.; Durand, J. O., Large pore mesoporous silica nanomaterials for application in delivery of biomolecules. *Nanoscale* **2015,** *7* (6), 2199-209.

85.   Santos, S. M. L.; Cecilia, J. A.; Vilarrasa-García, E.; Silva Junior, I. J.; Rodríguez-Castellón, E.; Azevedo, D. C. S., The effect of structure modifying agents in the SBA-15 for its application in the biomolecules adsorption. *Microporous and Mesoporous Materials* **2016,** *232*, 53-64.

86.   Anglin, E. J.; Cheng, L.; Freeman, W. R.; Sailor, M. J., Porous silicon in drug delivery devices and materials. *Advanced drug delivery reviews* **2008,** *60* (11), 1266-1277.

87.   Cecilia, J. A.; Moreno Tost, R.; Retuerto Millán, M., Mesoporous Materials: From Synthesis to Applications. *International Journal of Molecular Sciences* **2019,** *20* (13).

88.   Huh, S.; Wiench, J. W.; Yoo, J.-C.; Pruski, M.; Lin, V. S. Y., Organic Functionalization and Morphology Control of Mesoporous Silicas via a Co-Condensation Synthesis Method. *Chemistry of Materials* **2003,** *15* (22), 4247-4256.

89.   Slowing, I. I.; Trewyn, B. G.; Giri, S.; Lin, V. S. Y., Mesoporous Silica Nanoparticles for Drug Delivery and Biosensing Applications. *Advanced Functional Materials* **2007,** *17* (8), 1225-1236.

90.   Slowing, II; Vivero-Escoto, J. L.; Wu, C. W.; Lin, V. S., Mesoporous silica nanoparticles as controlled release drug delivery and gene transfection carriers. *Adv Drug Deliv Rev* **2008,** *60* (11), 1278-1288.

91.   Tang, F.; Li, L.; Chen, D., Mesoporous Silica Nanoparticles: Synthesis, Biocompatibility and Drug Delivery. *Advanced Materials* **2012,** *24* (12), 1504-1534.

92.   Botterhuis, N. E.; Sun, Q.; Magusin, P. C.; van Santen, R. A.; Sommerdijk, N. A., Hollow silica spheres with an ordered pore structure and their application in controlled release studies. *Chemistry* **2006,** *12* (5), 1448-56.

93.   Liu, J.; Qiao, S. Z.; Budi Hartono, S.; Lu, G. Q., Monodisperse yolk-shell nanoparticles with a hierarchical porous structure for delivery vehicles and nanoreactors. *Angew Chem Int Ed Engl* **2010,** *49* (29), 4981-5.

94.   Santhosh, P. B.; Ulrih, N. P., Multifunctional superparamagnetic iron oxide nanoparticles: promising tools in cancer theranostics. *Cancer Lett* **2013,** *336* (1), 8-17.

95.   Wu, H.; Zhang, S.; Zhang, J.; Liu, G.; Shi, J.; Zhang, L.; Cui, X.; Ruan, M.; He, Q.; Bu, W., A Hollow-Core, Magnetic, and Mesoporous Double-Shell Nanostructure: In Situ Decomposition/Reduction Synthesis, Bioimaging, and Drug-Delivery Properties. *Advanced Functional Materials* **2011,** *21* (10), 1850-1862.

96.   Zhang, L.; Wang, T.; Yang, L.; Liu, C.; Wang, C.; Liu, H.; Wang, Y. A.; Su, Z., General route to multifunctional uniform yolk/mesoporous silica shell nanocapsules: a platform for simultaneous cancer-targeted imaging and magnetically guided drug delivery. *Chemistry* **2012,** *18* (39), 12512-21.

97.   Wu, H.; Liu, G.; Zhang, S.; Shi, J.; Zhang, L.; Chen, Y.; Chen, F.; Chen, H., Biocompatibility, MR imaging and targeted drug delivery of a rattle-type magnetic mesoporous silica nanosphere system conjugated with PEG and cancer-cell-specific ligands. *Journal of Materials Chemistry* **2011,** *21* (9).

98.   Liong, M.; Lu, J.; Kovochich, M.; Xia, T.; Ruehm, S. G.; Nel, A. E.; Tamanoi, F.; Zink, J. I., Multifunctional Inorganic Nanoparticles for Imaging, Targeting, and Drug Delivery. *ACS Nano* **2008,** *2* (5), 889-896.

99.   Wu, P.; Zhu, J.; Xu, Z., Template-Assisted Synthesis of Mesoporous Magnetic Nanocomposite Particles. *Advanced Functional Materials* **2004,** *14* (4), 345-351.

100.   Zhao, W.; Gu, J.; Zhang, L.; Chen, H.; Shi, J., Fabrication of Uniform Magnetic Nanocomposite Spheres with a Magnetic Core/Mesoporous Silica Shell Structure. *Journal of the American Chemical Society* **2005,** *127* (25), 8916-8917.

101.   Uribe Madrid, S. I.; Pal, U.; Kang, Y. S.; Kim, J.; Kwon, H.; Kim, J., Fabrication of Fe3O4@mSiO2 Core-Shell Composite Nanoparticles for Drug Delivery Applications. *Nanoscale Res Lett* **2015,** *10*, 217-217.

102.   Purbia, R.; Paria, S., Yolk/shell nanoparticles: classifications, synthesis, properties, and applications. *Nanoscale* **2015,** *7* (47), 19789-873.

103.   Hallali, N.; Clerc, P.; Fourmy, D.; Gigoux, V.; Carrey, J., Influence on cell death of high frequency motion of magnetic nanoparticles during magnetic hyperthermia experiments. *Applied Physics Letters* **2016,** *109* (3).

104.   Zhao, Z.; Torres-Díaz, I.; Vélez, C.; Arnold, D.; Rinaldi, C., Brownian Dynamics Simulations of Magnetic Nanoparticles Captured in Strong Magnetic Field Gradients. *The Journal of Physical Chemistry C* **2017,** *121* (1), 801-810.

105.   Podaru, G.; Chikan, V., CHAPTER 1 Magnetism in Nanomaterials: Heat and Force from Colloidal Magnetic Particles. In *Magnetic Nanomaterials: Applications in Catalysis and Life Sciences*, The Royal Society of Chemistry: 2017; pp 1-24.

106.   Podaru, G. V.; Chikan, V.; Prakash, P., Magnetic Field Induced Ultrasound from Colloidal Superparamagnetic Nanoparticles. *The Journal of Physical Chemistry C* **2016,** *120* (4), 2386-2391.

107.   Munaz, A.; Shiddiky, M. J. A.; Nguyen, N. T., Recent advances and current challenges in magnetophoresis based micro magnetofluidics. *Biomicrofluidics* **2018,** *12* (3), 031501.

108.   Tombacz, E.; Turcu, R.; Socoliuc, V.; Vekas, L., Magnetic iron oxide nanoparticles: Recent trends in design and synthesis of magnetoresponsive nanosystems. *Biochem Biophys Res Commun* **2015,** *468* (3), 442-53.

109.   Wei, W.; Wang, Z., Investigation of Magnetic Nanoparticle Motion under a Gradient Magnetic Field by an Electromagnet. *Journal of Nanomaterials* **2018,** *2018*, 6246917.

110.   Hu, G.; He, B., Magnetoacoustic imaging of magnetic iron oxide nanoparticles embedded in biological tissues with microsecond magnetic stimulation. *Appl Phys Lett* **2012,** *100* (1), 13704-137043.

111.   Xu, Z.; Hou, Y.; Sun, S., Magnetic Core/Shell Fe3O4/Au and Fe3O4/Au/Ag Nanoparticles with Tunable Plasmonic Properties. *Journal of the American Chemical Society* **2007,** *129* (28), 8698-8699.

112.   Lyon, J. L.; Fleming, D. A.; Stone, M. B.; Schiffer, P.; Williams, M. E., Synthesis of Fe Oxide Core/Au Shell Nanoparticles by Iterative Hydroxylamine Seeding. *Nano Letters* **2004,** *4* (4), 719-723.

113.   Brown, K. R.; Walter, D. G.; Natan, M. J., Seeding of Colloidal Au Nanoparticle Solutions. 2. Improved Control of Particle Size and Shape. *Chemistry of Materials* **2000,** *12* (2), 306-313.

114.   Cheng, L.; Liu, Y.; Zou, B.; Yu, Y.; Ruan, W.; Wang, Y., Template-etching route to construct uniform rattle-type Fe3O4@SiO2 hollow microspheres as drug carrier. *Mater Sci Eng C Mater Biol Appl* **2017,** *75*, 829-835.

115.   Torchilin, V. P., Recent advances with liposomes as pharmaceutical carriers. *Nat Rev Drug Discov* **2005,** *4* (2), 145-60.

116.   Woodle, M. C., Sterically stabilized liposome therapeutics. *Advanced Drug Delivery Reviews* **1995,** *16* (2), 249-265.

117.   Charrois, G. J. R.; Allen, T. M., Rate of biodistribution of STEALTH® liposomes to tumor and skin: influence of liposome diameter and implications for toxicity and therapeutic activity. *Biochimica et Biophysica Acta (BBA) - Biomembranes* **2003,** *1609* (1), 102-108.

118.   Al-Jamal, W. T.; Al-Jamal, K. T.; Bomans, P. H.; Frederik, P. M.; Kostarelos, K., Functionalized-quantum-dot-liposome hybrids as multimodal nanoparticles for cancer. *Small* **2008,** *4* (9), 1406-15.

119.   Nappini, S.; Bonini, M.; Bombelli, F. B.; Pineider, F.; Sangregorio, C.; Baglioni, P.; Nordèn, B., Controlled drug release under a low frequency magnetic field: effect of the citrate coating on magnetoliposomes stability. *Soft Matter* **2011,** *7* (3), 1025-1037.

120.   Kloepfer, J. A.; Cohen, N.; Nadeau, J. L., FRET between CdSe Quantum Dots in Lipid Vesicles and Water- and Lipid-soluble Dyes. *The Journal of Physical Chemistry B* **2004,** *108* (44), 17042-17049.

121.   Nappini, S.; Bonini, M.; Ridi, F.; Baglioni, P., Structure and permeability of magnetoliposomes loaded with hydrophobic magnetic nanoparticles in the presence of a low frequency magnetic field. *Soft Matter* **2011,** *7* (10).

122.   Needham, D.; Dewhirst, M. W., The development and testing of a new temperature-sensitive drug delivery system for the treatment of solid tumors. *Advanced Drug Delivery Reviews* **2001,** *53* (3), 285-305.

123.   Ueno, M.; Yoshida, S.; Horikoshi, I., Characteristics of the Membrane Permeability of Temperature-Sensitive Liposome. *Bulletin of the Chemical Society of Japan* **1991,** *64* (5), 1588-1593.

124.   Ganta, S.; Devalapally, H.; Shahiwala, A.; Amiji, M., A review of stimuli-responsive nanocarriers for drug and gene delivery. *J Control Release* **2008,** *126* (3), 187-204.

125.   Hegh, D. Y.; Mackay, S. M.; Tan, E. W., Pulsatile release from pH triggered imidazoline switchable surfactant liposomes. *RSC Advances* **2016,** *6* (62), 56859-56866.

126.   Wu, G.; Mikhailovsky, A.; Khant, H. A.; Fu, C.; Chiu, W.; Zasadzinski, J. A., Remotely Triggered Liposome Release by Near-Infrared Light Absorption via Hollow Gold Nanoshells. *Journal of the American Chemical Society* **2008,** *130* (26), 8175-8177.

127.   Malekar, S. A.; Sarode, A. L.; Bach, A. C., 2nd; Bose, A.; Bothun, G.; Worthen, D. R., Radio Frequency-Activated Nanoliposomes for Controlled Combination Drug Delivery. *AAPS PharmSciTech* **2015,** *16* (6), 1335-43.

128.   Shirmardi Shaghasemi, B.; Virk, M. M.; Reimhult, E., Optimization of Magneto-thermally Controlled Release Kinetics by Tuning of Magnetoliposome Composition and Structure. *Sci Rep* **2017,** *7* (1), 7474.

129.   Wong, W.; Gan, W. L.; Liu, N.; Lew, W. S., Magneto-actuated cell apoptosis by biaxial pulsed magnetic field. *Sci Rep* **2017,** *7* (1), 10919.

130.   Goya, F. G.; Grazu, V.; Ibarra, R. M., Magnetic Nanoparticles for Cancer Therapy. *Current Nanoscience* **2008,** *4* (1), 1-16.

131.   Pankhurst, Q. A.; Connolly, J.; Jones, S. K.; Dobson, J., Applications of magnetic nanoparticles in biomedicine. *Journal of Physics D: Applied Physics* **2003,** *36* (13), R167-R181.

132.   Ahmed, S. E.; Moussa, H. G.; Martins, A. M.; Al-Sayah, M. H.; Husseini, G. A., Effect of pH, ultrasound frequency and power density on the release of calcein from stealth liposomes. *European Journal of Nanomedicine* **2016,** *8* (1), 31-43.

133.   Steinberg, Y.; Schroeder, A.; Talmon, Y.; Schmidt, J.; Khalfin, R. L.; Cohen, Y.; Devoisselle, J.-M.; Begu, S.; Avnir, D., Triggered Release of Aqueous Content from Liposome-Derived Sol–Gel Nanocapsules. *Langmuir* **2007,** *23* (24), 12024-12031.

134.   Józefczak, A.; Kaczmarek, K.; Hornowski, T.; Kubovčíková, M.; Rozynek, Z.; Timko, M.; Skumiel, A., Magnetic nanoparticles for enhancing the effectiveness of ultrasonic hyperthermia. *Applied Physics Letters* **2016,** *108* (26).

135.   Carrey, J.; Connord, V.; Respaud, M., Ultrasound generation and high-frequency motion of magnetic nanoparticles in an alternating magnetic field: Toward intracellular ultrasound therapy? *Applied Physics Letters* **2013,** *102* (23), 232404.

136.   Mehrmohammadi, M.; Qu, M.; Ma, L. L.; Romanovicz, D. K.; Johnston, K. P.; Sokolov, K. V.; Emelianov, S. Y., Pulsed magneto-motive ultrasound imaging to detect intracellular trafficking of magnetic nanoparticles. *Nanotechnology* **2011,** *22* (41), 415105.

137.   Callen, E.; Callen, H. B., Magnetostriction, Forced Magnetostriction, and Anomalous Thermal Expansion in Ferromagnets. *Physical Review* **1965,** *139* (2A), A455-A471.

138.   Love, J. C.; Estroff, L. A.; Kriebel, J. K.; Nuzzo, R. G.; Whitesides, G. M., Self-Assembled Monolayers of Thiolates on Metals as a Form of Nanotechnology. *Chemical Reviews* **2005,** *105* (4), 1103-1170.

139.   Nappini, S.; Fogli, S.; Castroflorio, B.; Bonini, M.; Baldelli Bombelli, F.; Baglioni, P., Magnetic field responsive drug release from magnetoliposomes in biological fluids. *J Mater Chem B* **2016,** *4* (4), 716-725.

140.   Das, M.; Dahal, U.; Mesele, O.; Liang, D.; Cui, Q., Molecular Dynamics Simulation of Interaction between Functionalized Nanoparticles with Lipid Membranes: Analysis of Coarse-Grained Models. *The Journal of Physical Chemistry B* **2019,** *123* (49), 10547-10561.

141.   Chakraborty, S.; Abbasi, A.; Bothun, G. D.; Nagao, M.; Kitchens, C. L., Phospholipid Bilayer Softening Due to Hydrophobic Gold Nanoparticle Inclusions. *Langmuir* **2018,** *34* (44), 13416-13425.

142.   Malekkhaiat Haffner, S.; Malmsten, M., Membrane interactions and antimicrobial effects of inorganic nanoparticles. *Adv Colloid Interface Sci* **2017,** *248*, 105-128.

143.   Liburdy, R. P.; Tenforde, T. S.; Magin, R. L., Magnetic Field-Induced Drug Permeability in Liposome Vesicles. *Radiation Research* **1986,** *108* (1), 102-111.

144.   Tenforde, T. S.; Liburdy, R. P., Magnetic deformation of phospholipid bilayers: Effects on liposome shape and solute permeability at prephase transition temperatures. *Journal of Theoretical Biology* **1988,** *133* (3), 385-396.

145.   Liu, J. F.; Neel, N.; Dang, P.; Lamb, M.; McKenna, J.; Rodgers, L.; Litt, B.; Cheng, Z.; Tsourkas, A.; Issadore, D., Radiofrequency-Triggered Drug Release from Nanoliposomes with Millimeter-Scale Resolution Using a Superimposed Static Gating Field. *Small* **2018,** *14* (44), e1802563.

146.   Hulangamuwa, W.; Acharya, B.; Chikan, V.; Rafferty, R. J., Triggering Passive Molecular Transport into Cells with a Combination of Inhomogeneous Magnetic Fields and Magnetic Nanoparticles. *ACS Applied Nano Materials* **2020,** *3* (3), 2414-2420.

147.   Tomitaka, A.; Takemura, Y.; Huang, Z.; Roy, U.; Nair, M., Magnetoliposomes in Controlled-Release Drug Delivery Systems. **2019,** *47* (6), 495-505.

148.   Monnier, C. A.; Burnand, D.; Rothen-Rutishauser, B.; Lattuada, M.; Petri-Fink, A., Magnetoliposomes: opportunities and challenges. *European Journal of Nanomedicine* **2014,** *6* (4).

149.   Fortes Brollo, M. E.; Domínguez-Bajo, A.; Tabero, A.; Domínguez-Arca, V.; Gisbert, V.; Prieto, G.; Johansson, C.; Garcia, R.; Villanueva, A.; Serrano, M. C.; Morales, M. d. P., Combined Magnetoliposome Formation and Drug Loading in One Step for Efficient Alternating Current-Magnetic Field Remote-Controlled Drug Release. *ACS Applied Materials & Interfaces* **2020,** *12* (4), 4295-4307.

150.   Acharya, B.; Chikan, V., Pulse Magnetic Fields Induced Drug Release from Gold Coated Magnetic Nanoparticle Decorated Liposomes. *Magnetochemistry* **2020,** *6* (4).

151.   Nappini, S.; Al Kayal, T.; Berti, D.; Nordèn, B.; Baglioni, P., Magnetically Triggered Release From Giant Unilamellar Vesicles: Visualization By Means Of Confocal Microscopy. *The Journal of Physical Chemistry Letters* **2011,** *2* (7), 713-718.

152.   Qiu, D.; An, X., Controllable release from magnetoliposomes by magnetic stimulation and thermal stimulation. *Colloids Surf B Biointerfaces* **2013,** *104*, 326-9.

153.   Hsu, M. H.; Su, Y. C., Iron-oxide embedded solid lipid nanoparticles for magnetically controlled heating and drug delivery. *Biomed Microdevices* **2008,** *10* (6), 785.

154.   Liu, T.-Y.; Hu, S. H.; Liu, K.-H.; Shaiu, R.-S.; Liu, D.-M.; Chen, S.-Y., Instantaneous drug delivery of magnetic/thermally sensitive nanospheres by a high-frequency magnetic field. *Langmuir : the ACS journal of surfaces and colloids* **2008,** *24 23*, 13306-11.

155.   Chen, Y.; Bose, A.; Bothun, G. D., Controlled Release from Bilayer-Decorated Magnetoliposomes via Electromagnetic Heating. *ACS Nano* **2010,** *4* (6), 3215-3221.

156.   Issa, B.; Obaidat, I. M.; Albiss, B. A.; Haik, Y., Magnetic nanoparticles: surface effects and properties related to biomedicine applications. *Int J Mol Sci* **2013,** *14* (11), 21266-305.

157.   Vlasova, K. Y.; Piroyan, A.; Le-Deygen, I. M.; Vishwasrao, H. M.; Ramsey, J. D.; Klyachko, N. L.; Golovin, Y. I.; Rudakovskaya, P. G.; Kireev, II; Kabanov, A. V.; Sokolsky-Papkov, M., Magnetic liposome design for drug release systems responsive to super-low frequency alternating current magnetic field (AC MF). *J Colloid Interface Sci* **2019,** *552*, 689-700.

158.   Choi, W. I.; Sahu, A.; Wurm, F. R.; Jo, S.-M., Magnetoliposomes with size controllable insertion of magnetic nanoparticles for efficient targeting of cancer cells. *RSC Advances* **2019,** *9* (26), 15053-15060.

159.   Toledo, E. J. L.; Ramalho, T. C.; Magriotis, Z. M., Influence of magnetic field on physical–chemical properties of the liquid water: Insights from experimental and theoretical models. *Journal of Molecular Structure* **2008,** *888* (1-3), 409-415.

160.   Wang, Y.; Wei, H.; Li, Z., Effect of magnetic field on the physical properties of water. *Results in Physics* **2018,** *8*, 262-267.

161.   Cai, R.; Yang, H.; He, J.; Zhu, W., The effects of magnetic fields on water molecular hydrogen bonds. *Journal of Molecular Structure* **2009,** *938* (1-3), 15-19.

162.   Sundaram, J.; Mellein, B. R.; Mitragotri, S., An Experimental and Theoretical Analysis of Ultrasound-Induced Permeabilization of Cell Membranes. *Biophysical Journal* **2003,** *84* (5), 3087-3101.

163.   Escoffre, J. M.; Mannaris, C.; Geers, B.; Novell, A.; Lentacker, I.; Averkiou, M.; Bouakaz, A., Doxorubicin liposome-loaded microbubbles for contrast imaging and ultrasound-triggered drug delivery. *IEEE Trans Ultrason Ferroelectr Freq Control* **2013,** *60* (1), 78-87.

164.   Singh, R. R. T.; Garland, J. M.; Cassidy, M. C.; Migalska, K.; Demir, K. Y.; Abdelghany, S.; Ryan, E.; Woolfson, D.; Donnelly, F. R., Microporation Techniques for Enhanced Delivery of Therapeutic Agents. *Recent Patents on Drug Delivery & Formulation* **2010,** *4* (1), 1-17.

165.   Weaver, J. C.; Chizmadzhev, Y. A., Theory of electroporation: A review. *Bioelectrochemistry and Bioenergetics* **1996,** *41* (2), 135-160.

166.   Novickij, V.; Grainys, A.; Novickij, J.; Markovskaja, S., Irreversible magnetoporation of micro-organisms in high pulsed magnetic fields. *IET Nanobiotechnol* **2014,** *8* (3), 157-62.

167.   Nomikou, N.; McHale, A. P., Exploiting ultrasound-mediated effects in delivering targeted, site-specific cancer therapy. *Cancer Lett* **2010,** *296* (2), 133-43.

168.   Duck, F. A., Chapter 4 - Acoustic Properties of Tissue at Ultrasonic Frequencies. In *Physical Properties of Tissues*, Duck, F. A., Ed. Academic Press: London, 1990; pp 73-135.

169.   Younes, M.; Lechago, L. V.; Somoano, J. R.; Mosharaf, M.; Lechago, J., Wide Expression of the Human Erythrocyte Glucose Transporter Glut1 in Human Cancers. *Cancer Research* **1996,** *56* (5), 1164-1167.

170.   Macheda, M. L.; Rogers, S.; Best, J. D., Molecular and cellular regulation of glucose transporter (GLUT) proteins in cancer. *J Cell Physiol* **2005,** *202* (3), 654-62.

171.   Barron, C. C.; Bilan, P. J.; Tsakiridis, T.; Tsiani, E., Facilitative glucose transporters: Implications for cancer detection, prognosis and treatment. *Metabolism* **2016,** *65* (2), 124-39.

Appendix A – Supporting Information from Chapter 2

Calculation of number of Lipid Molecules per Liposome

N(total) = [4π (d/2)^2 + 4π (d/2 - h)^2]/a

Where,

4π (d/2)^2 = Surface area of outer monolayer of liposomes

4π (d/2 - h)^2 = Surface area of inner layer of liposomes

'd' = diameter of liposomes (it is determined from the pore size of the membrane used during extrusion step of liposome preparation)

'h' = thickness of bilayer = approx. 5nm

'a' = Lipid head group area =approx. 0.71nm (for Phosphatidylcholine)

Thus, N(total)= 17.69 * [r^2 + (r-5)^2] ; where r= radius of Liposomes

Calculation of Number of Liposomes

N(liposomes) = [M * Avogadro's Number]/ [N(total) * 1000]

Where,

M= molar concentration of Lipid

In an experiment, 10 mg of Lipid (DPPC+DSPC+ Cholesterol) is used to prepare 1 mL of liposome sample solution in the hydration step. Since the amount of DPPC is significantly more than other components, the concentration of Lipid approximately refers to the concentration of DPPC.

The concentration of Lipid = (247 uL* 0.0545 M)/ (1000uL) = 0.0136M

Thus,

N(total) = 336552.25 (when Diameter of Liposomes is 200nm)

N(liposomes) is then approximately**,** 24.33e12 .

Note: The liposomes samples when passed through the column, for the separation of free dyes, process involves the dilution by 4 times (the concentration is nearly 6.08e12). Further, the experimental step involves the dilution of this sample 10 times (during the addition of nanoparticles).

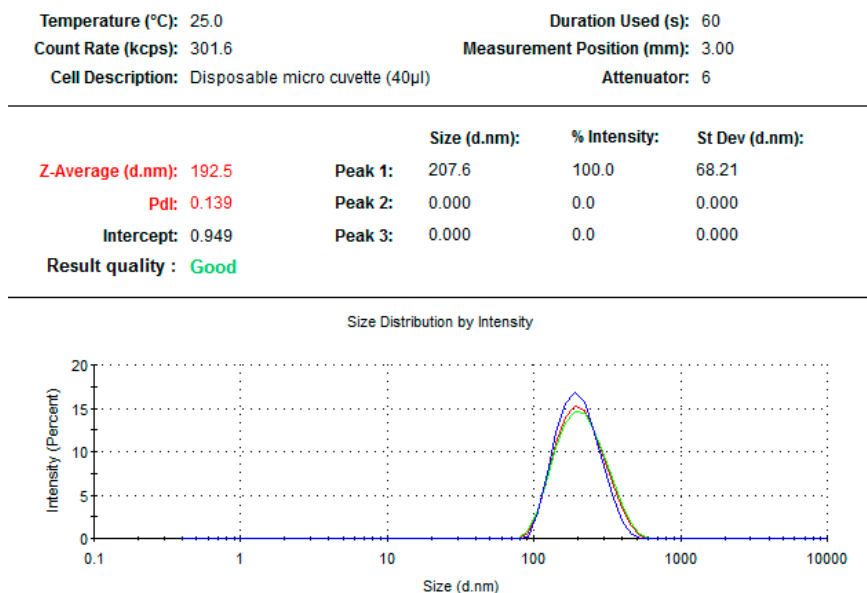**Release factor of CF from Thiolated liposomes diluted in distilled water**
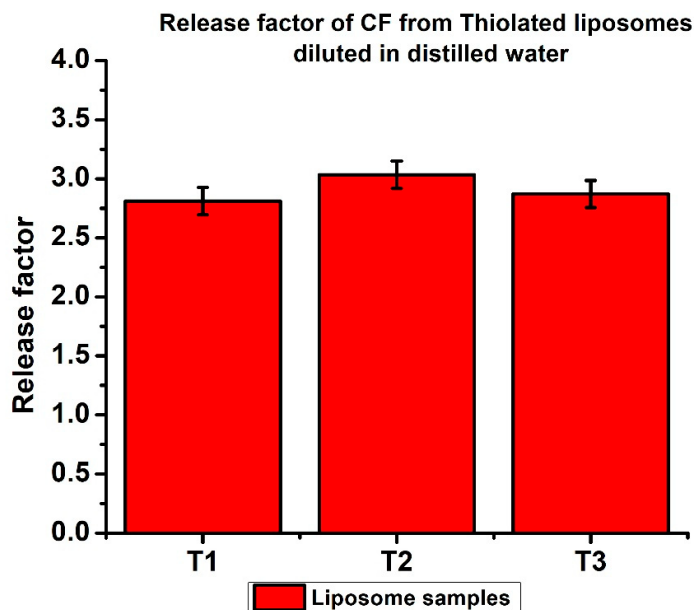
Figure A1. The normalized release factor of CF from thiolated liposomes after the completion of the thermal cycle is mentioned in section 4.4). This shows the reproducibility of the method of dyes

encapsulation as well as CF release assay.

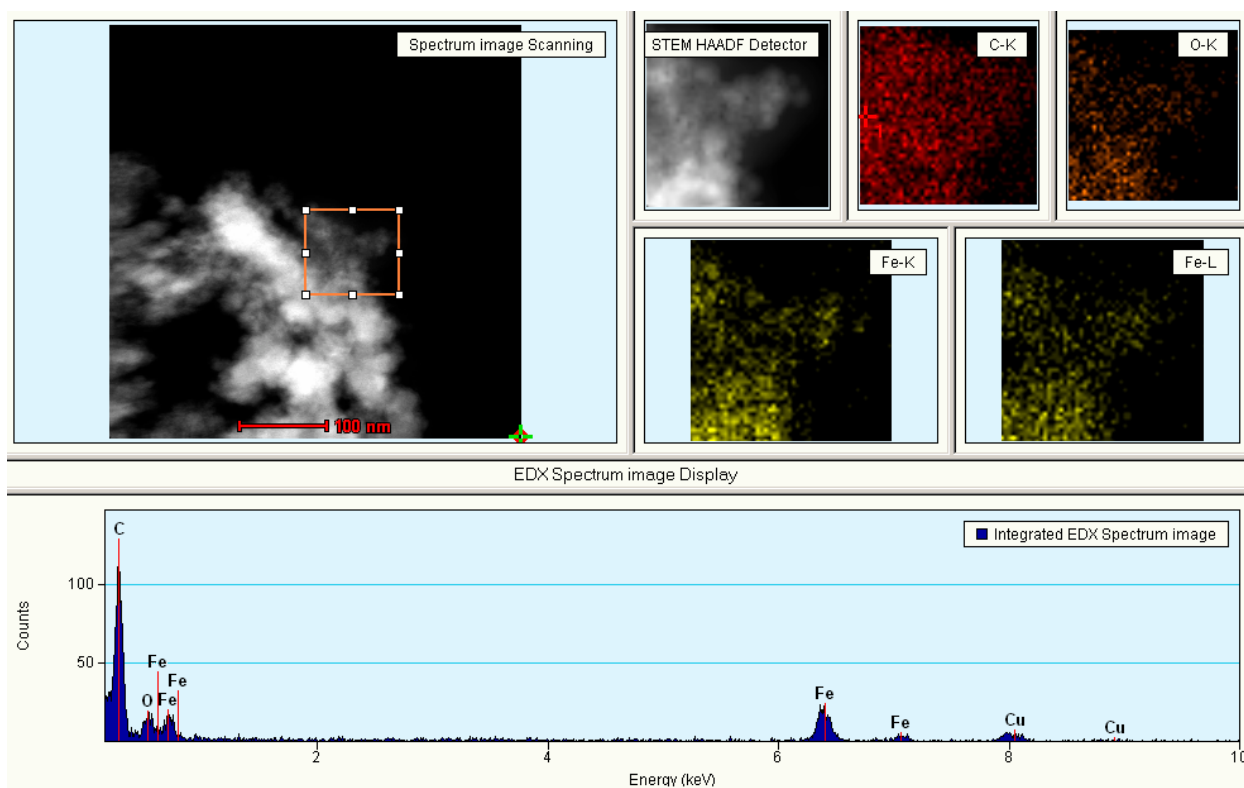**The Thermal profile for liposomes samples**
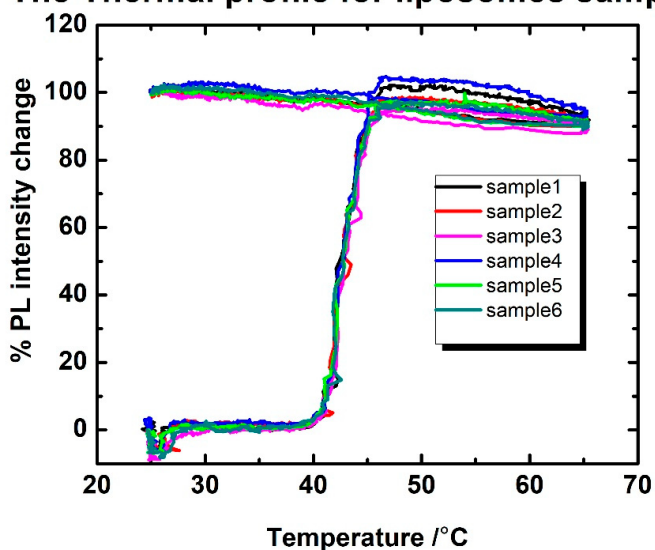
**Figure A2.** The comparison of thermal profile for percentage CF release from different samples. (n=6) showing reproducibility of the method used.

Appendix B – Supporting Information from Chapter 3

| | | | Size (d.nm): | % Intensity: | St Dev (d.nm): |

Temperature (°C): 25.0   Duration Used (s): 60
Count Rate (kcps): 301.6   Measurement Position (mm): 3.00
Cell Description: Disposable micro cuvette (40µl)   Attenuator: 6

		Size (d.nm):	% Intensity:	St Dev (d.nm):
Z-Average (d.nm): 192.5	Peak 1:	207.6	100.0	68.21
Pdl: 0.139	Peak 2:	0.000	0.0	0.000
Intercept: 0.949	Peak 3:	0.000	0.0	0.000
Result quality : Good				

Size Distribution by Intensity

Figure B1. The size distribution of liposomes.

Figure B2. The EDX analysis of synthesized iron oxide nanoparticles.
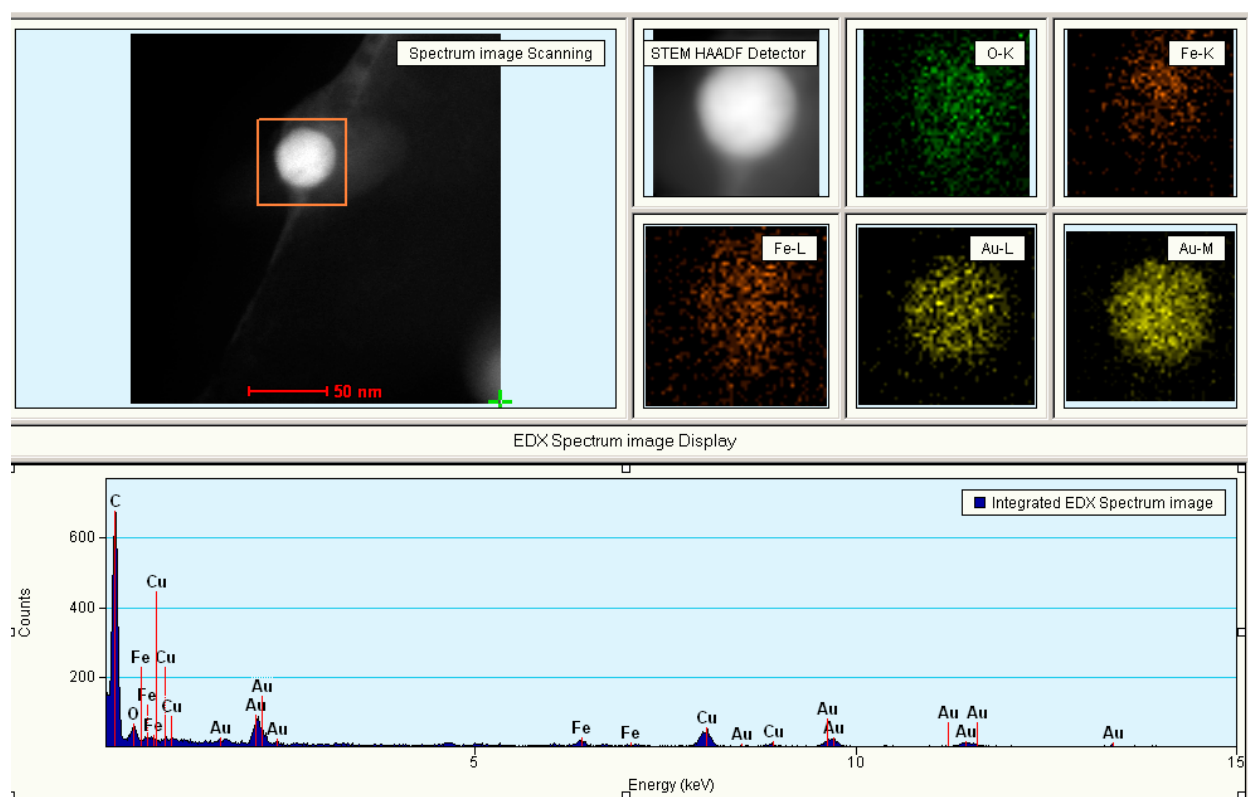
Figure B3. The EDX analysis of gold-coated commercial iron oxide nanoparticles.
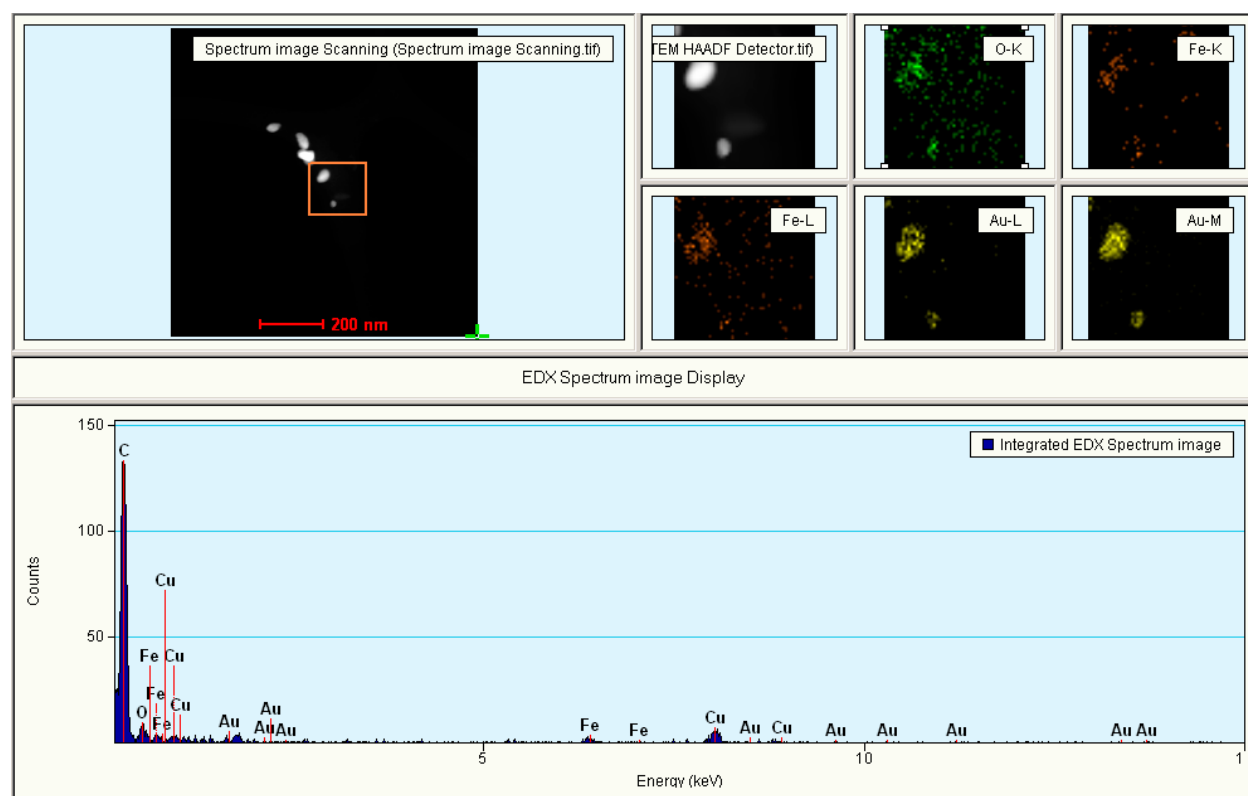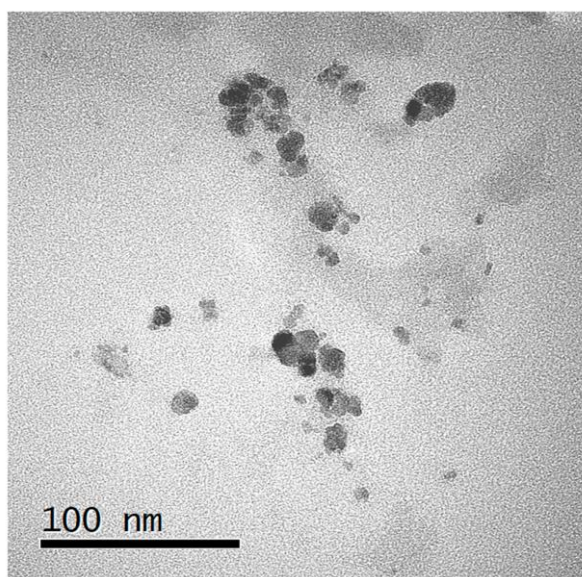

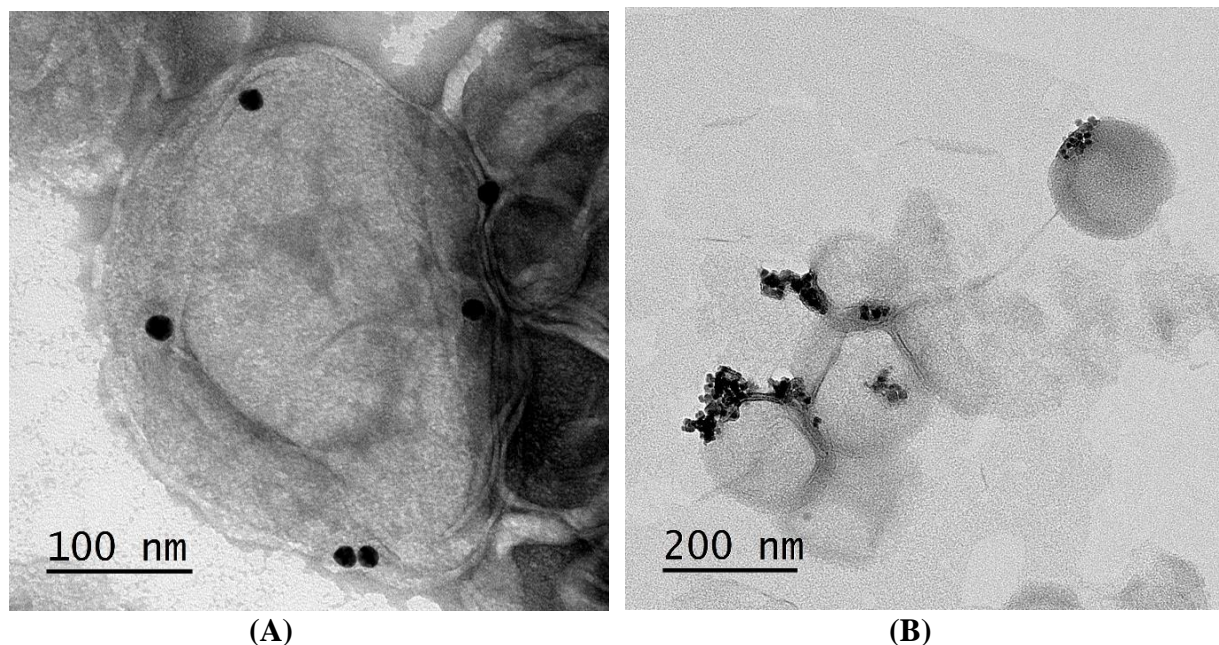**Figure B4.** The EDX analysis of gold-coated synthetic iron oxide nanoparticles.
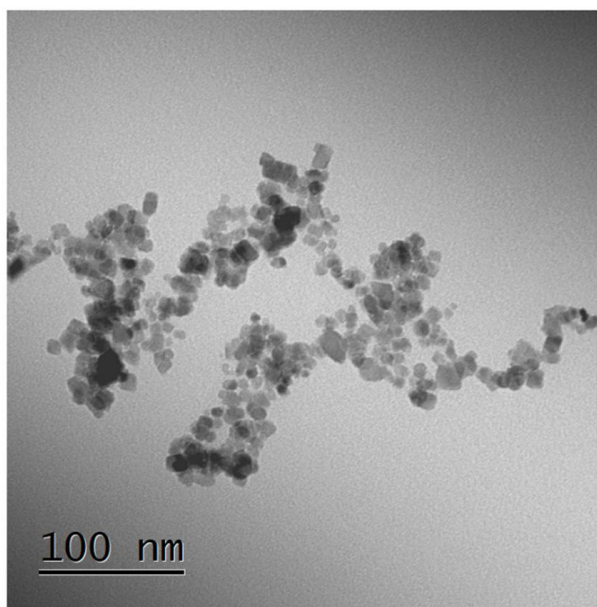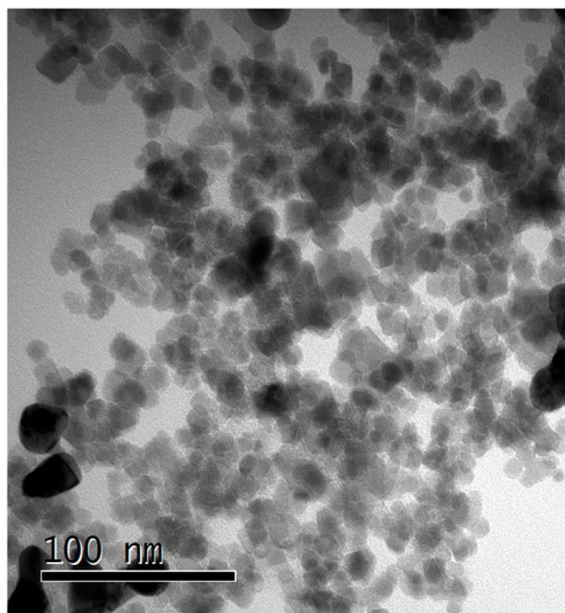
Figure B5. (A) TEM image of synthesized iron oxide nanoparticles; (B) TEM image of gold-coated synthesized iron oxide nanoparticles: (C) TEM image of gold-coated commercial iron oxide nanoparticles.

(A)   **(B)**

Figure B6. The images showing (A) gold-coated commercial iron oxide nanoparticles (B) synthetic iron oxide nanoparticles, on the liposomal surface provide evidence of Au-SH chemisorption.

Staining method used for liposomes and nanoparticles system:

Negative staining method

The details of the specimen are seen as unstained, electron-lucent structures (light) against electron-dense (dark) background Uranyl acetate (2% aqueous solution) is used as a negative stain. Place a drop of suspension of particulate specimens (in higher concentration) on a coated TEM. Grid and drain off the excess by blotting with filter paper from the edge of the TEM grid. Immediately add a drop of negative stain and allow to remain 3-5 minutes. Again, drain off the excess stain by blotting, dry the grid and observe under TEM.

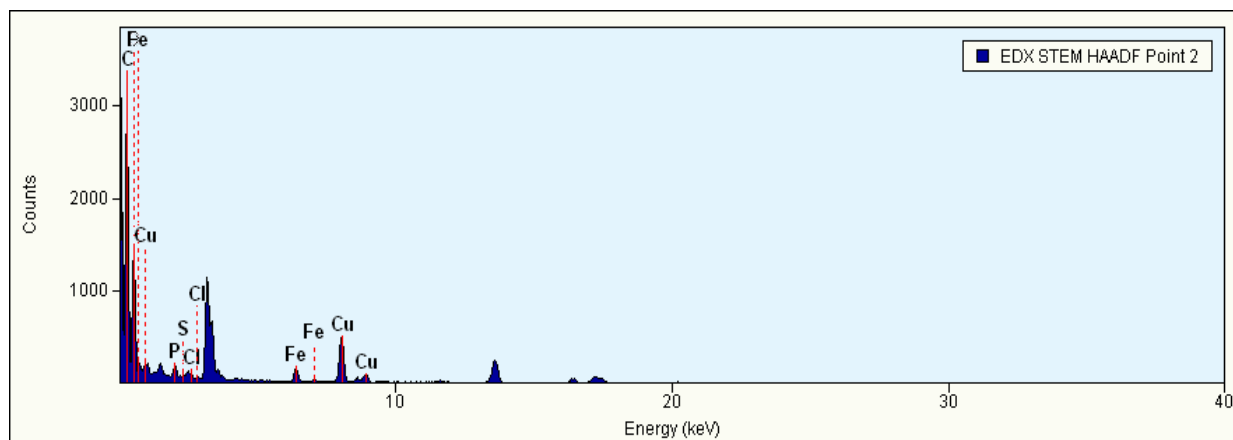# Appendix C – Supporting Information from Chapter 4

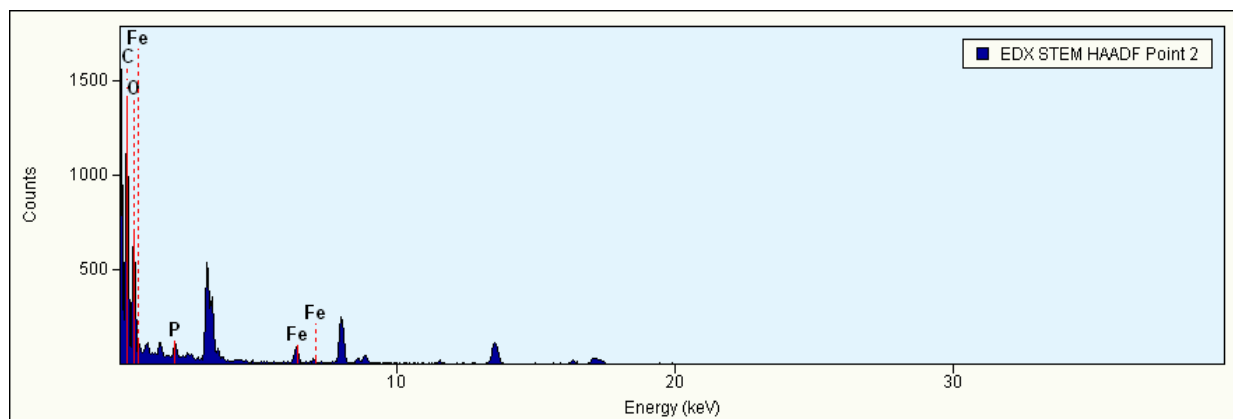Figure C1. EDX Spectrum for MNPs at Core (1:1)
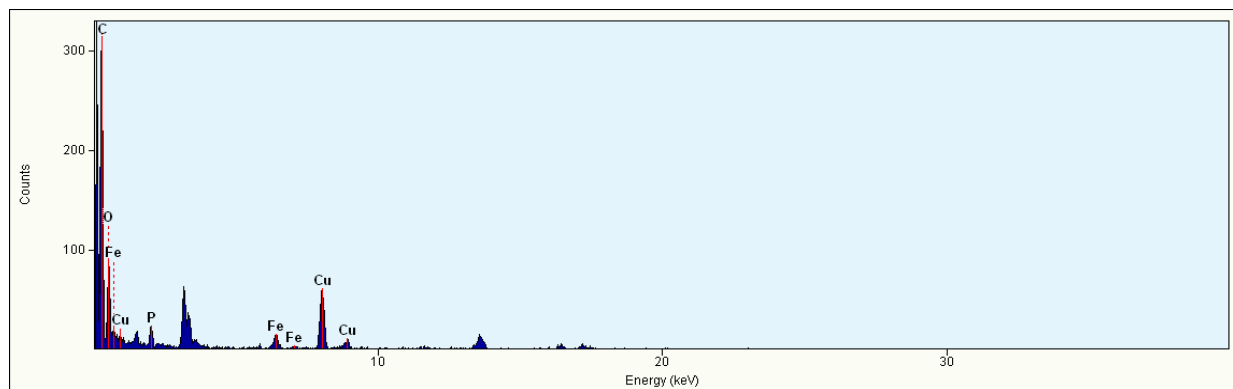

Figure C2. EDX Spectrum for MNPs at Core (1:4)

Figure C3. EDX Spectrum for MNPs at the bilayer